Exchange Processes between a Coniferous Forest and the Atmosphere

Uitwisselingsprocessen tussen een naaldbos en de atmosfeer

Fred C. Bosveld

Promotor: Dr. A. A. M. Holtslag,
               Hoogleraar in de meteorologie en luchtkwaliteit.

Co-promotor: Dr. ir. W. Bouten,
               Universitair hoofddocent, Universiteit van Amsterdam.

Exchange Processes between a Coniferous Forest

and the Atmosphere

Fred C. Bosveld

Stellingen behorende bij het proefschrift van Fred C. Bosveld:

"Exchange processes between a coniferous forest and the atmosphere",

Wageningen, 3 november 1999.

1) Voor het schatten van uitwisselingsfluxen boven bos uit gradiënten dienen in-situ uitwisselingscoëfficiënten bepaald te worden. (Dit proefschrift)

2) De ruwheidslengte voor warmte wordt mede bepaald door de turbulente structuur van de atmosferische ruwheidslaag. (Dit proefschrift)

3) In bossen treedt 's nachts vaak convectie op. Dit leidt tot een aanzienlijk sterkere thermische koppeling tussen atmosfeer en de bosbodem dan tot nu toe werd aangenomen. (Dit proefschrift)

4) De maximale oppervlakteweerstand is als indicator alleen niet voldoende om verdamping van bossen te vergelijken. (Dit proefschrift)

5) Transpiratiereductie van een nat Douglas sparrenbos wordt slechts in beperkte mate bepaald door blokkade van stomata. (Dit proefschrift)

6) De structuurparameter van de verticale wind kan redelijk geschat worden met een eenvoudig instrument dat de nuldoorgangen van de verticale wind detecteert. (Bosveld, 1999, KNMI-WR-99-03)

7) Goed bedoelde acties, zoals het dumpen van tweedehands schoenen in ontwikkelingslanden, leiden tot ernstige ontwrichting van lokale economieën in het zuiden.

8) Als p een priemgetal is dan is p een factor van 2^p-2 (de kleine stelling van Fermat). Er zijn slechts weinig samengestelde getallen waarvoor dit ook geldt.

9) Het recente eerherstel van Galileï door de Rooms-katholieke kerk toont aan dat niet alleen het aardse klimaatsysteem lange tijdschalen in zich bergt.

10) Uitspraken van voetbalcommentatoren zoals: 'de bal kreeg snelheid mee door het natte veld' getuigen van een goed ontwikkeld fysisch gevoel. (Stelling 11, Sander Tijm)

11) 'Ieder voordeel heeft zijn nadeel' geldt zeker voor het analyseren van zelf uitgevoerde metingen. (vrij naar Cruijff, 1997)

12) De keuze van de paranimfen is het exclusieve recht van de promovendus.

Voorwoord

Het voor u liggende boekje is de weerslag van een project waaraan ik met kleine en grote onderbrekingen vanaf 1988 aan gewerkt heb. Het was in 1987 dat Peter Hofschreuder en Aart Vermetten van de Landbouw Universiteit Wageningen contact legden met het KNMI. Mede als coördinatoren van de meetlokatie Speuld zijn zij van onschatbare waarde geweest voor het welslagen van alle activiteiten in Speuld gedurende het ACIFORN project. Met Anton Beljaars (nu op het ECMWF) stond ik in de top van de Wageningen mast in Speuld en we zeiden tegen elkaar, "ideaal is het niet". Een half jaar later stond er een tweede mast op de lokatie en konden de metingen beginnen. Anton, bedankt, op essentiële momenten heb jij richting gegeven aan mijn werk op het KNMI.

De mast bood een uniek uitzicht over de bossen van de noordwesthoek van de Veluwe. De hoge bomen bij Drie waarvan men zegt dat ze in vroeger tijden dienst deden als baken voor de scheepvaart op de Zuiderzee. Het 'Solsche Gat' waar de geest van Teunisz ooit rond dwaalde en dat eeuwen eerder dienst deed als trefpunt van druïden. Het bos met zijn kronkelende bomen. En niet te vergeten het melancholieke geluid van de tuien van de mast bij voldoende harde wind. In die mast waarvan ik zei dat je overal precies bij kon en waarvan Gerard zei dat je overal precies niet bij kon. Bedankt Gerard voor al je coördinerende steun tijdens onze veldexperimenten en voor alle prettige gesprekken tijdens onze expedities naar Speuld. Bedankt M.P.D. Jansse voor de perfecte coördinatie tijdens de opbouw fase van de infrastructuur; Mark van Wijngaarden en Louis van der Woerd voor het ontwerp- en tekenwerk; Leo Schiks, Willem Hovius en Roel Blankenstein die de zaak 'even' in elkaar gezet hebben; Benno Bannink van wie ik leerde hoe een cup-anemometer tegen de wind in kan draaien. In het bijzonder Sjaak Koster ('we zullen die hap zuurkool 's even wegwerken') voor het met veel geduld en precisie doormeten en afregelen van alle elektronica, en Rob van Krimpen voor het met even zoveel geduld en precisie ijken van de cup-anemometers. Die mooi uitgevoerde cupanemometers geleend van de LUW, bedankt Adrie Jacobs. De al ver voor mijn tijd ontwikkelde KNMI-psychrometers (goed dat er ter plaatse 220 aanwezig was om de Stefan ventilatoren draaiend te houden), bedankt S. Schoen en Wout Slob. De subtiele kneepjes van het turbulentie vak werden mij bijgebracht door Wim Kohsiek, Wim bedankt.

Jan Duyzer ('je kan de gradiënt zelfs ruiken') van TNO, bedankt voor de samenwerking. Ons perspectief wilde nog weleens verschillen gezien de foute marge die je in depositie metingen nu eenmaal hebt. Inmiddels had ik al een paar maal Willem Bouten mijn co-promotor van de UvA ontmoet, die het belang zag van het gelijktijdig meten door al die verschillende instituten en die mij dus wist te verleiden tot langdurige meetcampagnes. Willem, ik zeg niets te veel, zonder jouw enthousiasme en creativiteit was dit boekje er nooit gekomen. Het CORRELACI clubje, dus Willem Bouten (nogmaals), Peter Evers, Hans van Grinsven, Wilma Jans, Inge de Kort, M. van der Maas, E. van der Meulen, Frank Noppert, Ad Olsthoorn, Evelien Steingröver, W. Swart, Aaldrik Tiktak, Aart Vermetten (nogmaals) en Arie Versluis, bedankt.

Het informele flux-gradiënt clubje die voor mij een nieuwe impuls betekende

Contents

1   Introduction

1.1   Objective

Entering a forest is always a special experience for a meteorologist. Most notably are the low wind speeds and low radiation levels. Geiger (1961) shows that the actual micro-climate depends on the density of the forest. In general the air in the interior of the forest is cooler and more humid than aloft during daytime. This effect is more pronounced for a dense forest. Forests form one of the few canopies of which the interior can be entered and experienced without special instruments. Although the large size of trees compared to the human scale is not a principle difference, the influence of forest on atmospheric and hydrological processes differs substantially from low vegetation. Most notable forest characteristics are a low albedo, a large rainfall interception reservoir and high aerodynamic roughness (Jarvis et al., 1976).

  The physical interaction of a forest with the atmosphere can be described in terms of radiative and thermodynamic energy, momentum, water and matter exchange. The atmospheric control is given in terms of forcing variables and forcing surface fluxes. The forcing variables are temperature, specific humidity, wind speed and matter concentrations at a certain reference height above the forest surface. The forcing surface fluxes are short wave incoming radiation, long wave incoming radiation and precipitation. The dependent surface fluxes, i.e. the outgoing fluxes of short wave radiation and long wave radiation, the sensible heat and latent heat fluxes, the momentum flux, and the matter fluxes are a result of the atmospheric forcing. These dependent surface fluxes are modified by tree and soil processes. This thesis deals with the exchange of radiation, sensible heat, latent heat and momentum between a Douglas fir forest and the atmosphere. This includes the energy and water balances as well as turbulent transport. As such it offers a comprehensive insight into the micro-meteorology of a forest site near Garderen, the Netherlands. The major scientific question that we address in this thesis is:

-    What processes are relevant in controlling the dependent surface fluxes and how can this control be quantified?

To answer this question we will use well established concepts related to aerodynamic transport, the surface energy budget and the surface water budget. A detailed study of matter fluxes, apart from water vapour, is outside the scope of this thesis. However, parts of this thesis are relevant to the subject of matter exchange.

1

1.2   Motivation

A fair amount of micro-meteorological studies on forests has appeared in the literature during the past decades, see among others, Monteith (1976), Hutchinson and Hicks (1985) and Jarvis et al. (1989). From these studies very useful information can be extracted to predict forest exchange in relation to specific forest conditions. In the study of exchange processes between forests and the atmosphere, three main factors are of importance: tree species, soil type and climate. Although these three factors are partly correlated, still a large amount of different combinations are found on this planet. This means that each thorough study of a forest site adds valuable information to our knowledge on forest ecosystems. Much progress has been made in measurement techniques over the last decades. This results not only in more accurate measurements, but also in measurements on more appropriate scales, both temporal and spatial. Improved measurement techniques opens the way for more detailed forest studies than have been possible in the past. The current thesis is based on a continuous measuring program during the growing season of a Douglas fir forest. It incorporates measurements from micro-meteorology, hydrology and tree physiology. The study aims to contribute to research on the effects of air pollution, weather and climate, and remote sensing of the earth surface.

Effects of air pollution

Coordinated by the Dutch Priority Programme on Acidification (Heij and Schneider, 1991) the ACIFORN project (*Acidification research on Douglas fir Forest in the Netherlands*) aimed at assessing the impact of air pollution on tree vitality. The experimental part of the project was operational from 1986 to 1989 and culminated in a coordinated experimental effort in 1989 by a number of Dutch institutes at the Speulderbos research location, near the village of Garderen, the Netherlands. They are the Agricultural University of Wageningen (Air pollution department), the Research Institute for Forestry and Urban Ecology (Wageningen), University of Amsterdam (Environmental Sciences), State University of Leiden (State Herbarium), TNO (Delft), KEMA (Arnhem) and KNMI (De Bilt).

Air pollution components are deposited on the earth surface through rain (wet deposition), fog and cloud water (cloud deposition) and by gas/particle exchange (dry deposition) (Fowler et al, 1991). Here we concentrate on dry deposition. The measurement of dry deposition fluxes is time consuming and expensive. For modelling purposes, networks of long term monitoring stations are established at which concentrations of the various air pollution components are measured. To estimate the load of trace gases onto the earth surface, assumptions are made on the influence of the surface on the deposition process (Erisman, 1992). For reactive species as HNO_3 and HCL dry deposition rates are not controlled by the vegetation. For other species like SO_2 and NO_2 the uptake takes place primarily

2

through the stomata of the vegetation. For such species, the vegetation controls the dry deposition rates. NH_3 seems to be partially controlled by stomata. Wet canopies exhibit enhanced deposition rates of SO_2 and NH_3. To model the process of dry deposition appropriately, stomatal conditions have to be known as function of environmental conditions. Establishing model parameters that relate to dry deposition involves direct observations of dry deposition fluxes over various kinds of vegetation.

One way to estimate dry deposition rates on a forest is by measuring vertical fluxes of gasses in the turbulent air layer just above the forest. Direct flux measurements can be performed if a fast response sensor (< 1 s) of the constituent under consideration is available. For many trace gasses fast response sensors are not available or they are not suited for long term measurements in an outdoor environment. In such cases one has to rely on the measurement of vertical concentration differences. Well established flux-profile relations exist, which describe the translation from vertical concentration differences to vertical fluxes as function of weather conditions. However, these relations are only valid in the surface layer which is the atmospheric layer extending from a few times the vegetation height to typically 10% of the atmospheric boundary layer height. For high vegetations, like forests, the lower limit of the surface layer is often above practical heights for obtaining measurements. One is forced to perform measurements in the roughness sublayer, which is the atmospheric layer below the surface sublayer, extending downward to the top of the vegetation.

This thesis contributes to the research on effects of air-pollution in two ways. Firstly, by establishing relations between concentration differences gradients and deposition/emission fluxes for trace gasses close to the forest canopy. Secondly, by analysing the dynamics of water vapour exchange between the forest and the atmosphere for dry conditions. In this way relations are established between stomatal behaviour and environmental conditions. This knowledge can be used to infer dry-deposition rates of trace gasses like SO_2, NO_2 and O_3, of which uptake rates are at least partly controlled by stomatal opening.

Climate and weather research

The earth surface forms the lower boundary condition of the atmosphere. As such it strongly modulates the internal dynamics of the atmosphere. The distribution of land and sea and the location of mountain ridges are of importance for the large scale variations in weather and climate. But also land surface types and their variation over the globe have an important impact on global and regional climates. Predicted climates are sensitive to surface albedo, soil water availability, surface roughness and stomatal control (Shuttleworth, 1993). Feedbacks on the diurnal scale occur through the coupling between evapotranspiration on the one hand and boundary layer development and boundary layer cloud formation on the other hand (Cuenca et al., 1997). On the seasonal scale the coupling of soil water availability with atmospheric precipitation is of importance (Beljaars et al., 1996). At even longer

3

time scales, changes in vegetation cover are to be considered. For weather prediction in the short range (3 days) the impact of land surface cover is less important due to the process of continuous assimilation of observations. However, a correct representation of surface processes is still of great importance for the translation of large scale weather to the surface, where most of human activities takes place.

Over the years, Soil-Vegetation-Atmosphere-Transfer Schemes (SVATS) in global atmospheric models have become more complex in order to represent exchange processes more realistically on the various time scales involved (Dickinson, 1986; Sellers et al., 1986; Viterbo and Beljaars, 1995). Also soil hydrology is treated in some detail in modern SVATS to represent the hydrological feedbacks in those models. More complex soil/vegetation models are used in process studies. Some of these models put more emphasis on the canopy processes like radiation transport, turbulent transport and assimilation (Goudriaan, 1977). Others are more detailed in describing soil processes like water uptake by the roots (Tiktak and Bouten, 1992). The use of such models in global atmospheric models is impractical and even disadvantageous because of the numerous parameters that have to be known for each vegetation and soil type over the globe.

Long term observations of surface fluxes of precipitation, radiation, sensible and latent heat and momentum can contribute to the evaluation of SVATS. An example is the use of time series of the KNMI Cabauw grassland site for the Project for Intercomparison of Landsurface Parameterization Schemes (PILPS) (T.Chen et al., 1997; Beljaars and Bosveld, 1997) and for the ECMWF Re-Analysis (ERA) (Bosveld et al., 1998a). Other examples are HAPEX-Mobilhy (Jacquemin and Noilhan, 1990), FIFE (Betts et al, 1992) and BOREAS (Betts et al, 1998).

This thesis contributes to weather and climate research by describing quantitatively the interaction between a forest and the atmosphere in terms of radiation, heat and momentum fluxes as a function of environmental factors. Moreover, it provides a data set, with emphasis on both micro-meteorology and hydrology, which can be used for the evaluation of SVATS.

At KNMI the *Tropospheric Energy Balance Experiment* (TEBEX) aims at improving the representation of processes related to radiation, clouds, turbulent transport and surface exchange in weather and climate models. The experimental programme was operational during 1995-1996 and emphasised on long term monitoring of cloud parameters, boundary layer profiles and surface fluxes on the typical scale of a model grid box. The Speulderbos location was selected as one of the two surface flux stations, the other being Cabauw where KNMI operates a 200 m meteorological tower. By performing process studies on the basis of the 1989 observations of the Speulderbos site, this thesis contributes to the characterisation of one of the TEBEX land surface sites.

Remote sensing

With the advent of satellite based observation systems, global observations of the

4

earth surface become available. Characterisation of various parameters related to land surface type can be obtained on a global scale by using radiance observations. Although still hampered with various kind of problems, (atmospheric transmission, cloud detection, linking observed parameters to canopy parameters) satellite based observations seems to be the way forward to improve on describing the lower boundary condition of the atmosphere on a global scale. Ground based observations are essential to interpret these remote sensing data.

Surface temperature is a key variable in the description of the components of the surface energy balance. The temperature difference between the surface and the atmosphere is related to the division of the available energy into its components. Various methods are under consideration to estimate the evapotranspiration from observations of infrared radiation temperature (Van den Hurk et al., 1997; Anderson et al., 1997; Bastiaanssen, 1998). For a good interpretation of these observations, we need a thorough understanding of the various processes that contribute to the surface temperature.

This thesis contributes to the use and interpretation of remote sensing observations. We investigate the relation between the observed radiation surface temperature and the sensible heat flux of the forest within the context of existing theory. We also identify forest processes that may lead to significant deviations from theory.

1.3   Forest processes

To understand forest-atmosphere exchange processes in relation to environmental factors, we have to introduce some basic concepts from micro-meteorology and hydrology. These concepts are related to aerodynamic transport, surface energy budgets and surface water budgets, and will be used throughout this thesis to interpret forest observations.

Aerodynamic transport

To relate the atmospheric forcing variables like temperature, wind speed and humidity, to their corresponding surface values and fluxes, we have to quantify the aerodynamic transport properties in the air adjacent to the forest canopy. Close to the surface the air is, in general, in turbulent motion. The surface layer is the lowest part of the atmosphere where fluxes are nearly equal to their surface values (Tennekes, 1982). The top of the surface layer is typically 0.1 times the height of the atmospheric boundary layer. The reference height at which the forcing variables are measured is assumed to be below the top of the surface layer. The surface layer is limited from below by the assumption that its turbulent flow structure is not influenced by individual surface obstacles. Thus the lower limit must be several times above the typical surface obstacle height. In the surface layer the turbulent structure is determined by only three basic quantities, i.e. height, friction velocity

and buoyancy flux. The latter is primarily determined by the sensible heat flux. From the three basic quantities one dimensionless stability parameter can be formed. Surface layer similarity theory (Monin and Obukhov, 1954) states that quantities related to surface layer turbulence, and made dimensionless with the appropriate turbulent scales, are a function of only the stability parameter. From similarity it follows that stability effects become negligible when the buoyancy flux disappears, but also when approaching the surface.

Below the surface layer, the interaction of the flow with individual obstacles has increasing impact on the turbulent structure of the flow. This region is called the roughness sublayer. Although averaged over horizontal surfaces there still exist a constant flux layer, dimensionless relations valid for the surface layer will breakdown because the structure of the turbulence has changed. As a first approximation we may assume that this change can be described with one new length scale, related to the dimensions of the surface obstacles. Thus dimensionless quantities become a function of stability and the ratio of height and obstacle length scale. For low vegetation stability effects are very small at the heights of concern here. For high vegetation as forests this may not be the case. The roughness sublayer is limited from below by the canopy sublayer. This layer is defined by the presence of sinks and sources for momentum and other quantities and starts at the top of the vegetation.

The roughness layer of a forest extends to typically 2 times the tree height. From a measurement point of view it is therefore often impractical to place the reference height in the surface layer above the forest. Moreover at such height horizontal inhomogeneities in the upwind terrain may complicate the structure of the surface layer to such an extend that no simple flux gradient relations are found (Businger, 1986). The relation between fluxes and profiles of state variables can be expressed in terms of an aerodynamic resistance (r_a). Chapter 2 of this thesis deals with the aerodynamic resistance in the roughness sublayer of the forest.

All exchanged quantities are transported through the vegetation/atmosphere interface by molecular diffusion. Momentum can also be transported by the process of form drag, a process which has no equivalent for other quantities. Quantities that are transferred only by molecular diffusion are called scalar quantities. The difference in transport resistance of a scalar quantity compared to momentum is often expressed in terms of an excess resistance (r_b). This is the subject of chapter 3 and 4.

For mass exchange between the surface and the atmosphere a surface resistance (r_c) may exist which is related to the hinderance of transport from the interior of the canopy or soil to the interface between surface and air. For water transport this resistance is related to the opening of stomata which resides on the needles of the trees. Through the stomatal opening the tree can regulate its water loss. This is the subject of Chapter 5. For a fully wet surface this resistance is zero. Chapter 6 deals with the interaction of dry and wet parts in a partially wet canopy.

Surface energy budgets

6

The conservation of thermodynamic energy requires a balance between the radiation transformed at the earth surface and the heat transported from the surface. Short wave incoming radiation and long wave incoming radiation provide the energy input at the earth surface. Short wave radiation originating from the sun, arrives at the earth surface as direct and as diffuse radiation. Long wave radiation is emitted as thermal radiation by different layers of the atmosphere. It is strongly modified by the presence of clouds. Radiation loss is by reflected short wave radiation (described by the surface albedo) and by emission of long wave radiation (determined by the surface temperature and emissivity). Part of the radiation energy, the net radiation, is transformed at the surface into three components, sensible heat which heats the atmospheric air, latent heat which is associated with the evaporation of surface water, and storage heat flux which accounts for the heating of soil and biomass.

As an example, Figure 1.1 shows typical measurements of the components of the energy balance for both a grassland site (Cabauw, the Netherlands) and the current forest site (Garderen, the Netherlands) for the same clear day (21 May 1989). The figure shows that for the same short wave incoming radiation (SRD), higher net radiation (QN) occurs at the forest site. This is related to the difference in albedo, 0.11 for the forest and 0.23 for the grassland site. But also, daytime surface temperatures are much lower for the forest site, due to the high roughness of the forest, leading to a smaller upward long wave radiation as compared to the grassland site. Transpiration rates (LHF) are very different. The grassland site is on a well watered clay soil, whereas the forest site is on a sandy soil with ground water table at -40 m below the forest floor. At the grassland site transpiration is so high that reversal of atmospheric stability, indicated by a change of sign of the sensible heat flux (SHF), occurs 3 hours earlier than at the forest site. The diurnal variation of the storage heat flux (G) is much larger at the forest site due to the significant amount of standing biomass. Note that at the grassland site G is generally positive due to the prevailing increase in temperatures over the days for this period. The large difference in sensible heat flux between the sites suggests that atmospheric boundary layer height will be higher over forest than over low vegetation. This is confirmed by studies of Jacobs et al. (1991) and Holtslag and Ek (1996) for the HAPEX-Mobilhy experimental region.

Surface hydrological budget

The energy budget is coupled to the water budget through the latent heat flux. We start the description of the surface water budget with precipitation entering the canopy system. Part of the precipitation, depending on the canopy density, is intercepted in the canopy and evaporated back into the atmosphere without reaching the forest floor. Another part reaches the forest floor as throughfall and infiltrates into the soil. There it may evaporate or it may be uptaken by the root system to be released into the atmosphere by the process of transpiration. The remaining part drains to deeper layers of the soil beyond the root zone. This water eventually
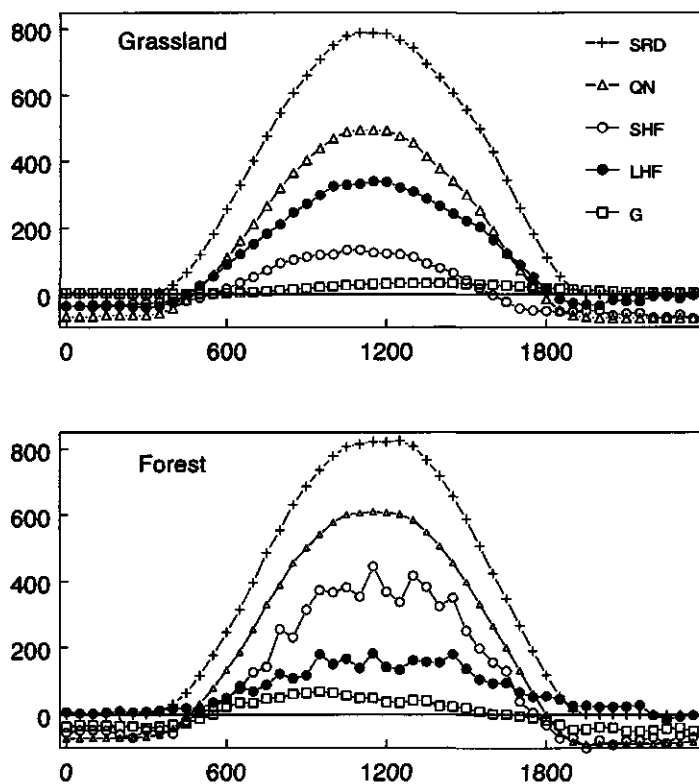
Figure 1.1. Comparison of radiation and heat fluxes for one day (21 May 1989) at a grassland site (Cabauw) and a forest site (Garderen).

enters the ground water and on the long run may be transported to the sea.

Building on the concept of transport resistances Monteith (1965) and Reitema (1965) derived the so-called combination equation for evapo-transpiration of a canopy. The derivation is based on energy conservation, the assumption that latent and sensible heat are transported evenly effective and on the assumption that inside the needles water vapour is saturated at the needle temperature. The last assumption results in the elimination of the surface temperature which is otherwise particularly difficult to specify. The advantage of the Penman-Monteith equation is that a clear distinction is made between the atmospheric control and the plant control of the transpiration.

1.4   Methods and measurements

In the preceding paragraphs we have outlined the research question, sketched the context of our research and described concepts which can be used as a framework to analyse measurements. We are now in a position to define the measuring strategy of our research.

Diagnosis of surface response

In this study we want to establish relations between the forcing variables and the surface response in terms of outgoing fluxes. Preferably these relations are diagnostic, which means that there is a one to one correspondence between the atmospheric forcing and the surface response. In practice however, there are buffers between the input and the output of the forest system.

Processes related to buffers in the forest system are: a) Atmospheric buffer of heat and momentum between reference height and surface, on time scales of minutes, b) water buffer capacity of the plant tissue on a time scale of hours, c) intercepted rain water which is a function of the balance of rates rain, evaporation and drainage, on the time scale of rain events, d) soil and biomass heat flux which is a function of temperature evolution, dominated by the diurnal cycle, and e) soil water content which is a function of the balance between various hydrological process on timescales of rain events to seasons. Shoot growth and tree activity are other important processes that have influence on the surface response. They are determined by the development of the weather, but also by the availability of nutrients and the development of diseases.

To keep to a diagnostic analysis, different solutions have been sought for the various processes described above. The atmospheric buffer can be quantified by using profile measurements of wind, temperature and humidity from the reference level to the surface. The plant tissue buffer is of importance in using tree stem sap flow observations as a measure for forest transpiration. Here the problem is solved by using only daily averaged values. Intercepted rain water and soil water are measured and both can be added to the list of forcing variables. Soil and biomass

heat flux is obtained from a separate prognostic model driven by appropriate temperature measurements and calibrated against residuals in the night time energy balance. With respect to plant physiology only the development related to bud-growth in the spring is taken into account by prescribing an observed variation of LAI over the seasons.

The forest site and instruments

The experimental site is located 2 km North of the village Garderen in the north-west part of the Veluwe, in the Netherlands. The geographical coordinates are $52^{o}15'$N, $5^{o}41'$E. The terrain is situated at 52 m above mean sea level. The site is situated in an extended forested area. The forest stand in which the research station is situated consists of 2.5 ha of Douglas-fir (*Pseudotsuga menziesii*) planted in 1962. In 1989 the tree height varied between 15 and 20 m, average height was 18 m. Tree density is 785 trees ha^{-1}. The average tree diameter at breast height (DBH) is 20 cm.

Bosveld et al. (1998b) describe the technical details of the instruments, performance, calibrations and the data set. Here we give a short summary. The micro meteorological measurements by KNMI were performed along a 36 m tall open structured guyed mast. Booms with instruments and maintaining platforms were positioned at 4, 18, 24, 30 and 36 m height. At each height wind, dry-bulb temperature and wet-bulb temperature were measured. Turbulence measurements were performed at the 30 m level.

Wind was measured with small cup anemometers produced at the Agricultural University of Wageningen. Calibration was performed in the KNMI wind tunnel. Dry bulb- and wet bulb temperatures were measured with ventilated and shielded psychrometers developed at KNMI. The temperature sensors consisted of Cu/Co thermocouple junctions, which enabled accurate measurement of vertical temperature differences. Absolute temperature was obtained by thermally connecting one thermocouple junction to a Pt-500 resistance. All temperature sensors were calibrated at KNMI.

Wind direction was measured at the top of the mast, with a wind-vane manufactured at KNMI. Short wave radiation was measured with a Kipp pyranom-eter at the top of the mast. Calibration was performed at KNMI. Net radiation was measured with a Funk-type net radiometer, produced by Middleton. The instrument was mounted on a separate boom at the 36-m level. Calibration for short wave radiation was performed at KNMI. Infrared radiation temperature of the crown layer was measured with a Heiman infrared thermometer. Calibration was performed at KNMI. The instrument was placed at the top of the mast and looks downward in the North direction. A rain grid sensor, manufactured by ECN, was placed at the top of the mast.

Fast response wind and temperature measurements were obtained from a sonical wind/thermometer-device manufactured by Kaijo-Denki (DAT300/TR61A). Static calibration of the wind and its angle response are performed by KNMI in the

10

wind tunnel of TNO-Apeldoorn. Static calibration of temperature is performed at KNMI. Humidity fluctuations were measured with a Ly-α hygrometer manufactured by Electromagnetic Research Corporation. Static calibration is performed at KNMI. The Ly-α hygrometer was operated at approximately 50 days. For the other instruments almost continuous time series were obtained from April to December 1989. Main problems arose a) in the sonic temperature during rain and b) with wet-bulb temperature vertical differences during very dry conditions. Measurements were performed at a rate of 1 Hz. Data were reduced on-line on a 10 minute basis and stored. Afterwards a quality control was performed by means of graphical presentations. Data were further reduced to half hourly and hourly values.

A number of observations used in this thesis were measured by other institutes. Rain amounts were measured by the University of Amsterdam at a clearing 3 km North of the research site. Sap flow measurements were measured by the KEMA (Noppert et al, 1990). Soil water content was measured by the University of Amsterdam (Tiktak and Bouten, 1990). Crown water storage amounts were measured by the University of Amsterdam (Bouten et al., 1990). Bio-geometrical measurements, among which leaf area index, were obtained by the Institute for Forestry and Urban Ecology (Jans et al, 1994) and State Herbarium Leiden (De Kort 1990). Root density was measured by the University of Wageningen (Olsthoorn and Tiktak, 1991).

Bosveld (1999) describes a number of important corrections on the measurements. These are corrections related to limitations of measuring techniques and corrections related to malfunctioning of instruments. An important role plays the structure parameter of the vertical wind. This quantity is a measure for the turbulence intensity in the inertial subrange. During the campaign it was measured with the sonic anemometer. The theory of structure parameters is treated and corrections are derived for limited instrumental response. The structure parameter is used to estimate cup-anemometer overspeeding. The overspeeding correction is tested in situ by comparing the 31-m level cup anemometer with the sonic anemometer readings. High frequency loss on eddy-covariances due to line averaging is estimated on the basis of work of Kristensen and Fitzjarrald (1984) who postulate an axi-symmetric three-dimensional spectrum for scalar fluxes. It is found that for the current measuring height high frequency spectral loss is negligible. Low frequency loss due to finite averaging times is estimated on the basis of spectra published by Kaimal et al. (1972). This loss is important and the magnitude of the loss has some uncertainty due to the uncertainties in the low frequency part of the co-spectrum. The sonic anemometer is calibrated in a large wind tunnel at all relevant angles of onflow. Especially transducer shadow effects are important. A method is developed to handle the complex calibration information in a consistent way. This method is tested in situ by comparing with the cup anemometer at the 31-m level. The sonic anemometer calibration results obtained in a laminar wind tunnel flow had to be related to the time averaged measurements obtained in an environment with high turbulence intensity. Mall functioning of the D/A converter of the sonic anemometer resulted in a small jump in the vertical

11

wind speed at the point of zero crossing. Corrections for the vertical turbulent fluxes and for the structure parameter of the vertical wind were derived. This involved the parameterisation of the frequency of zero-crossings of the vertical wind. A tilt in the net radiometer was found. Corrections were calculated on the basis of estimated direct short wave radiation. Direct short wave radiation was estimated from 10 minute averaged total short wave radiation.

1.5   Organisation of the thesis

Chapters 2 to 6 are integral copies of manuscripts that were published, accepted or submitted to relevant scientific journals. In each chapter the information on research site and instrumentation, relevant for that chapter is given. The thesis is organised according to the transport resistances outlined in section 1.3, i.e. aerodynamic, scalar excess and surface resistance.

Chapter 2 describes the aerodynamic resistance for momentum and sensible heat in the roughness sublayer (Bosveld, 1997). This chapter is closely related to dry deposition research. A procedure is developed for the derivation of deposition fluxes for trace gasses on the basis of gradient measurements.

Chapter 3 and 4 exploit the observations of crown layer infrared radiation temperature. Chapter 3 deals with the excess resistance for scalar quantities and the influence of the roughness layer for day time cases (Bosveld et al., 1999a). Chapter 4 analyses night time cases and shows that differences occur between surface radiation temperature and aerodynamic surface temperature. These cases are accompanied by downward movement of cold air from the crown to the interior of the forest. A simple two layer radiation/energy balance model is constructed to relate the difference between the two surface temperatures to atmospheric conditions (Bosveld et al., 1999b).

In chapter 5 we turn to the surface resistance for water vapor. On the basis of latent heat flux observations, the bulk canopy resistance in the Penman-Monteith equation is parameterised following a model of Jarvis. The main variables influencing transpiration are identified. A variation on the Jarvis formulation described recently by Monteith (Monteith, 1995) is investigated and the performance of the Priestley-Taylor equation is evaluated (Bosveld and Bouten, 1999a). Chapter 6 describes the interaction between evaporation and transpiration during wet episodes. Canopy water storage observations and sap flow observations are used to discriminate between evaporation of intercepted crown water and transpiration of water taken up by the root system. A generalisation of the Penman-Monteith equation is formulated to obtain a consistent description of both components (Bosveld and Bouten, 1999b).

Chapter 7 gives a summary, and the results are compared to other forest studies described in the literature.

A number of technical topics are treated as appendices to the chapters. In Appendix 2.A the structure parameter of the vertical wind is defined. Corrections

12

for spectral loss are discussed. It is shown that this structure parameter is a convenient measure for small scale turbulence intensity. Corrections for overspeeding of cup anemometers in terms of structure parameters are derived and applied. In the same appendix a problem in the D/A converter of the sonic anemometer is described. Corrections for fluxes and structure parameters are derived. In appendix 2.B the difference between cup anemometer wind speed and vectorial wind speed is treated. This is of importance because of the very high turbulence intensity in the roughness layer of the forest. Appendix 4.A treats a storage heat flux model driven by the forest interior air temperature. Appendix 6.A describes the calibration procedure of xylem sapflow measurements against eddy covariance measurements and soil water budget measurements.

2 Derivation of fluxes from profiles over a moderately homogeneous forest.[1]

Abstract

Measurements of fluxes and profiles of wind and temperature are performed in the roughness layer of a moderately homogeneous forest location. It is investigated to what extent vertical scalar fluxes can be derived from profile measurements. The influence of inhomogeneities in the upwind terrain is investigated with footprint analysis and with an inhomogeneous surface layer model. Four methods to estimate displacement height are suggested, among them is a method involving the structure parameter of the vertical wind. All methods give a decrease of displacement height with increasing wind speed, while roughness length is found to increase with increasing wind speed. For near neutral conditions dimensionless temperature gradients are found to be substantially lower than the surface layer values found in literature for homogeneous terrain with low vegetation. Dimensionless shear however is comparable with the surface layer value. The height of the roughness layer is 20 times the roughness length. Two schemes with locally derived surface parameters are tested to derive friction velocity and sensible heat flux from the profile measurements. These site specific schemes perform satisfactory. A third scheme based on a priori chosen surface parameters from the literature, performs significantly worse especially for low wind speed and unstable cases.

2.1 Introduction

In the context of air pollution research it is often desirable to determine scalar fluxes from gradient measurements. This is true for those components for which no fast response instruments are available, prohibiting the use of direct turbulent flux estimates by the method of eddy-correlation. As part of the project "ACIdification of FORest in the Netherlands", an interdisciplinary research programme on the influence of air pollution on tree vitality (Vermetten et al.,1986; Evers et al.,1987), gradients of several air pollution components were monitored over a Douglas fir forest at the Speulderbos location in the centre of the Netherlands. These measurements were used to derive flux estimates for ammonia (Duyzer et al., 1992), sulphur dioxide (Vermetten et al., 1992) and carbon dioxide (Vermetten et al., 1994). In these studies adapted surface layer flux profile relations were used to incorporate roughness layer effects based on local temperature profile measurements, wind measurements and eddy-correlation measurements of

---

momentum and heat fluxes (Bosveld, 1991). In the present paper a detailed analysis is presented of the behaviour of dimensionless temperature and shear as well as the surface parameters displacement height and roughness length. In addition to the relations derived by Bosveld (1991), three more flux profile schemes are developed with different degrees of complexity. It is investigated how well the relations between gradients and turbulent fluxes of heat and momentum are defined for such a location and how much detail is necessary to obtain reliable flux estimates.

In a number of forest studies e.g. Thom et al. (1975), Garratt (1978), Raupach (1979), Denmead and Bradley (1985), Högström et al. (1989) and Fazu and Schwerdtfeger (1989), it has been shown that close to forests the usual universal functions relating fluxes with gradients (Dyer, 1974) over low vegetation, do not apply. In this so-called roughness layer new length scales, apart from the height, come into play related to the particular geometry of the trees. In a more recent study Cellier and Brunet (1992) summarise a number of studies and conclude that for open forest both the exchange of heat and momentum are enhanced relative to the surface layer relations in approximately the same amount. For dense forests however the heat exchange remains enhanced whereas the exchange for momentum tends to the classical surface layer values. Raupach (1979) argues that, whereas the enhancement of exchange can probably be attributed to enhanced mixing due to wake turbulence generated at the tree tops, the suppression of exchange for momentum over dense forest should probably be attributed to a steep wind gradient developing close above the forest. This gives the vorticity field a tendency to a two dimensional structure. In two-dimensional turbulence it is vorticity and not momentum that is transported equally efficient as heat (Taylor, 1932).

Wind speed dependence of displacement height and roughness length over forests has been reported by Voght and Jaeger (1990) for a pine forest on the basis of profile measurements. For the Thetford forest, Molion and Moore (1986) also give some evidence for a wind speed dependence, but they are hesitant to draw firm conclusions because of possible instrumental problems especially at low wind speeds. Changes in roughness length and displacement height with wind speed arise because of streamlining of individual shoots with increasing wind speed, see Thom (1971) and Monteith (1973). The partitioning between form drag and viscous drag depend on needle/leaf Reynolds number (Monteith, 1973). This in turn may influence penetration depth. We can think of other factors such as a changing stratification in the trunk space of the forest, leading to a higher displacement height at low wind speeds when stratification is most likely to occur. Movement of trees may influence the turbulent structure in the roughness layer. Also the clustered movement of trees when localised gusts strike the crowns may result in a more open structure of a dense forest with a deeper penetration of momentum into the forest at higher wind speeds.

In section 2.2 a footprint analysis and an inhomogeneous surface layer model are used to assess the influence of limited fetch on the measurements. Section 2.3 describes the measurements and discusses corrections. Section 2.4 presents the theory of surface layer scaling. In section 2.5 evidence is given for a wind speed

dependent displacement height and roughness length. Section 2.6 presents an analysis of flux gradient measurements for wind and temperature. Section 2.7 presents a comparison of four flux profile schemes. Section 2.8 gives a discussion of the results and provides conclusions. Appendix 2.A gives some background on the structure parameter of the vertical wind and on the way these parameter is used to derive cup anemometer overspeeding corrections. Appendix 2.B treats the transformation from mean cup anemometer scalar wind to the length of the mean vector wind for high turbulence intensities. The latter is the more fundamental quantity that arises in the Reynolds formulation of the momentum conservation equation.

2.2   Research site and fetch

Research location

The research was carried out in a 2.5 ha Douglas fir plantation, located within a large forested area in the Netherlands. The stand has a tree density of 785 trees ha^{-1}. The firs were planted in 1962. In 1989, the year that the measurements were performed, the trees had reached a mean height of 18 m and a mean diameter at breast height of 0.21 m. The single sided leaf area index varies between 8 and 11 m^{2}m^{-2} throughout the year (Evers et al., 1991).

Topography and surrounding stands

The topography is slightly undulating with height variation of 10 to 20 m over distances of 1 km. Figure 2.1 shows the topography within a kilometre of the research location. The area is divided in stands with typical dimension of a few hectares. In the neighbourhood the dominant stand species are Douglas fir, Beech, Japanese Larch and Scotch Pine. A small clearing is situated just north of the mast. On a larger scale a large clearing is situated just 1 km to the south-east of the mast, and one at more than 2 km south-west of the mast. The edge of a large heather area is at a distance of 1.5 km to the east. In all other directions the forest extends for more than 3 km.

A field survey by eye from a measuring tower at 36 m above the forest floor yields the following classification of the upwind terrain up to a distance of approximately 200 m. In all sectors except the sector 30-125° the stands are somewhat more open in structure then the local stand. The sector -30 to 30° containes a small clearing at approximately 100 m distance. The sector 30-125° has approximately the same structure as the local stand. In the sector 150-210° the upwind terrain consists of stands with somewhat lower trees then in the local stand. Tree height variation is small. For the sector 240-300° the upwind terrain consists of stands with trees which are somewhat taller and with more variation in height than

N

40

df

jl

cl

45

sp

df

be

df

55

be

sp

50

hl

45

40

35

cl Clearing
df Douglas fir
jl Japanese Lark
be Beech
sp Scotch Pine
hl Hemlock

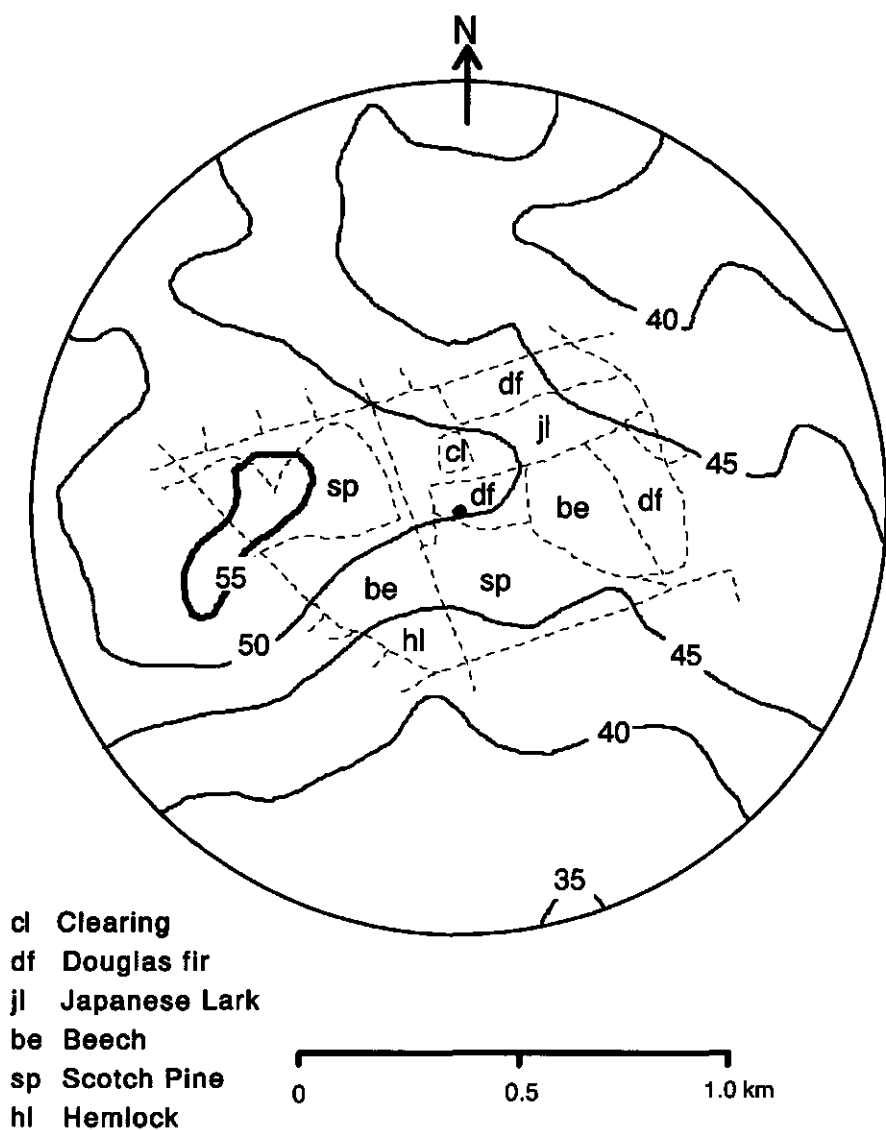| | | |
0   0.5   1.0 km

Figure 2.1. Topography and forest stands around the research location. Solid lines are height contours in meters above mean sea level. Dotted lines are stand borders. Black dot is position of mast.

18

the local stand. In the sector 330-360° tree height is the same as in the local stand.

The influence of limited fetch

To estimate the area for which the measured fluxes are representative footprint analysis is particularly useful. Estimates of footprints for different stability were made using the methods of Leclerc and Thurtell (1990) who use a Lagrangian approach and of Schmid (1994) who bases his footprint model on the surface layer dispersion model of Gryning et al. (1987). We had to extrapolate the results a bit outside their claimed range of validity to incorporate a roughness length of 2 m encountered over this forest. Results are derived for a roughness length of 2 m, a displacement height of 12 m and measuring height of 30 m. The source area in the method of Schmid (1994) is the area, with equal contributions at points of the boundary (an ellipse like shape), from which 50% of the flux at the sensor location comes from. The distance of the most upstream point is at 100 m for $L = -50$ m, at 200 m for $L = \infty$, at 300 m for $L = 200$ m and at 750 m for $L = 50$ m. Leclerc and Thurtell (1990) present their results integrated over lines perpendicular to the mean wind speed. For neutral conditions the line upstream of which 50% of the flux originates is at 75 m distance. Comparison of the two methods is not straight forward. We proceed with the observation that for the method of Schmid the 50% lateral line will be down wind of the point half way the most upwind point, thus at 100 m. It will be upwind of the point with maximum contribution, which is at 60 m for neutral conditions. We assume that the actual 50% line is approximately halfway, e.g. at 80 m. Both models thus give comparable results. It should be noted that both models are intended to be used in the surface layer and not in the roughness layer of a forest. As will be shown shortly the atmospheric mixing for heat is enhanced relative to the surface layer values at least for unstable and neutral conditions. This may imply that the source areas are somewhat closer to the measuring point than indicated by the present calculations. Nevertheless in all but the most unstable cases, footprint areas reach well over the boundaries with the neighbouring forest stands.

For flux estimates based on profiles, serious problems arise when surface roughness changes occur in the upwind terrain. Since turbulent flux and profiles have different adaptation timescales, an imbalance occurs in the relation between flux and gradient which results in a deviation of the dimensionless gradient from the usual surface layer relations. The influence of surface roughness transitions in the upwind terrain on dimensionless gradients was investigated using an E-ε model of the inhomogeneous surface layer (Bosveld and Beljaars, 1987; Beljaars et al., 1987; Beljaars, 1982). A roughness change of a factor of 2 at a distance of 500 m gives a deviation of 10% in the dimensionless gradients. The smooth to rough transition (roughness change a factor of 10) at 1.5 km to the east gives 5-15% (for z from 21 to 33 m) increase in dimensionless shear and dimensionless potential temperature gradient. Since in the roughness layer mixing is enhanced these deviations may be less, especially for heat transfer.

2.3   Instruments and corrections

Level	Temperature	Wind-cups	Sonic
4 m	3.71	4.16	
18 m	17.67	18.12	
24 m	23.67	24.12	
30 m	30.51	30.96	29.67
36 m	35.49	35.94	

Table 2.a. Height of the instruments above the foot of the mast in meters

A technical description of the measuring facility is given in Bosveld et al. (1998b). Here the main points are highlighted. Measurements are performed along a 36 m high mast with a triangular bases with sides of 1.2 m. The mast has an open structure. The effective diameter of the mast for potential flow is circa 0.3 m (Wessels, 1983). At four levels above and one level inside the forest cup-anemometers and thermometers are mounted on booms extending 3 m from the centre of the mast, all in a southerly direction. Fast response instruments are mounted on a separate boom of equal length at 30 m above the forest floor, also in a southerly direction. Table 2.a gives the measuring heights above the forest floor. Measurements with wind direction between -30 and 45° are excluded from most analyses due to mast interference.

Wind speed profiles are measured with three-conical-cup anemometers manufactured at the Agricultural University of Wageningen (the Netherlands). Output signal is derived from a photo-chopper system. The response length is 1.3 m and the threshold speed is circa 0.3 ms^{-1}. Calibration is performed in the wind tunnel at the Royal Netherlands Meteorological Institute, hereafter KNMI (Monna, 1983). The calibrations did show a slightly non-linear sensitivity, therefore second order polynomial calibration curves were used. Inspection of successive calibrations indicates that the error in the wind differences is of the order of 0.05 m s^{-1}. For wind speeds lower than 1 m s^{-1} the calibration curve is not reliable. These data are excluded from the analyses. Since only 10 minute averages and standard deviations of the wind speeds are retained, stalling of the cup-anemometers was not detected. The same criterion of wind speed smaller than 1 m s^{-1} is used to exclude periods with stalling. Overspeeding correction is made based on a method described by

20

Kristensen (1993) and adapted for the roughness layer involving measurements of the structure parameter of the vertical wind (see appendix 2.A). In appendix 2.B a method is described to transform from mean scalar wind to mean vector wind which gives good results for turbulence intensities (ratio of standard deviation of lateral wind component and cup anemometer windspeed) less than 0.6. Data with higher turbulence intensities are rejected. Unless stated otherwise, vector wind is used in the subsequent analysis.

Dry and wet bulb temperature differences are measured with copper-constantan thermocouples. The shielding is a modified version of the KNMI type sensor described by Slob (1978). Both ends of the thermocouple chain are thermally coupled in an aluminium block giving the opportunity to check for malfunctioning of the system. Calibration is performed at KNMI. Dependence of the thermocouple sensitivity on temperature is accounted for. Standard KNMI thermocouple amplifiers are used. Of main concern is the occurrence of offsets in the thermocouple system and amplifiers. The system was regularly checked by replacing the sensors by short circuits and assuring thermal equilibrium over the dummy sensors. Variations of 0.01 K occurred on time scales of a day but were not correlated with the diurnal change. To check performance during the measuring period neutral conditions were selected with high wind speed and approximately zero heat flux, derived from the eddy-correlation measurements. The three temperature differences each showed a constant offset in the range of 0.00 to 0.02 K for the whole measuring period of 9 month. This offset is subtracted from the measurements. Accuracy for the dry-bulb temperature differences is estimated at 0.02 K under dry conditions.

Wind speed fluctuations and sonic temperature fluctuations are measured with a Kaijo Denkij sonic anemometer DAT 310, probe TR-61A. The probe was mounted on a thin 1 m high stem to diminish flow obstruction. The stem was placed on an inclinometer which measured the tilt out of the horizontal plane in two directions. The wind components of the sonic anemometer are calibrated every two years (Kraan and Oost, 1989). The sonic temperature sensor is calibrated in a climate chamber at KNMI. No significant deviations were found in successive calibrations.

With a fixed averaging time the low frequency loss becomes wind speed dependent. Corrections are performed on the basis of surface layer co-spectra given by Kaimal et al. (1972). For friction velocity the correction is circa 0.02 m s^{-1} for unstable and neutral conditions, almost independent of wind speed. For heat flux the correction ranges from 8% at 2 ms^{-1} to 3% at 5 m s^{-1}. High frequency loss due to line averaging is negligible for the current measuring height.

Tilt as measured with the inclinometer was usually less than 1°. Flux measurements are transformed to the horizontal plane as indicated by the inclinometer. Momentum flux measurements are corrected for flow obstruction around the probe as shown in Duyzer and Bosveld (1988). A method was developed to correct for changes in horizontal wind speed sensitivity due to transducer shadowing and frame obstruction. The method is based on wind tunnel calibrations as described in Kraan and Oost (1989). This method is accurate for angles of

onflow within 40°. Measurements involving the horizontal wind speed fluctuations are rejected when the onflow is outside this angle.

Sonic temperature fluxes are corrected for moisture flux and horizontal wind speed influences as described by Schotanus et al. (1983). The moisture flux is derived from the Penman-Monteith equation with a model for the canopy resistance following Stewart (1988). Input variables to the model are net radiation, short wave incoming radiation, specific humidity, temperature and soil water. These quantities were monitored during the relevant period. Parameters for the bulk stomatal response on moisture deficit, short wave incoming radiation, soil water and leaf area index are optimised against 43 days of eddy correlation Lyman-α measurements performed throughout the present campaign. The residuals between the model latent heat flux and the observations show a standard deviation of 30 W m^{-2} for hourly values. This results in a standard deviation of the moisture correction in the sonic heat flux of 3 W m^{-2}.

Sonic temperature variances are corrected for wind effects as described by Schotanus et al. (1983). The buoyancy flux needed in the calculation of the Obukhov length scale is taken as the wind corrected sonic temperature flux (Kaimal and Goyner, 1991).

A problem in the D/A converter of the vertical wind speed introduced a reproducible jump of 0.14 m s^{-1} each time the sign of the vertical wind speed changed. Under the assumption of a joint Gaussian distribution of the fluctuations it can be shown that the fractional correction in the fluxes are proportional to the ratio of the jump and the standard deviation of the vertical wind. Corrections to the fluxes range from 5% for unstable conditions to 10% for stable conditions.

Structure parameters of the vertical wind were derived from the sonic anemometer measurements. Structure parameters are also corrected for the D/A converter problem mentioned above. Corrections for spectral loss where applied. Both correction procedures are outlined in Appendix 2.A.

A wind speed comparison was made of the 31 m cup anemometer with the sonic anemometer at 30 m height after all the corrections were performed. Cup anemometer wind was transformed to 30 m height with help of the 24 m level measurements. To avoid differences between vector wind and scalar wind both wind speeds are transformed to the square root of the average of the square of the instantaneous wind speed. In appendix 2.B it is shown that this can be calculated exactly if the standard deviations of the different wind components are known. For wind speeds above 2 m s^{-1} the differences found were less than 0.04 m s^{-1}.

Wind direction is measured with a standard KNMI vane at the top of the mast. A rain indicator is operated at the top of the mast.

Measurements were performed continuously from April to December 1989. The sonic anemometer was turned into the expected wind direction for the coming days every few days. Instruments were inspected and cleaned at least every week. Instruments were sampled at 1 Hz. Data reduction to averages, standard deviations and covariances were performed on-line. 10 minute values are screened. Finally hourly mean values were calculated. This procedure assures a detrending on a time

22

scale of 10 minutes.

2.4 Surface layer scaling

The profiles of wind speed and temperature measured in the roughness layer are analysed in terms of surface layer similarity. This is a convenient context to assess the influence of roughness layer effects on the measurements. In doing so we first have to define our reference surface layer profiles. In the surface layer Monin-Obukhov similarity applies. Quantities are made dimensionless with the length scale $z-d$, the height above the displacement height, friction velocity u_*, defined as $\sqrt{(-\tau_x/\rho)}$ where τ_x is the component of the surface stress vector along the mean horizontal wind vector and ρ is the density of air, and the turbulent temperature scale $\theta_* = -\langle wt \rangle / u_*$, where $\langle wt \rangle$ is the vertical turbulent temperature flux. The dimensionless quantities are functions of stability ζ only. Here $\zeta = (z-d)/L$, where $L = (T/kg)u_*^2/\theta_*$ is the Obukhov length, T is absolute temperature, g is earth gravitational acceleration and k the Von Karman constant ($k = 0.40$). We then define the dimensionless shear and the dimensionless potential temperature gradient by:

$$\frac{k(z-d)}{u_*}\frac{dU}{dz} = \phi_M(\zeta)$$
$$\frac{k(z-d)}{\theta_*}\frac{d\theta}{dz} = \phi_H(\zeta)$$

(2.1)

where U is wind speed and θ is potential temperature. From this the integrated flux profile relations are derived:

$$U(z_2)-U(z_1) = \frac{u_*}{k}\left(\ln(\frac{z_2-d}{z_1-d}) - \psi_M(\zeta_2) + \psi_M(\zeta_1) \right)$$
$$\theta(z_2)-\theta(z_1) = \frac{\theta_*}{k}\left(\ln(\frac{z_2-d}{z_1-d}) - \psi_H(\zeta_2) + \psi_H(\zeta_1) \right)$$

(2.2)

For the wind speed we can integrate to the level where wind speed is zero, assuming that the suurface layer extents down to the vegetation and obtain an expression which involves the roughness length z_0:

$$\frac{U(z)}{u_*} = \frac{1}{k}\cdot\left(\ln(\frac{z-d}{z_0}) - \psi_M(\zeta) \right)$$

(2.3)

For the unstable case we use the functions proposed by Dyer (1974):

23

$$\phi_M^2(\zeta)= \psi_H(\zeta)= x^{-2}, \; x = (1-16\zeta)^{1/4}$$
$$\psi_M(\zeta)= \ln((1+x^2)(1+x)^2/8)-2\;\arctan(x)+\pi/2 \tag{2.4}$$
$$\psi_H(\zeta)= 2\;\ln(1/2+x^2/2)$$

where the integration is from Paulson (1970). For the stable case we use the integrated form given by van Ulden and Holtslag (1985) based on Cabauw tower measurements and we derive the differential form from that:

$$\phi_M(\zeta)=\phi_H(\zeta) = 1+a\zeta+b\cdot((1+c)\zeta-f\zeta^2)e^{-f\zeta}$$
$$\psi_M(\zeta)=\psi_H(\zeta) = -a\zeta-b\cdot(\zeta-c/f)\cdot e^{-f\zeta}-bc/f \tag{2.5}$$

with $a = 0.7$, $b = 0.75$, $c = 5$ and $f = 0.35$. This form has the familiar neutral limit of $1+5\zeta$ but gives lower values for stabilities larger than 0.5, which is also consistent with findings of Carson and Richards (1978).

Surface layer scaling for the structure parameter of the vertical wind gives:

$$\frac{C_w^2\;(z-d)^{2/3}}{u_*^2} = f_C(\zeta) = \begin{matrix} 4.9([1-16\zeta]^{-1/4}-\zeta)^{2/3} & ;\zeta<0 \\ 4.9(1+4\zeta)^{2/3} & ;\zeta>0 \end{matrix} \tag{2.6}$$

For the definition and stability function of C_w^2 we refer to appendix 2.A.
Surface layer scaling of the standard deviation of temperature gives:

$$-\frac{\sigma_\theta}{\theta_*} = f_\theta(\zeta) = a\cdot(\zeta_0-\zeta)^{-1/3} \quad ;\zeta<0 \tag{2.7}$$

where ζ_0 is minus the stability from which free convection start to dominate. Rotach (1994) suggests $\zeta_0=0.020$ and $a = 0.95$.

2.5   Displacement height and roughness length

The displacement height (d) arises in the formulation of the logarithmic wind profile as a measure of the effect of the elevation of the vegetation on the wind profile. In the scale analysis for the neutral surface layer we can define the effective height $z_e = z - d$ as the scale height that makes the dimensionless shear independent of height. The scale length z_e can be derived from the friction velocity and shear by:

$$z_e=\frac{u_*}{k}\left(\frac{dU}{dz}\right)^{-1} \tag{2.8}$$

From this perspective the displacement height is related to the effective depth that eddies feel at certain height. For low vegetation the relation between the effective eddy depth and the geometrical depth remains clear since practical measuring heights are well within the surface layer and the displacement height is much smaller then the measuring height. For a forest this relation may break down because typical measuring heights are within the roughness layer and displacement

height is not much smaller than measuring height.

On the other hand d is related to the geometry of the vegetation. A rule of thumb is 0.7 times the vegetation height, but there is also a dependency on vegetation density (see for example Raupach, 1992). Thom (1971) found for an artificial rod like vegetation in a wind tunnel experiment that the displacement height corresponds with the effective height of impulse destruction. For more complex vegetation types no comparable measurements exists. Despite the thorough analysis of Jackson (1981) it remains to be shown that the displacement height in the logarithmic wind profile is necessarily equal to the effective height of impulse destruction in the canopy. Since there is no physical law that prescribes this relation it is more likely that the different ways of estimating a displacement height from vegetation geometry at best define a relevant length scale for this parameter.

From the perspective of an effective measuring height related to the eddy size several estimates of z_e can be given which are equivalent in the neutral surface layer but may deviate in the roughness layer. Estimates of effective measuring height can be obtained from

- the dimensionless shear through Equation (2.1),
- the dimensionless potential temperature through Equation (2.1),
- the product of dimensionless wind gradient and potential temperature gradient,

$$\frac{k^2 z_e^2}{<wt>} \frac{d\theta}{dz} \frac{dU}{dz} = \phi_M(\zeta) \cdot \phi_H(\zeta), \quad \phi_M(0)\phi_H(0)=1 \tag{2.9}$$

- the dimensionless structure parameter of the vertical wind through Equation (2.6), C_w-method,
- the dimensionless standard deviation of temperature through Equation (2.7), σ_T-method.

The third definition, Equation (2.9), is incorporated because it avoids the use of friction velocity which is particularly difficult to measure accurately. The fourth definition is included because it is independent of profile measurements. The fifth definition is based on Rotach (1994), who uses the surface layer scaling relation of the standard deviation of temperature, Equation (2.7), to estimate displacement heights over a very rough urban environment.

The first and fourth form are particularly well suited to be used for neutral conditions. The fifth form makes use of the convective limit behaviour of temperature variance, as such it gives effective measuring heights representative for a convective roughness layer. One has to keep in mind that roughness layer effects and the presence of inhomogeneities may lead to deviations of the dimensionless quantities for neutral conditions from the surface layer values.

Wind speed dependence of displacement height
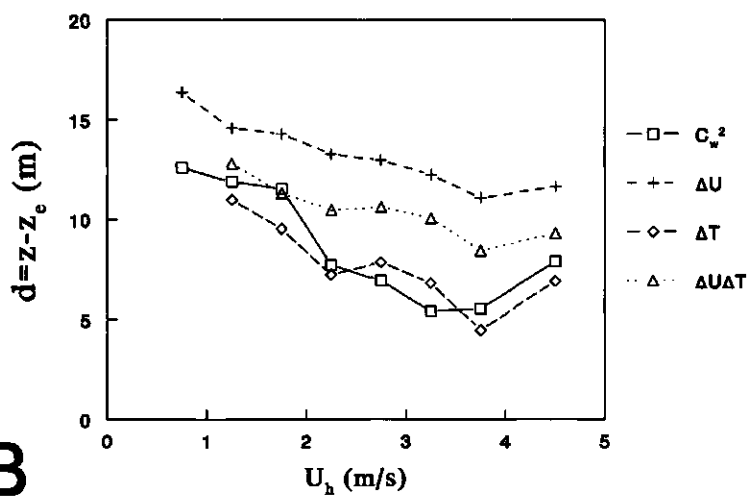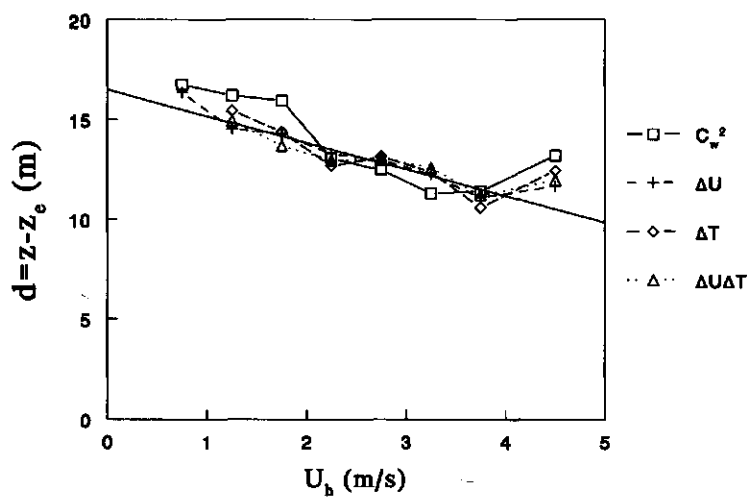
Figure 2.2. Displacement heights as function of wind speed classes for four methods. A) derived with neutral surface layer dimensionless values, B) derived with adapted dimensionless values.

In a preliminary analysis it was found that for neutral conditions dimensionless gradients were different for high and for low wind speeds. Detecting such an effect can be seriously hampered by instrumental problems. Especially for cup anemometers subtle changes in their performance with changing windspeed may occur. By using a number of more or less independent methods we hope to exclude this problems. To be sure that no stability effects interfere with the search for wind speed dependence only near neutral cases are used. This excludes the temperature variance method from the analysis. Data are used from the wind sector 45-125°. Here and in following sections special analysis are performed on data from the sector 45-125° since this sector has the most homogeneous fetch within a distance of 500 m. It is assumed that changes in displacement height are related to the interaction of the tree tops with the atmospheric flow. As the characteristic wind we choose the wind speed at $z = 18$ m (U_h) which is just above the top of the vegetation. This is the only occasion that cup anemometer windspeeds below 1 m s^{-1} are retained, since accuracy for this wind speed is less critical than it is in profile analysis. Moreover scalar wind is used here to avoid to many rejected data in the proces of transforming to vector wind. In Figure 2.2a estimates of the displacement height according to the first four definitions are displayed. The turbulence measurements are taken at 30 metre height, the profile differences are taken between 36 and 24 m height above the forest floor. Near neutral cases are selected $(L < -100$ m) and extrapolated to neutral with the surface layer relations of Equation (2.2). Data are grouped into classes of wind speed U_h. The Equations (2.1) and (2.6) are rewritten with the denumerator of the l.h.s. moved to the r.h.s..For each wind speed class a linear fit with fixed zero offset is performed to arrive at an estimate of the effective measuring height. A typical standard deviation in the class averaged displacement heights is 0.5 m. It is observed that all definitions give different values for the displacement height. However, all definitions show a decreasing displacement height with increasing wind speed. The different absolute values arise because of roughness layer effects and probably also from inhomogeneities in the upwind terrain. In Figure 2.2b the neutral values of the dimensionless quantities are adapted such that estimated displacement heights coincides best with each other. As a reference is taken the shear derived displacement heights. At a relatively high wind speed of $U_h = 3$ m s^{-1} the displacement height of this method corresponds with the independent estimate 0.7 times the vegetation height. For the temperature definition we had to choose $\phi_H(0) = 0.75$. For the structure parameter we had to choose $\phi_C(0) = 4.0$ a value substantially lower than the surface layer value of 4.9. We describe the wind speed dependence of the displacement height with:

$$d(U_h) = d^{ref} - 1.33 \cdot (U_h - 3) \ (m) \tag{2.10}$$

where U_h is in m s^{-1}. d^{ref} is the displacement height at $U_h = 3$ m s^{-1}. For the wind direction sector 45-125° we assume $d^{ref} = 12.5$ m.

Stratification inside the forest

27

Often the air inside the forest is cooler than above the forest. Especially during low wind conditions before noon the biomass thermal inertia prevents the forest air from warming. During such periods the small turbulent kinetic energy of the flow above the forest compared to the potential energy of stratification limits the penetration of eddies into the forest. We define a bulk Richardson number by

$$Ri_{veg} = \frac{g}{T} \cdot \frac{\theta_h - \theta_i}{U_h^2} \tag{2.11}$$
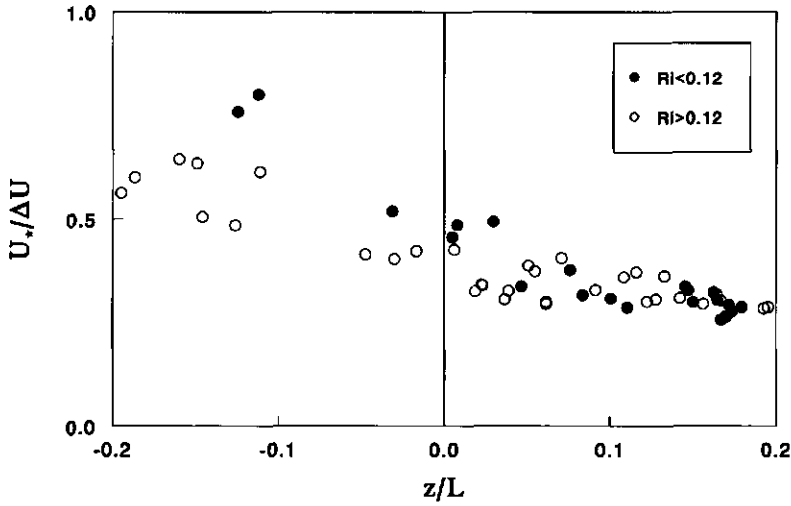
Figure 2.3. Ratio of friction velocity and wind difference between 36 and 24 m as a function of stability. U_h is between 1.0 and 1.4 m/s. Data are classified according to vegetation Richardson number.

where θ_h and θ_i are the potential temperatures at the top of the forest and in the interior respectively. For flows with stable stratification buyoncy destruction of turbulence starts to dominate over shear production when $Ri > 0.2$. The current measurements show that Ri_{veg} is often larger than 0.2. Thus we expect for these cases that eddy penetration is limited and that displacement height is increased. Discriminating a Richardson number effect on displacement height from a wind speed effect is difficult since the Richardson number itself depends on wind speed. In fact one has to show that in a given small class of wind speeds there remains a dependence on Richardson number. Here we analyse dimensionless wind differences between 36 and 24 m, which is sensitive to changes in displacement height. Ri_{veg} is derived from temperature measurements at 18 and 4 m above the forest floor and

28

wind speed at 18 m. Figure 2.3 shows for U_h between 1 and 1.4 m s^{-1} the inverse dimensionless wind difference between 36 and 24 m as a function of stability. Data are classified into small and large Richardson numbers. Wind direction is between 45 and 125°. For the stable cases no difference is observed. Around neutral and for unstable cases data with stable interior stratification seem to be lower than data with less stratification. At higher wind speed no cases with $Ri_{veg} > 0.12$ are found. This limited number of data suggests that there is some influence of forest interior stratification, but this occurs only for the lowest wind speeds. It is not enough to account for the total observed wind speed dependency of the displacement height.

Displacement height as function of wind direction

Due to inhomogeneities in the upwind terrain we may encounter roughness layers with different height and structure for different wind directions. It seems therefor unwise to use dimensionless gradients methods, which are particularly sensitive to inhomogeneities, to investigate the wind direction dependence of effective measuring heights. Here we use the σ_T-method and the C_w-method.

Figure 2.4 shows for wind direction classes of 30° the standard deviation of

Figure 2.4. Standard deviation of temperature (σ_T) and structure parameter of vertical wind (C_w) scaled on corresponding surface layer values with d=12.5 m as function of wind direction.

temperature and the square root of the structure parameter of the vertical wind both relative to their expected surface layer values with a displacement height of 0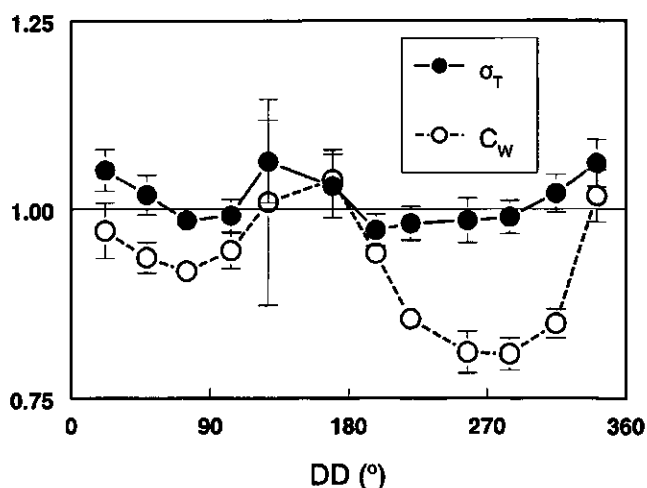.7 times vegetation height (= 12.5 m). Here we use wind corrected sonic temperature fluctuations. For the structure parameter near neutral cases ($L < -100$ m) are selected and corrected for small stability effects with Equation (2.6). To avoid interference with the wind speed dependence of displacement height only data with $U_h > 3$ m s^{-1} are retained. For the temperature data unstable cases are selected which are close to the convective limit. Equation (2.7) is used to correct for the small deviations from true convective behaviour. Both quantities have the same dependency on the effective measuring height, i.e. $z_e^{-1/3}$. Thus, a large value in the figure means a large displacement height. For each class a similar linear regression procedure is used as in the preceeding section on wind speed depency. Standard errors in the mean are displayed aswell. It is observed that the temperature variance method gives values close to 1, which corresponds to d-values close to 12.5 m. The C_w-method gives lower values. The two methods show the same trend as a function of wind direction. However, the range of variation of the C_w-method is much larger especially for the rough sector 240-300°. In appendix 2.A it is shown that turbulent dissipation ε and C_w^2 are closely connected. Using the E-ε model to estimate the influence of roughness changes on ε and thus on C_w^2 we found that typical roughness changes could explain only 25% of this variation. Deviations may arise since the balance between between production, dissipation and turbulent transport of kinetic energy in the roughness layer differ from this balance in the surface layer (Raupach, 1981). The σ_T-method shows a very robust behaviour. Under convective conditions footprints are small, this may explain the small and hardly significant variation with winddirection. In the following we shall use $d^{ref} = 12.5$ m as defined in Equation (2.10) for all winddirections.

Wind speed dependence of roughness length.

A changing displacement height with wind speed will have implications for the roughness length. It seems reasonable to assume that with a deeper penetration of eddies into the forest, caused by less thermal stratification inside the forest or by the more open structure at higher wind speeds will lead to an increase of momentum destruction rate. However this argument is probably not valid if deeper penetration is induced by a reduction of viscous drag on the needles at higher wind speed. In such conditions momentum destruction decreases at the top levels which is then the very reason why eddies penetrate deeper. In Figure 2.6 sonic anemometer wind speeds at 30 m and wind speeds derived from cup anemometer observations (interpolated to 30 m) are shown as a function of friction velocity for near neutral cases ($L < -200$ m) and wind direction between 45 and 125°. Wind speeds are corrected for the small stability effects. Drawn are a linear regression line with zero offset (solid) and with free offset (dashed). A linear relation through the origin doesn't adequately describe the data. The free offset regression gives for the offset 0.49±0.07 ms^{-1}. This suggests that dimensionless wind is wind speed dependent.

30
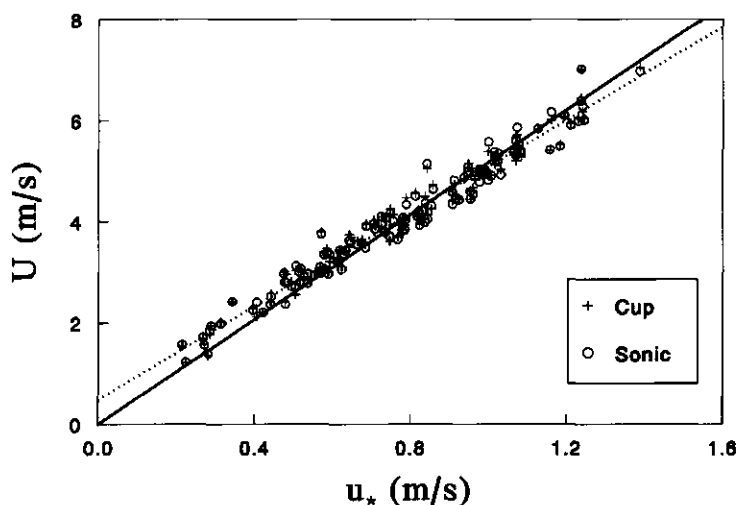
Figure 2.5. Wind speed as function of friction velocity for cup anemometer and sonic anemometer. Near neutral data. Data are corrected for stability. Linear regression curves: (solid) zero offset, (dashed) free offset .

The wind speed of both systems show the same trend suggesting that cup anemometer stalling and uncertainties in the calibration at low wind speeds doesn't play a role. In Figure 2.6 the roughness length is calculated from sonic anemometer wind observations with Equation (2.3). The open circles are calculated with displacement height taken constant at 12.5 m, the filled circles are calculated with displacement height taken wind speed dependent following Equation (2.10). It is observed that roughness length varies over a larger range when wind speed dependent displacement height is used. The wind speed dependency of the roughness length is parameterised by:

$$z_0(U_h) = z_0^{ref} + 0.4 \cdot (U_h - 3) \ (m) \tag{2.12}$$

where U_h is in m s^{-1}. z_0^{ref} is the roughness length at $U_h = 3$ m s^{-1}. For the winddirection sector 45-125° we have $z_0^{ref} = 2.2$ m.

Dimensionless wind as function of stability

For completeness dimensionless wind at 36 m is analysed for wind direction between 45 and 125°. Data are selected with $U_{36} > 2$ m s^{-1}. By rewriting Equation (2.3) the stability function can be retrieved. The displacement height is calculated

31
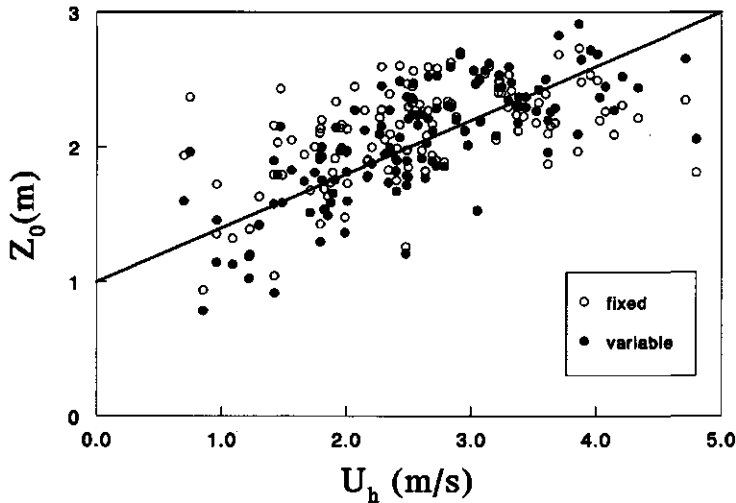
Figure 2.6. Roughness length derived from near neutral cases with fixed displacement height and with wind speed dependent displacement height.

from Equation (2.10). Roughness length is calculated from Equation (2.12). Figure 2.7 shows the measured stability function. Near neutral values are displayed enlarged in the figure. The solid line represents the surface layer function Equations (2.4) and (2.5). The data follow the surface layer curve quite well.

Roughness length as function of wind direction

To investigate roughness as a function of wind direction the neutral values of the dimensionless wind for different wind directions are determined. Data are selected with $U_{36} > 3.5$ m s^{-1}. Near neutral data are chosen ($|L| > 200$ m) and a stability correction is performed from Equation (2.3) to extrapolate to the neutral value. Figure 2.8 shows these stability corrected values as a function of wind direction. A definite variation is observed with a very sharp increase in roughness from 180 to 240°. This corresponds with what is observed by eye (see description in section 2.2). Table 2.b gives the corresponding roughness length for wind direction steps of 30°. Linear interpolation then gives the roughness length for arbitrary wind directions. A consequence of the variation of roughness length is that profiles will not be in equilibrium with the local fluxes for some wind directions.
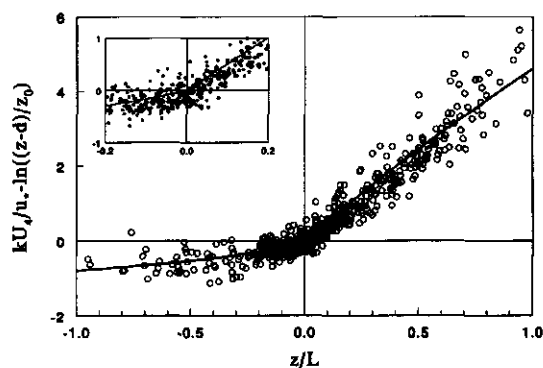
Figure 2.7. Dimensionless wind speed as function of stability for wind direction within 45-125°.

DD (°)	z_o (m)	DD-class (°)	z_o (m)	DD-class (°)	z_o (m)
0	[1.7]	120	1.9	240	3.5
30	1.9	150	1.3	270	3.6
60	2.2	180	1.4	300	3.5
90	2.1	210	2.2	330	2.6

Table 2.b. Roughness length as function of wind direction based on U(z=36 m) and d=12.5 m for high wind speeds (U_h=3 m/s). Values between brackets are influenced by mast interference.

2.6 The relation between fluxes and gradients of wind and temperature

Here we deal with the behaviour of dimensionless quantities as a function of stability and, for neutral cases, as a function of wind direction.

Dimensionless shear

In the surface layer dimensionless shear is a function of stability only. Here we investigate the behaviour of the dimensionless shear in the roughness layer of the forest. Dimensionless gradients are estimated from the cup anemometer

33
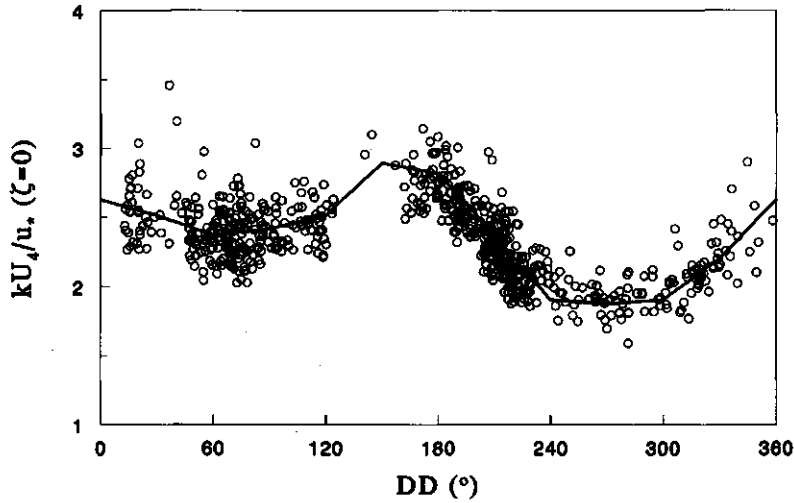
Figure 2.8. Dimensionless wind for neutral conditions as a function of wind direction.

measurements for the three height intervals in the profile. To convert from differences to gradients we use the logarithmic approximation (Arya, 1991):

$$\phi_m = \frac{k\, z_e}{u_*} \frac{dU}{dz} \approx \frac{k}{u_*} \cdot \frac{U_2 - U_1}{\ln(z_2 - d) - \ln(z_1 - d)}$$

$$z_e = \sqrt{(z_2 - d)\cdot(z_1 - d)}$$

(2.13)

where z_e is the effective height for which the gradient is estimated and d is derived from Equation (2.10). Figure 2.9 a-c shows, for wind direction between 45 and 125°, the dimensionless shear as a function of stability for the three differences in the profile. In all cases data are selected with wind speed at the lowest level of the interval greater than 2 m s^{-1}. For the highest two intervals near neutral values are displayed enlarged in the figure. The solid lines are the surface layer functions. It is observed that at all levels dimensionless shear is larger than the surface layer values. Few data points are retained for the lowest interval due to the prevailing low wind speeds and high turbulent intensity, which makes transformation from scalar wind to vector wind impossible.

Figure 2.10 a-c shows the dimensionless shear between the successive levels for near neutral conditions ($|L| > 200$ m) as a function of wind direction. Data are corrected for stability. In all cases data are selected with wind speed at the lowest

34

Figure 2.9. Dimensionless shear as function of stability for the three profile intervals. A) 36-31 m, B) 31-24 m and C) 24-18 m.
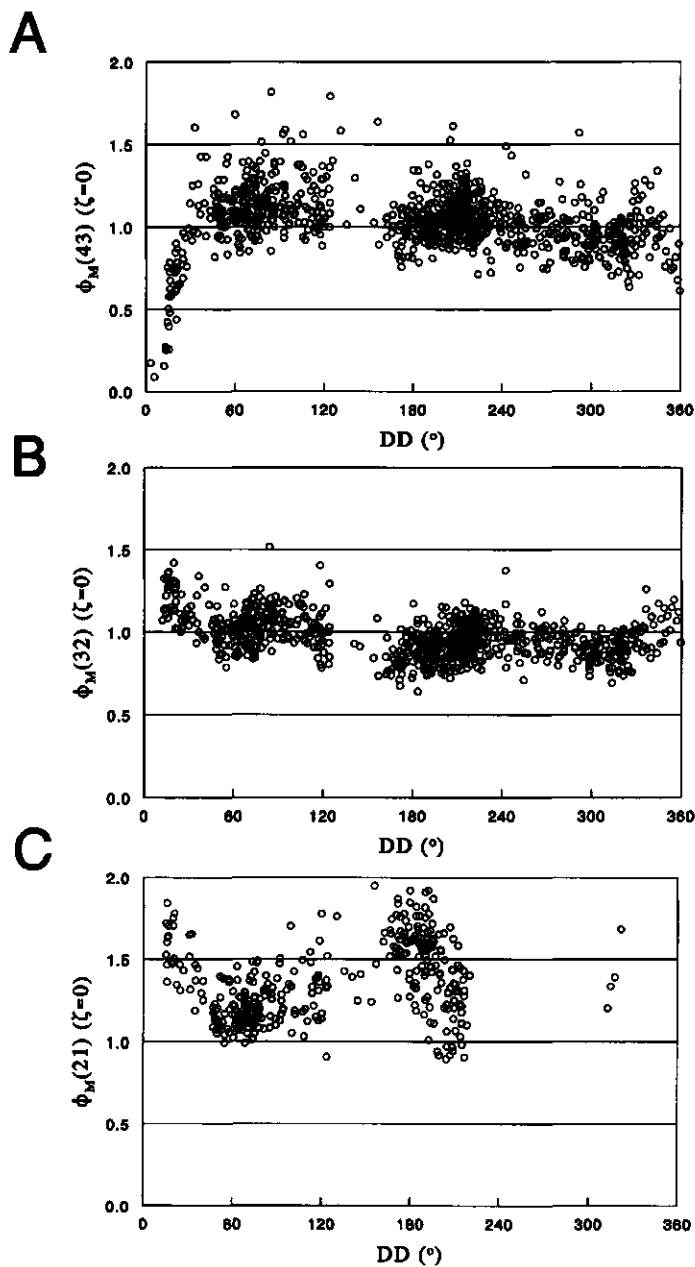
Figure 2.10. Dimensionless shear for neutral conditions as function of wind direction for A) 36-31 m B) 31-24 m and C) 24-18 m.

level of the interval greater than 2 m s^{-1}. Here again few data points for the lowest interval are retained. This is especially the case for the roughest wind direction between 240 and 300°. Moreover the lowest level is obstructed by a tall tree at the south introducing a high shear which is not representative for the upstream terrain. It is observed that for wind directions between -30 to 45° mast obstruction influences the measurements. For the two highest intervals the values scatter around the homogeneous surface layer value of 1 but a trend to lower values with wind direction going from south over west to north is observed.

Dimensionless potential temperature gradient in the roughness layer

Dimensionless potential temperature gradient is defined by Equation (2.1). To examine stability dependence of ϕ_H, data are selected with wind direction between 45 and 125°. For too small temperature fluxes data becomes very scattered and biases in the temperature system start to dominate. Data with $|<w\theta>|/u_* < 0.05$ K are excluded.

Figure 2.11 shows for the three height intervals the dimensionless potential temperature gradient as a function of stability. Solid lines represent the surface layer relations. Especially for near neutral and unstable cases values are lower than the surface layer relation. This is more pronounced for the lower levels in the profile.

Determination of the neutral crossing value is less straightforward than in the wind shear case since values close to neutral are very scattered. Unstable data with $L < -100$ m where selected and corrected for stability by dividing by the surface layer relations. Using stable data significantly increased the scatter. These data are excluded. Figure 2.12a-c shows the dimensionless potential temperature gradient stability corrected for the successive levels 4-3, 3-2 and 2-1 as a function of wind direction. Values are significantly lower than 1, but the same trend of decreasing values with veering wind is observed as was found in the shear case. Only at the lowest interval around wind direction of 180° significant variation occurs induced by a nearby tall tree.

2.7 Derivation of fluxes from profiles

To arrive at a practical scheme for profile derived fluxes we have to incorporate the observed roughness layer effects in the description of the dimensionless shear and temperature gradients. Let α_M and α_H be the neutral crossing values of dimensionless shear and potential temperature gradient respectively. On the basis of the Figures 2.9 and 2.11 the following adapted functions are proposed:

$$\phi^R(\zeta) = \alpha - 1 + \phi^S(\zeta) \quad , \zeta > 0$$
$$\phi^R(\zeta) = \alpha \phi^S(\zeta) \quad \quad , \zeta < 0 \tag{2.14}$$

where ϕ^S is the surface layer dimensionless gradient and ϕ^R is the adapted roughness layer form. For the stable side a constant shift is prescribed and for the

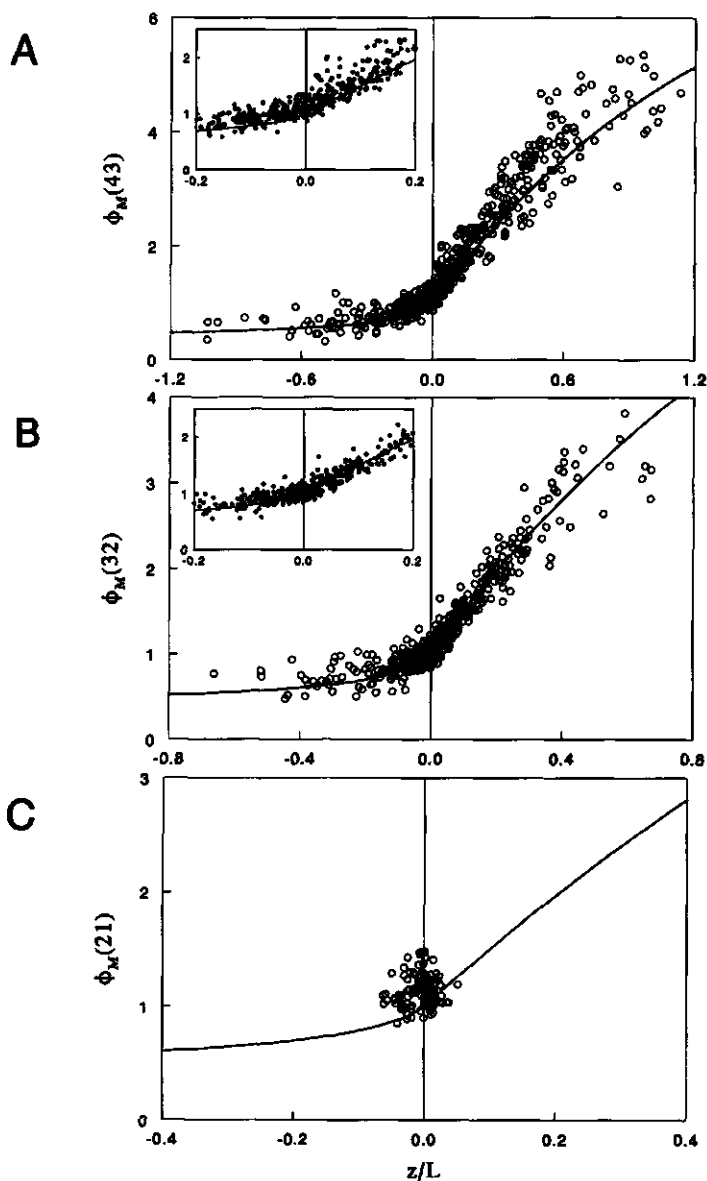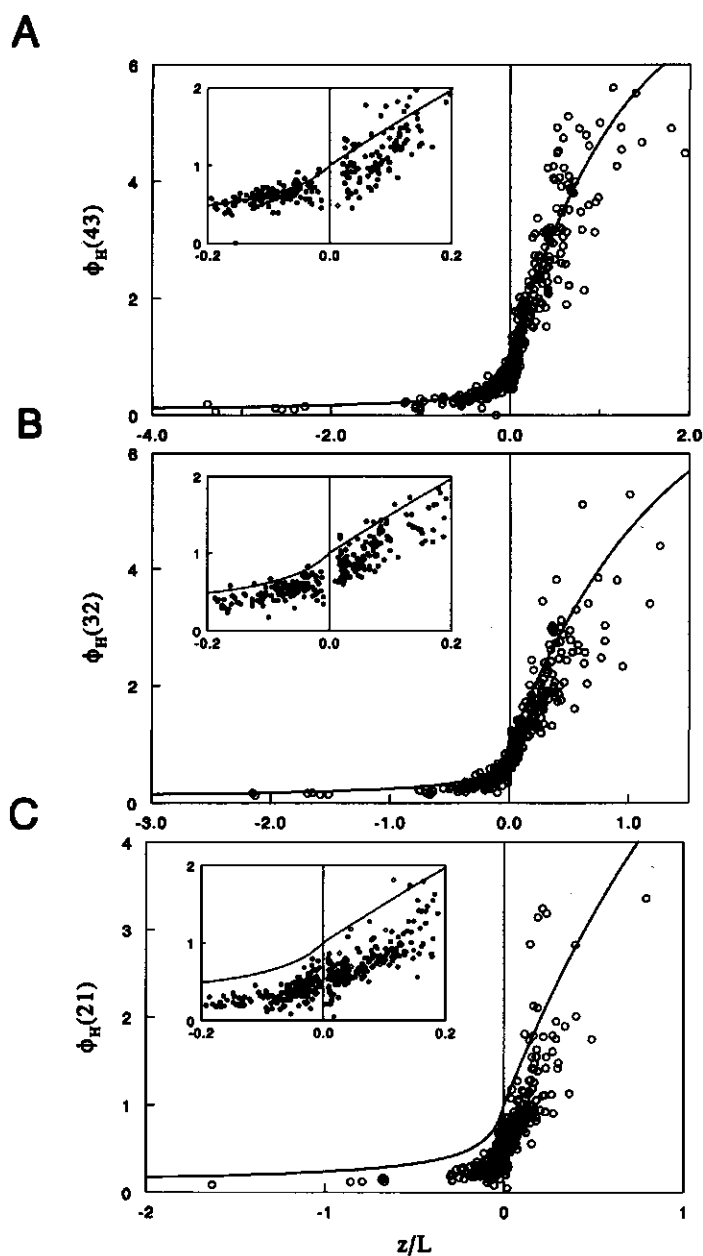*Figure 2.11*. Dimensionless potential temperature gradient as function of stability for the three profile intervals. A) 36-31 m, B) 31-24 m and C) 24-18 m.
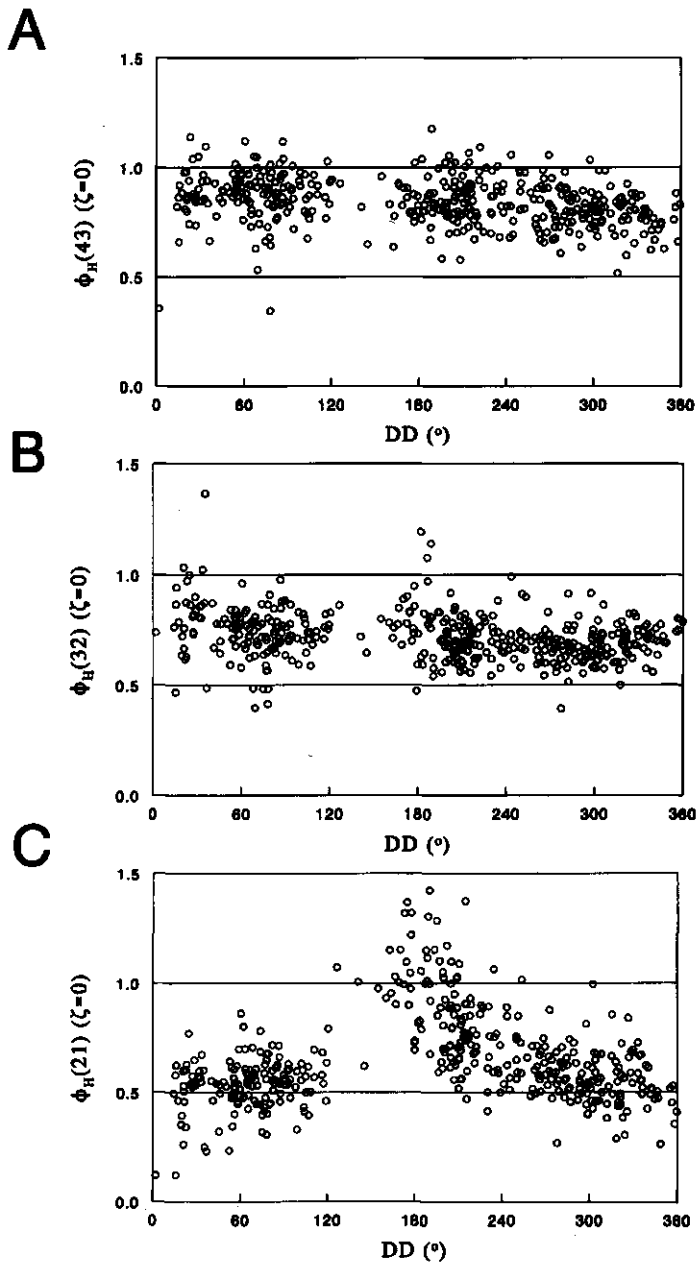
Figure 2.12. Dimensionless temperature gradient as function of wind direction for A) 36-31 m B) 31-24 m and C) 24-18 m.

Height interval	Effective height	α_M	α_H
36-30 m	20.3 m	1.10±0.10	0.90±0.10
30-24 m	14.2 m	1.05±0.05	0.75±0.10
24-18 m	8.0 m	1.15±0.10	0.60±0.10

Table 2.c. Neutral crossing values α_M and α_H for the three height intervals and wind direction between 45 and 125°. Effective height above the displacement height (d=12.5 m) is given.

unstable side a fraction of the surface layer value is prescribed. Different α values are allowed for momentum and heat. Also α may vary with height. From the Figures 2.10 and 2.12 it is observed that especially the α_H values are height dependent. Here we assume that the α values are not dependent on stability. Table 2.c gives α values derived from the Figures 2.10 and 2.12 for the three intervals in the profile measurements for the wind directions between 45 and 125°. Standard deviations of the hourly values around the mean are given.

For the derivation of fluxes from profiles in the surface layer two approaches can be found in the literature. In both approaches a vertical temperature difference is used to assess stability and heat flux. The two methods differ in the way wind measurements are incorporated. One way is to use wind difference measurements, this method does not need information on the roughness length. A second approach uses wind speed at one level together with a roughness length which if necessary can be taken wind direction dependent as in our case. Four schemes are evaluated:

DD (°)	z_o (m)	DD-class (°)	z_o (m)	DD-class (°)	z_o (m)
0-30	[1.75]	120-150	1.58	240-270	2.88
30-60	2.03	150-180	1.50	270-300	3.18
60-90	2.09	180-210	1.83	300-330	2.48
90-120	1.93	210-240	2.38	330-360	[1.87]

Table 2.d. Roughness length as function of wind direction for the scheme S0. Value between brackets are influenced by mast interference.

S0   The original scheme proposed by Bosveld (1991). One wind level (z = 36 m)

40

with wind direction dependent roughness length (no wind speed dependence) given for 30° wind direction classes in Table 2.d. A fixed displacement height ($d = 12.5$ m) and temperature difference ($z = 36\text{-}24$ m, $\alpha_H = 0.88$). Wind speed is scalar wind here and uncorrected for overspeeding.

S1   One wind level ($z = 36$ m) and a fixed roughness length (no wind speed and no winddirection dependence) ($z_0 = 2$ m), temperature difference ($z = 36\text{-}24$ m, $\alpha_H = 0.80$) and a fixed displacement height ($d = 12.5$ m).

S2   One wind level ($z = 36$ m) with wind speed and wind direction dependent roughness length, temperature difference ($z = 36\text{-}24$ m, $\alpha_H = 0.80$) and wind speed dependent displacement height. Roughness length is calculated from Table 2.b by interpolation.

S3   Wind difference in profile ($z = 36\text{-}24$ m, $\alpha_M = 1.05$), no roughness length, temperature difference ($z = 36\text{-}24$ m, $\alpha_H = 0.80$) and wind speed dependent displacement height.

Wind speed dependent roughness length is calculated from Equation (2.12) by substituting values derived from Table 2.b for z_0^{ref}. Wind speed dependent displacement height is derived from Equation (2.10). Equation (2.14) can be integrated to arrive at analogous equations as the surface layer Equation (2.2). A complication occurs because the α's are height dependent. This is resolved by using a constant effective α representative for the height interval of integration. For the relation between 36 m wind and friction velocity the usual surface layer relation is used ($\alpha_M = 1$) assuming that this level is close to the top of the roughness layer as suggested by the trend in α_H values with height listed in Table 2.c. Note that the integration constant z_0 incorporates both surface roughness and deviations of the profile in the roughness layer. Hourly fluxes are derived by solving the equations iteratively.

SO uses as input scalar wind speeds and was derived before the w-jump correction and the low frequency corrections on the flux data were performed, as described in section 2.3. S2 and S3 are based on site derived parameters, whereas S1 is based on typical values of roughness length and displacement height found in the literature for a closed forest, except perhaps the value for α_H, and can be seen as an a priori estimate. S1 also serves to investigate the influence of the wind dependent d and z_0 used in S2 and S3.

In table 2.e statistics of the comparison between observed eddy correlation fluxes and the four schemes are presented. Results are classified into unstable ($L < 0$) and stable ($L > 0$) cases. Furthermore, the data are stratified into low wind speed ($U_h < 2$ m s^{-1}) and high wind speed ($U_h > 2$ m s^{-1}) classes. For neutral conditions a wind speed of 2 m s^{-1} at vegetation height corresponds to approximately 4 m s^{-1} at $z = 36$ m. For each sub-class the number of observations N is given together with the average of the eddy correlation friction velocities $<u_*(ed)>$ and sensible heat fluxes

Unstable								
	$\langle u_*(pr)\rangle$	σ_y	bias	R	$\langle H(pr)\rangle$	σ_y	bias	R
$U_h<2$	N=685 $\langle u_*(ed)\rangle$=0.45 m/s				N=685 $\langle H(ed)\rangle$= 105 W/m^2			
S0	0.54	0.05	+19%	0.94	113	40	+8%	0.91
S1	0.49	0.08	+7%	0.87	131	46	+26%	0.91
S2	0.48	0.06	+5%	0.93	100	39	-4%	0.92
S3	0.45	0.06	+0%	0.93	101	39	-4%	0.92
$U_h>2$	N=432 $\langle u^*(ed)\rangle$=0.85 m/s				N=431 $\langle H(ed)\rangle$= 168 W/m^2			
S0	0.93	0.06	+10%	0.96	157	35	-6%	0.96
S1	0.84	0.11	-2%	0.89	170	40	+1%	0.95
S2	0.89	0.09	+4%	0.93	165	36	-2%	0.96
S3	0.86	0.07	+1%	0.95	163	37	-3%	0.96
Stable								
	$\langle u_*(pr)\rangle$	σ_y	bias	R	$\langle H(pr)\rangle$	σ_y	bias	R
$U_h<2$	N=1510 $\langle u_*(ed)\rangle$= 0.28 m/s				N=1510 $\langle H(ed)\rangle$= -27 W/m^2			
S0	0.33	0.05	+15%	0.96	-32	10	+18%	0.89
S1	0.29	0.07	+3%	0.90	-28	13	+6%	0.81
S2	0.31	0.08	+7%	0.94	-28	11	+6%	0.84
S3	0.28	0.06	-2%	0.93	-25	12	-6%	0.83
$U_h>2$	N=247 $\langle u_*(ed)\rangle$= 0.81 m/s				N=246 $\langle H(ed)\rangle$= -49 W/m^2			
S0	0.85	0.07	+5%	0.96	-44	13	-10%	0.85
S1	0.80	0.11	-2%	0.88	-43	13	-10%	0.85
S2	0.81	0.09	-0%	0.92	-43	15	-12%	0.82
S3	0.77	0.07	-5%	0.96	-39	16	-19%	0.79

Table 2.e. Comparison of eddy correlation measurements with three profile methods. Data are classified into low and high wind speed and into stable and unstable classes. See text for explanation of columns.

$\langle H(ed)\rangle$, where brackets indicate average over a sub-class. For each model the subclass averaged fluxes $\langle u_*(pr)\rangle$ and $\langle H(pr)\rangle$, σ_y the standard deviation of the hourly observations (bias corrected), the relative bias in percentages ($100\%\bullet(\langle model\rangle/\langle observation\rangle-1)$) and the correlation coefficient R are given. Here

all eddy correlation data are used, e.g. also those data where the sonic anemometer is not turned into the wind direction. Grant and Watkins (1989) show that the influence of transducer shadow effects on the vertical wind speed are not large, thus eddy-correlation heatflux is not much affected. The transducer shadow correction procedure applied here for the horizontal wind components, which influences the u_* observations, is still accurate up to a few percent for flow directions larger than the 40° limit applied for the analysis of the preceding section. Therefor also all eddy correlation friction velocity data are used in this analysis.

Scheme S0 systematically overestimates friction velocity. Sensible haet flux is overestimated at low wind speeds and underestimated at high wind speed. Scheme S1 shows a large overestimation of sensible heat flux at low wind speed under unstable conditions. Scheme S2 has a better overall performance. Scheme S3 performes even somewhat better except for sensible heat at high wind under stable conditions. Thus the introduction of wind speed dependent displacement and roughness length has a positive effect on the performance of the schemes S2 and S3.

Figure 2.13 shows hourly values of the three models against eddy correlation measurements of u_* and H for the wind direction class 125-240°. It is observed that correlation in friction velocity for S3 is higher than for the other schemes. Thus despite the introduction of a wind direction and wind speed dependent roughness length in S2 it still has a less satisfactory performance than S3. Scheme S1 shows a different behaviour for friction velocity at low values than at high values, corresponding to the differences at low wind speed and high wind speed. For sensible heat flux an overestimation is observed.

2.8   Discussion and conclusions

Profiles and fluxes of momentum and temperature are measured in the roughness layer of a forest. Data are analysed in the context of Monin-Obukhov similarity theory. It is observed that dimensionless gradients are not only a function of stability but also to some extent a function of wind speed. Two potential instrumental problems which artificially may lead to this observation were analysed. Possible instrumental problems with the cup anemometer observations, especcially at low wind speeds were excluded with by means of a comparison of sonic anemometer wind observations. The influence of spectral loss on the high frequency side of the spectrum is negligible at this measuring height. However, the fixed finite averaging time used here gives rise to a wind speed dependent low frequency loss in the eddy-correlation fluxes. Based on the spectra given by Kaimal et al. (1972), corrections were performed. This correction did not remove the wind speed dependency. Four partly independent methods gave comparable results. This makes it likely that the observed wind speed dependent displacement height is real and not caused by instrumental artifacts. The decreased dimensionless wind with increasing wind speed suggests an increase in roughness. Thus it seems that at higher wind

temporal distribution of the sources of momentum, temperature and other scalars, a memory that is gradually lost when approaching the surface layer. Thus it remains to be shown that scalars with a significantly different source distribution both in space and time, compared to temperature, will have the same exchange coefficients in the roughness layer. Moreover, the evaluation of the schemes in terms of sensible heat flux is not entirely adequate for trace gases. In the present evaluation, weight is put on the large heat flux cases. In general this need not be the high flux cases for trace gases.

An important observation of this study is that momentum and heat eddy diffusivities differ in magnitude even for neutral conditions. This is in line with the observation of Cellier and Brunet (1992) that, with increasing canopy density heat exchange remains enhanced in the roughness layer, whereas momentum exchange approach surface layer values. The enhancement of scalar exchange in the roughness layer may be related to possibility for eddies to penetrate below the level $z = d$ which from a surface layer point of view is a rigid surface. This means that going down to the canopy the effective eddy size will decrease more slowly than the geometric height. The less efficient momentum exchange in the roughness layer then may be attributed to the operation of pressure effects on the eddies, which in principle give a lower effective mixing length since the momentum excess of a parcel of air travelling to a different level is relatively efficiently destroyed due to these pressure forces. This effect will probably be more pronounced in closed vegetation where the wind gradient in the top layer of the canopy is high.

The height of the roughness layer z_* can be defined as the upper level where deviations in dimensionless gradients from the surface layer values are detectable. As observed from Figure 2.10, no meaningful estimate from the wind profile can be made. For temperature however we estimate from Figure 2.12 typical α_H values of 0.85, 0.70 and 0.55 for the subsequent intervals. By linear extrapolation we arrive at a height of 39 m above the forest floor as the top of the roughness layer for neutral conditions, which corresponds to 20 times the roughness length. This is comparable to the ratio 25 suggested for the Thetford forest (Thom et al., 1975) but much lower than the ratio 100 obtained by Garratt (1980) for a more open forest. Garratt (1980) suggests that tree spacing δ is the main parameter that determines the roughness layer height. Cellier and Brunet (1992) compile results for forests and sugar-cane crop indicating typical values for z_* ranging from 3δ to 4.5δ. Here tree spacing is approximately 4 m leading to $z_* = 10\delta$. The large difference remains unclear at this stage.

2.A   Structure parameter of the vertical wind

The structure parameter of the vertical wind C_w^2 is a measure of the turbulent intensity in the inertial subrange. C_w^2 is used in this paper for cup anemometer overspeeding correction and for an alternative way to estimate displacement height. The second order structure function of the vertical wind speed is defined as:

$$D_w^2(x) = <[w(y+x)-w(y)]^2>$$ (2.15)

where w is vertical wind speed, y is a vector in space, x is a difference in space and the brackets indicate averaging over an appropriate domain in space. In the inertial subrange the structure function is proportional to the 2/3 power of the spatial difference. For horizontal homogeneous conditions and differences in the horizontal plane and takking averages over a horizontal plane we define the structure parameter:

$$C_w^2 = \frac{D_w^2(x)}{x^{2/3}}$$ (2.16)

which then is independent of spatial difference in the inertial subrange. Often structure functions are derived from single point time series by means of Taylor hypothesis. In that case x is replaced by $<S>\tau$ where $<S>$ is the average of the length of horizontal wind velocity and τ is the time lag.

The measurement of structure parameters and their related structure functions in the inertial subrange of turbulence close to the earth surface poses serious demands on the spectral resolution of the instruments. With a typical spatial resolution of the sonic anemometer of 0.2 m and lag distance (wind speed times lag time) in the inertial subrange of 0.5 to 2 m it is clear that significant corrections have to be performed. Two correction procedures are developed. The first procedure (P1) assumes local isotropy of the inertial subrange turbulence. Simultanious corrections are calculated for the effect of:

- the filter characteristics of the D/A converter of the sonic anemometer including the effect of sample and hold,
- line averaging along the transducer path,
- Time delay between upward and downward going sound pulses of the vertical transducer.

A second correction procedure (P2) is based on the observation that for the structure functions all these corrections are almost independent of lag time. This can by shown by writing the structure function as

$$D_w^2(x) = 2 (R_{ww}(0)-R_{ww}(x))$$ (2.17)

where R_{ww} is the auto-correlation function of the vertical wind speed. Thus the structure function is the difference between the total variance and the auto-correlation at lag x. The first term contains all spatial scales down to the smallest, whereas the latter contains only scales of the order x and larger. Filtering with a characteristic spatial scale l smaller than x will mainly affect the variance and only slightly the lagged auto-correlation. The effect on the lagged auto-correlation can be shown to be of the order $(l/x)^2$. The effect of spectral loss on the variance can be estimated if we realise that

relation between lateral and longitudinal velocity components and α_u is the Kolmogorov constant for the one dimensional u-spectrum, here assumed 0.5 (Wyngaard and Coté, 1971). With the scaling relation for the dissipation:

$$\frac{kz\varepsilon}{u_*^3} = f_\varepsilon(\zeta) \tag{2.25}$$

where by definition $f_\varepsilon(0) = 1$, and the stability function for dissipation according to Garrat (1972)

$$
\begin{aligned}
f_\varepsilon(\zeta) &= (1-16\zeta)^{-1/4}-\zeta \qquad ;\zeta<0 \\
f_\varepsilon(\zeta) &= 1+4\zeta \qquad\qquad\qquad ;\zeta>0
\end{aligned} \tag{2.26}
$$

Equation (2.6) is derived.

Cup anemometer overspeeding and its relation to structure parameters of the vertical wind

Kristensen (1993) gives a review of the problem of cup anemometer overspeeding and shows the simplifications that can be made for surface layer turbulence. Here we follow his work. The relative overspeeding δ is to a good approximation given by:

$$\delta = \frac{l}{l+\Lambda}\frac{1}{U^2}\int_{-\infty}^{+\infty}\frac{k^2 l_0^2}{1+k^2 l_0^2}F_U(k)dk+\frac{\mu_2}{2}\frac{\sigma_w^2}{U^2} \tag{2.27}$$

where l is the calibration length, Λ is an instrumental length scale which is small compared to l, l_0 is the cup anemometer response length, U is windspeed, μ_2 is a coefficient characterising the response to elevated onflow, σ_w^2 is the variance of the vertical wind, $F_U(k)$ the longitudinal wind spectrum as a function of wave number k.

   The first term on the r.h.s of Equation (2.27) is the u-bias. It shows that the instruments bias is determined by the high frequency part of the spectrum and the response length of the instrument sets the length scale below which fluctuations are not followed well by the instrument and contribute to the overspeeding. The second term is proportional to the vertical velocity variance and contains no dynamic response characteristics of the instrument. Since the response length of the current cup anemometers is an order of magnitude lower than the effective measuring heights it follows that overspeeding is primarily determined by the inertial subrange turbulence. Were Kristensen proceed to express the r.h.s of Equation (2.27) in terms of the dissipation and its surface layer scaling behaviour, we can also make progress by expressing the r.h.s of Equation (2.27) in terms of C_w^2 which measures the intensity of the inertial subrange. Doing so we arive at:

$$\delta = 4.01\frac{\pi}{\sqrt{3}}\frac{l}{l+\Lambda}\frac{C_w^2 \cdot l_0^{2/3}}{U^2} + \frac{\mu_2}{2}\frac{\sigma_w^2}{U^2} \tag{2.28}$$

50

σ_w^2 and C_w^2 are measured at one level in the profile. Surface layer scaling relations are used to transform them to the subsequent cup anemometer levels in the profile.

2.B The relation between scalar wind speed and the length of the average wind velocity

Cup anemometers measure the scalar windspeed, i.e the length of the horizontal wind vector. A cup anemometer - wind vane combination, propellor vanes and 3-dimensional sonic anemometers are capable of measuring the horizontal wind vector. It is the average of the wind vector that appears in the momentum conservation equations of the atmospheric boundary layer. Here we concentrate on the relation between the scalar wind speed to the average of the length of the wind vector. We will not bother about instrumental imperfections as limited response distances and time or angle responses, but we concentrate on the fundamental differences. This question is raised because over forest turbulence intensity is high and measurements are taken so close to the forest that even a second order correction as is traditionally done seems doubtfull. This leeds us with the choice to reject a large number of windspeed measurements especially those close to the canopy or to develop a method to correct for higher turbulence intensities adequately.

Let us assume a statistically stationary turbulent wind field. We denote the horizontal windfield by:

$$U = (<U>+u)\cdot\vec{e}_1 + v\cdot\vec{e}_2 \qquad (2.29)$$

where $<U>$ is the length of the average wind velocity, u is the deviation of the wind velocity in the average winddirection, v is the deviation perpendicular to the average winddirection. The average wind direction is defined by the requirement that $<v> = 0$. The scalar wind S is defined as:

$$(<S>+s)^2 = (<U>+u)^2 + v^2 \qquad (2.30)$$

From this we immediately derive the exact relation wich is interesting in its own right:

$$<S>^2 + \sigma_s^2 = <U>^2 + \sigma_u^2 + \sigma_v^2 \qquad (2.31)$$

where σ_i^2 denote the variance of quantity i. To find a relation between the average scalar windspeed and the length of the average wind vector we have to take the square root of Equation (2.30) and average. If the deviations u and v are small relative to $<U>$ we can rely on Taylor expansion. This leads after averaging to the relation:

$$<S> = <U> \left(1 + \frac{1}{2}\frac{\sigma_v^2}{<U>^2} + O^4\right) \qquad (2.32)$$

51

aerodynamic surface temperature that determines the sensible heat transfer from the surface to the atmosphere, and the storage surface temperature that drives the change in the heat content of the soil and biomass. These temperatures are some kind of weighted average over the air soil/canopy interface, and they will differ in their weighting functions. Ideally, their mutual differences are much smaller than other relevant temperature differences in the system at hand. In that case a model based on surface-layer similarity, and with a single surface temperature, may be appropriate to describe both the sensible heat exchange and the radiation exchange between the canopy and the atmosphere.

No practical method exists to measure aerodynamic surface temperature for complicated surfaces such as canopies. In general, radiative surface temperature is used instead. Justification for such a procedure is found when this leads to a simple relation between atmosphere-surface temperature difference and sensible heat flux in terms of surface layer similarity theory. This leads to the concept of roughness length for heat, z_{0H}. A number of studies show that surfaces with sparse canopy cover (Brutsaert and Sugita, 1992; Stewart et al., 1994; Verhoef et al., 1996) and surfaces with occasional obstacle elements (Beljaars and Holtslag, 1991) may have extremely large values of the ratio z_{0M}/z_{0H}, where z_{0M} is the roughness length for momentum. These unrealistic values for z_{0H} may hint at the incapability of the single surface temperature model to describe sensible heat exchange, but it also may hint at a difference between aerodynamic surface temperature and radiative surface temperature. A fine example of the latter is given by Sun and Mahrt (1995) for a Boreal forest. Recent developments in multi-layer vegetation models may explain these phenomena (Blyth and Dolman, 1995; McNaughton and van den Hurk, 1995). For a dense canopy, the z_{0M} to z_{0H} ratio is better behaved (Garratt and Hicks, 1973) and has been satisfactory modelled by, amongst others, Brutsaert (1982).

In general the radiation surface temperature is derived from observations of broadband or narrowband infrared radiation fluxes. The advantage of working with narrowband sensors in the atmospheric window is that atmospheric emissivity can be neglected for most ground based applications. Huband and Monteith (1986), Kohsiek et al. (1993) and Mölder and Lindroth (1999) already showed the importance of the orientation of the instrument relative to the sun due to shading effects. Longwave emissivity that is smaller than one can lead to underestimation of the surface radiation temperature during clear sky conditions when longwave cooling is high (Feijt and Kohsiek, 1995).

For dense vegetation it is often assumed that z_{0H} is a true surface parameter, fully determined by the geometry and other characteristics of the surface and independent of the atmospheric conditions. As such z_{0H} is typically one order of magnitude smaller than z_{0M} (Garratt and Hicks, 1973). However, since z_{0H} is a surface-layer parameter that incorporates effects of the vegetation and of the flow structure in the lowest atmospheric layers, including the roughness sublayer, this assumption can be questioned. For forests the structure of the roughness sublayer is particularly well documented (Thom et al., 1975; Garratt, 1978a; Raupach, 1979; Denmead and Bradley, 1985; Fazu and Schwerdtfeger, 1989; Högström et al., 1989;

Mölder et al., 1999, Simpson et al., 1998). These studies show that exchange coefficients for heat and momentum are in general enhanced as compared to surface layer values. Moreover, enhancement may differ for the two quantities depending on canopy density (Cellier and Brunet, 1992). For the current forest these effects are quantified in Bosveld (1997), hereafter abbreviated to B97.

Lowering the displacement height in the inertial sublayer formulation of flux-profile relationships leads to higher estimated mixing coefficients. The possibility of adapting displacement heights for momentum (d_M) and heat (d_H) has been raised by Hicks et al. (1979) and by Raupach (1979) to explain enhanced mixing in the roughness sublayer of forests. Raupach (1979) showed that, for the closed Thetford forest, this leads to unrealistic estimates for d_H. The same conclusion can be derived from the results presented by B97 for the current forest. In the inertial sublayer d is in fact the only vegetation parameter that enters the scaling parameters for gradients and turbulent quantities; d enters through the effective height $z - d$ which is assumed to be proportional to the eddy-size, where z is the height above the surface. If we neglect stability effects, then the eddy size distribution is determined by the distance between the observation height and the displacement height for momentum. When the source level of heat is below this displacement height for momentum, the larger eddies will transport a greater part of the heat and this results in a smaller displacement height for heat than for momentum. Paw U and Meyers (1989) used a canopy model with 4th-order closure to assess this problem. They indeed found substantial differences in displacement heights for momentum, heat and moisture for their simulated soy bean canopy. However, they are not specific about how well their model simulates a realistic roughness sublayer. For a dense forest we may expect that the effective source level for heat does not differ much from the effective sink level for momentum, and thus a single value of d can be used for momentum and heat.

Only a few experimental studies exist that give reliable estimates of z_{0H}/z_{0M} or related quantities for forests. Garratt (1978b) gives results for a rather open structured forest and arrives at a ratio of 1 to 12. Mölder and Lindroth (1999) for a denser forest arrives at a ratio of 1 to 1.

In this study the behaviour of surface temperature of a very dense Douglas fir forest is examined in relation to sensible heat transfer. This is done by means of observed crown radiation temperatures and observed eddy-correlation heat fluxes. As a theoretical framework, we use surface layer similarity and a single surface temperature model to interpret the observations. In section 3.2 the research site and experiment are described. The section also gives details on the calibration of the infrared radiation thermometer. Section 3.3 describes surface layer similarity theory and the extension for the roughness sublayer of this forest based on the previous study of B97. In section 3.4 the roughness length for heat is derived from near neutral observations. An alternative definition of the roughness length for heat is proposed in section 3.5, based on an extrapolation of the appropriate roughness sublayer profiles for temperature and momentum; for neutral conditions the two definitions are equivalent.

Given the roughness-sublayer stability functions presented by B97, it is shown in section 3.6 that for unstable conditions the two definitions of z_{0H} give different predictions for the relation between the temperature difference over the roughness sublayer and the heat flux. This difference becomes significant when the stability parameter at the top of the roughness sublayer, Z_R/L, is of order 1 (Z_R being the roughness sublayer height relative to the displacement height, and L the Obukhov length). This is a condition that is not exceptional over forest and we analyse to what extent the observations support the modified definition of z_{0H}. Results for stable conditions are also presented in this section. In section 3.7 the relation between trunk-space air temperature and atmospheric air temperature is analysed; section 3.8 gives a discussion of the results and conclusions.

3.2   Forest location and instruments

The Speulderbos research location is a 2.5 ha Douglas fir plantation, located within a large forested area in the Netherlands (52° 15′ N, 5° 41′ W, 52 m above sea level). The shortest distance between the forest research site and the lower vegetation is 1.5 km. The stand has a tree density of 785 trees per hectare, and the firs were planted in 1962. In 1989, the year the measurements were performed, the trees had reached a mean height of 18 m and a mean diameter at breast height of 0.21 m. The single sided leaf area index (LAI) varied between 8 and 11 throughout the year (Evers et al., 1991). The forest floor is covered with a needle layer on which little vegetation is present; a trunk space and a crown layer can be discriminated, while trunk space with few branches and needles reaches to approximately 10-m height. The topography is slightly undulating with height variations of 10 to 20 m over distances of 1 km. The forest consists of stands with typical areal dimensions of a few hectares. In the neighbourhood of the research site the dominant stand species are Douglas fir, Beech, Japanese Lark and Scotch Pine. With a footprint analysis based on the work of LeClerc and Thurtell (1990) and Schmid (1994), B97 showed that footprints extend well over the edge of the current Douglas fir stand. However, in the wind direction sector 45 to 125°, the forest stands have comparable geometry to the local stand. In the other directions differences are larger. In this study only data with wind direction between 45 and 125° are used.

Temperature and wind speed measurements were performed along an open mast at 4, 18, 24, 30 and 36 m height above ground. The lowest level was in the trunk space of the forest, with the 18-m level just above the tree tops. Eddy correlation fluxes of temperature and horizontal momentum were measured at 30 m. Continuous observations were obtained during the period April-December 1989; instruments and correction procedures are described in B97.

Crown radiation temperature was measured with a Heimann infrared radiation thermometer (KT-24), with a spectral window of 8-35 μm. The instrument was maintained at a temperature of 30°C in order to avoid temperature gradients in

56

the instrument during rapid external temperature changes. The instrument was oriented to the northwest from the top of the mast with a zenith angle of 45°; the field of view was 22°, giving a view area at tree crown level of approximately 100 m². Calibration was performed against an enclosed water bath at the Royal Netherlands Meteorological Institute (KNMI).

An in situ calibration is derived by constructing a reference temperature T_{ref} from the meteorological observations, which resembles the radiative surface temperature as observed by the infrared sensor. Then a regression of the sensor output (V_H) against this reference temperature is performed. From laboratory calibration it was already found that the relation between V_H and radiation temperature is well described by a second order polynomial,

$$T_{ref} = aV_H^2 + bV_H + c \ . \tag{3.1}$$

Only near-neutral strong wind cases are used in the procedure. This ensures good coupling of the crown with the air above and consequently small temperature differences between the forest crowns and the air above the forest.

For the construction of the reference temperature the following considerations are important. Although the forest is rather dense at the crown level it is possible that the instrument also sees parts of the deeper layers of the forest, which tend to be at the forest trunk-space temperature. By selecting data with high wind speeds and small heat fluxes we ensure that temperature differences between the air above the forest and the forest trunk space are small, a measured few tenths of a kelvin at most.

Huband and Monteith (1986), Kohsiek et al. (1993) and Mölder and Lindroth (1999) already showed the importance of the orientation of the instrument relative to the sun. Indeed, systematic higher radiation temperatures of several tenths of a kelvin are found when the sun is behind the instrument, minimising the tree shades in the view area of the instrument.

A longwave emissivity ε smaller than one can lead to underestimation of the surface radiation temperature during clear sky conditions when longwave cooling is high (Feijt and Kohsiek, 1995). Part of the upward longwave radiation is comprised of reflected downward longwave radiation. For typical emissivities of vegetated surfaces and clearsky conditions deviations can be several tenths of a kelvin. Emissivity is higher for forest with high *LAI* than for low vegetation due to increased multiple scattering.

Expressed as a formula, we assume that the infrared radiation thermometer sees a reference temperature T_{ref} given by:

$$T_{ref} = T_{18} + \Gamma(z - z_{rad}) - \alpha\theta_* + \beta(T_4 - T_{18}) + \eta\frac{\Delta L^*}{4\sigma T_{18}^3} + \mu\frac{S^\downarrow}{\max(U_{18},1)}\cos(\phi_s - \phi_0) \ , \tag{3.2}$$

where T_{18} is air temperature at 18 m (tree top height). The second term accounts for the adiabatic lapse rate $\Gamma = 0.01$ K m^{-1} between this height (z) and the effective radiation level (z_{rad}); the latter level will be just above the level where the crowns

meet to form a closed layer. For the current forest this is close to the displacement height and we choose z_{rad} = 12.5 m. The third term reflects the difference between crown temperature and air temperature due to diabatic effects; θ_* is the turbulent temperature scale $-<w\theta>/u_*$ where $<w\theta>$ is the turbulent temperature flux and u_* is the friction velocity. α is a function of atmospheric stability, but due to the near-neutral selection criterion can be taken constant for this purpose. The fourth term reflects the effect of the contamination of the radiation temperature by the trunk-space temperature, here represented by the forest trunk-space air temperature at 4-m height (T_4). The fifth term represents the effect of longwave emissivity being smaller than 1. Net longwave radiation flux (ΔL^*) is derived from observations of net radiation and shortwave incoming radiation ($S^\downarrow$), together with an estimated forest albedo of 0.11. The denominator is the temperature derivative of the black body radiation law of Planck in which σ is the Stephan-Boltzman constant. Since the spectral window of the infrared radiation sensor differs from the effective spectral window of the combined net radiation and shortwave radiation system, the free parameter η is only an approximation to $1 - \varepsilon$. The sixth term represents the effect of instrumental view angle relative to the direction of the sun, where the functional form was found from an analysis of residuals. Here U_{18} is the wind speed at canopy height in m s^{-1}, ϕ_s is the azimuth of the sun and ϕ_0 is the azimuth to which the rear of the instrument points (150° degrees from North).

From the available data 91 hourly averaged infrared temperatures were selected with U_{18} > 2.5 m s^{-1} and $0 < -\theta_* < 0.2$ K. Here no selection on wind direction was made. Equation (3.1) is used to relate the output signal of the infrared radiometer to T_{ref}. A multi-linear regression is performed to obtain the three calibration coefficients and the four parameters in the formulation of the reference temperature (Equation (3.2)) simultaneously. Figure 3.1 shows T_{ref} as a function of V_H. Also shown is the in situ calibration curve. The selected hourly values are in the temperature range of 5 to 28 °C, which is broad enough to be representative for the whole data set. Moreover the selected data are reasonably spread over the nine months observation period and the residuals did not show a trend with time, suggesting a stable calibration over the observation period. The standard deviation in the residuals is 0.13 K; $\alpha = 2.8 \pm 0.2$, $\beta = 0.11 \pm 0.05$, $\eta = 0.004 \pm 0.003$ and $\mu = 0.0020 \pm 0.0002$. The contributions of the third and sixth term are typically 0.4 K, while the contributions of the fourth and the fifth term are typically smaller than 0.1 K. The η value suggests a longwave emissivity larger than 0.995.

The difference between the in situ calibration and the laboratory calibration, using an enclosed thermostatted surface, ranged from 0 to 1 K over the range 0 to 30 °C. Unfortunately, the instrument could not be recalibrated due to malfunctioning after the field campaign, and the nature of the difference with the laboratory calibration could not be traced. To obtain consistency within the data set the in situ calibration was adopted.

Having established the calibration of the radiation thermometer, we now have to establish the relation between the observed radiation temperature and the surface radiation temperature. From the preceding analysis it is found that emissivity is very

58
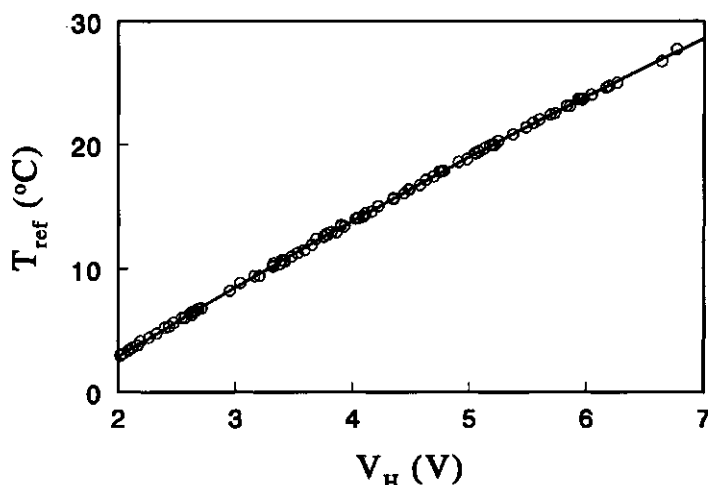
Figure 3.1. In situ calibration reference temperature as a function of output voltage of the infrared radiometer for 91 strong wind cases. Also drawn is the regression line used as calibration curve in this study.

close to 1, therefore the influence of reflected longwave radiation is ignored. The influence of shading related to the relative angle between instrument and the sun is of importance. To arrive at a representative surface radiation temperature T_s we use:

$$T_s = aV_H^2 + bV_H + c - 0.002 \frac{S^\downarrow}{\max(U_{18}, 1)} \cos(\phi_s - \phi_0) \, , \qquad (3.3)$$

where the coefficients are taken from the regression result. Those data points used in this in situ calibration that have wind direction between 45 and 125°, the good fetch sector, are excluded from the subsequent analysis.

3.3 Surface layer similarity and surface characteristics

Surface layer

Exchange of momentum and heat between the earth's surface and the surface layer of the atmosphere can be described with surface layer similarity theory. For the dimensionless shear ϕ_M and potential temperature gradient ϕ_H we have, according to

59

$$kB^{-1} = \ln(\frac{z_{0M}}{z_{0H}}) \ . \tag{3.12}$$

In turbulent flow kB^{-1} is, in general, positive. The smaller resistance to transfer for momentum is attributed to the presence at the surface of form drag, a process that does not affect scalar transport. The compilation of Garratt and Hicks (1973) shows that for rigid surfaces kB^{-1} is a strongly increasing function of the roughness Reynolds number $Re_* = u_* z_{0M}/v$, where v is the kinematic viscosity of air. For more fibrous and flexible surfaces, as for most vegetation, kB^{-1} is more or less constant. A typical value of 2.3 is found with a slight decreasing trend for rougher vegetation and/or vegetation with high LAI (Brutsaert, 1982). For sparse canopies much higher values are found, due to the sheltering effect of large areas of the surface that still take part in the heat exchange process.

As a start, we may utilise Equation (3.8) to estimate z_{0H} from the available observations. The top of the roughness sublayer z_R is only slightly above the highest measuring level at 36 m. Therefore, we use the observations of potential temperature at this height, θ_{36}, as a surface layer value. Surface temperature is obtained from the infrared radiometer. Hourly observations of u_* and $\langle w\theta \rangle$ as measured by the eddy correlation system at $z = 30$ m are used. Near-neutral unstable data are selected with $L < -200$ m and with wind direction corresponding to the best fetch, i.e $[45:125°]$. In this sector a roughness length for momentum z_{0M} of 2.2 m is found at a wind speed of $U_{18} = 3$ m s^{-1}. Data already used for the in situ calibration of the infrared radiometer are excluded.

To avoid unwanted scatter due to division of two small quantities, both sides of Equation (3.8) are multiplied by $\langle w\theta \rangle /k$. In Figure 3.2 observations of $-u_*(\theta_{36} - \theta_S)$ are shown as a function of $(\langle w\theta \rangle /k)f(Z_R, L, z_{0H})$, where $f(Z_R, L, z_{0H})$ represents the r.h.s. of Equation (3.8). Stability corrections are small and calculated according to Equation (3.9). The open dots represents values where z_{0H} (in the expression plotted along the x-axis) is taken as 2.0 m; the closed dots represents values where z_{0H} is taken wind speed dependent. Here z_{0H} is taken proportional to z_{0M} according to Equation (3.11), with a value of 2 m at $U_{18} = 3$ m s^{-1}. In both cases d is taken as a function of wind- speed according to Equation (3.11). Using a fixed value for d of 12.5 m, which is a typical value for moderate winds, has only minor influence. The straight lines indicated by z'_{0H} show the expected values of $-u_*(\theta_{36} - \theta_S)$ if the actual roughness length for heat had been 1.5, 2.0 and 2.5 m respectively, and give an indication of the uncertainty with which z_{0H} is determined. It is seen that the fixed z_{0H} formulation is in concordance with $z'_{0H} = 2.0$ m. Using a wind speed dependent z_{0H} (= var) leads to decreased values along the x-axis at high temperature flux. This is the case, since large heat fluxes are found only at high wind speeds, owing to the near-neutral selection criterion.

Two things are worth mentioning. Firstly, the limited accuracy of the temperature difference observations in near-neutral conditions precludes definite conclusions on any wind-speed dependence of z_{0H}. Secondly, it is remarkable that the roughness length for heat is approximately equal to the roughness length for
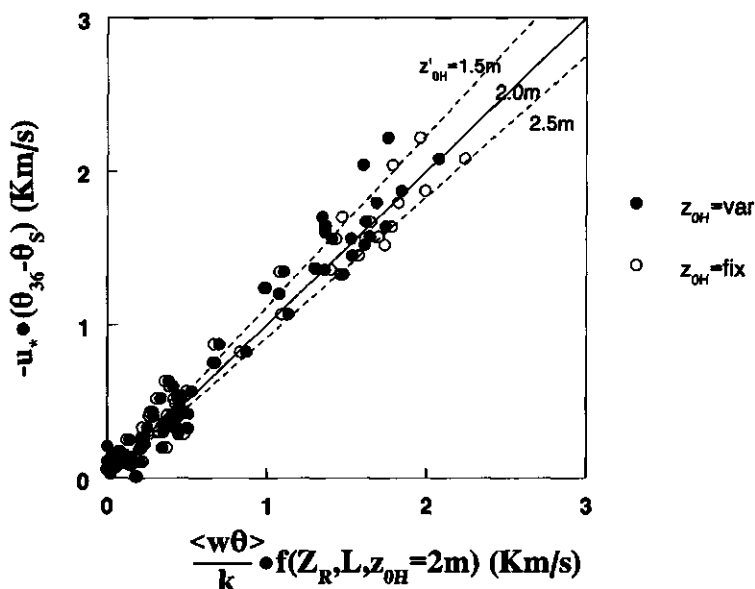
Figure 3.2. Observed temperature difference between 36 m and the surface (θ_S) against model, both multiplied by u_*, for fixed and variable z_{0H}. See text for explanation.

momentum for this forest and thus kB^{-1} is approximately 0. Mölder and Lindroth (1999) found approximately the same low value for a boreal forest and concluded that roughness sublayer effects are significant. Such a low value of kB^{-1} is inconsistent with the expected excess resistance for heat over momentum. The roughness lengths for momentum and heat are defined as the heights (above the displacement height) where U and θ become equal to their surface values when the logarithmic profiles are extrapolated through the roughness sublayer. Consequently z_{0H} and z_{0M} are integration constants that combine the effects of the roughness sublayer and the actual vegetation-atmosphere interfacial transport. In the next section we will quantify the importance of both effects.

3.5   Roughness length for heat incorporating roughness sublayer effects

The relation between turbulent transfer and vertical gradients in the horizontal homogeneous neutral surface layer is characterised by only one length scale, i.e., the height above the displacement height $z - d$. The surface layer is limited below by the so-called roughness sublayer, within which additional length scales related to the geometry of the canopy are important. For the present forest B97 used observed

eddy-correlation fluxes of momentum and heat, together with wind-speed and temperature differences in the roughness sublayer, to arrive at dimensionless shear and temperature gradients at three levels in the roughness sublayer. For neutral conditions his data are well described by:

$$\phi_M(\zeta = 0) = 1 - p_M + p_M \frac{(z-d)}{Z_R} \; ; \qquad h - d < z - d \le Z_R \; , \tag{3.13}$$

$$\phi_H(\zeta = 0) = 1 - p_H + p_H \frac{(z-d)}{Z_R} \; ; \qquad h - d < z - d \le Z_R \; , \tag{3.14}$$

where p_M and p_H are empirical parameters that define the deviation of the dimensionless gradients relative to the surface-layer values; $Z_R = 26.5$ m, which is 12 times the roughness length for momentum. This level is just above the highest measuring level. For this site it was found that $p_M = 0$ and $p_H = 0.6$, values typical for a very dense canopy. For more open canopies $p_M \approx p_H \approx 0.5$ is found (Cellier and Brunet, 1992).

From Equations (3.13) and (3.14) we note that the neutral roughness sublayer profile for momentum ($p_M = 0$) is equivalent to the surface-layer profile and that the profile for temperature ($p_H = 0.6$) deviates from the surface-layer profile. Thus, the extrapolation of surface-layer profiles through the roughness sublayer to calculate surface roughness is correct for momentum but not so for temperature. Here we seek to exclude the effects of different turbulent transport in the roughness sublayer between momentum and heat on calculation of the roughness length for heat. This is done by deriving the counterpart of Equation (3.8) for neutral conditions in the roughness sublayer through integrating Equation (3.14) from $z - d = Z_R$, the top of the roughness sublayer, downward. We find:

$$\frac{k \, [\theta_R - \theta_S]}{\theta_*} = (1 - p_H) \, \ln(\frac{Z_R}{z_{S,H}}) + p_H \, (1 - \frac{z_{S,H}}{Z_R}) \; , \tag{3.15}$$

where $z_{S,H}$, the modified roughness length for heat, is an integration constant analogous to z_{0H}. The ratio between $z_{S,H}$ and z_{0M} presumably better resembles the difference in transport efficiency at the vegetation/air interface between heat and momentum. Figure 3.3 shows schematically the difference between z_{0H} and $z_{S,H}$. In a more general treatment where $p_M \ne 0$ one would need to define a modified roughness length for momentum ($z_{S,M}$) as well.

Neglecting the ratio $z_{S,H}/Z_R$ in the last term, and equating Equation (3.15) to the neutral limit of Equation (3.8) with $z - d = Z_R$, we find a relation between z_{0H} and $z_{S,H}$:

$$z_{S,H} = z_{0H} \left(\frac{e \cdot z_{0H}}{Z_R} \right)^{p_H/(1-p_H)} \tag{3.16}$$

Taking $z_{0H} = 2.0$ m and $p_H = 0.6$, we find $z_{S,H} = 0.23$ m, which is about 0.1 times

64
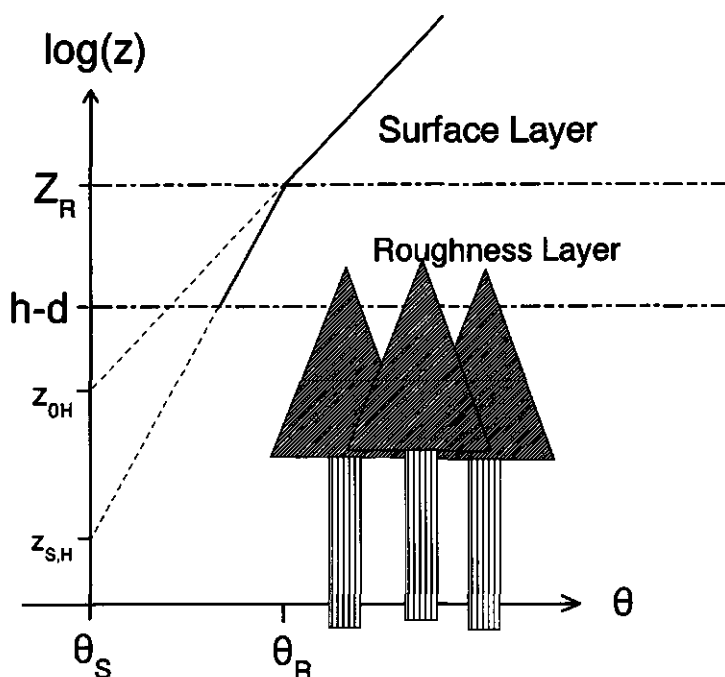
Figure 3.3. Schematic representation of the extrapolation procedure to arrive at roughness length for heat. Both the classic method and the modified method are shown.

z_{0M} for this forest. This suggests that the excess resistance to transfer of heat over momentum comprises two components; the well-known effects of form drag represented here by $z_{S,H}/z_{0M} = 0.1$ and the larger turbulent transfer efficiency for heat than for momentum in the roughness sublayer. For the current forest the two components tend to cancel, resulting in a value of kB^{-1} close to zero.

3.6   Diabatic conditions.

Until now the introduction of $z_{S,H}$ has given us insight into the way z_{0H} depends on the turbulent structure of the roughness sublayer, which itself is related to the density of the vegetation. For near neutral conditions however, the two formulations of roughness length for heat give the same dimensionless potential temperature difference between the surface and the lowest level of the surface layer (Z_R) and thus cannot be distinguished by observations taken in the surface layer. Let us now turn to unstable conditions.

For non-neutral conditions it is common practice to relate the air temperature in the surface layer and the surface temperature by extrapolating the diabatic surface-layer profiles to the level z_{0H} above the displacement height as is done in

Equation (3.8). Thus, z_{0H} is assumed to be independent of stability. As we have seen in the previous section, z_{0H} depends on the structure of the roughness sublayer. The independency of z_{0H} on stability therefore depends on the behaviour of diabatic roughness-sublayer profiles.

In B97 it is found that the dimensionless potential temperature gradient in the roughness sublayer for unstable cases can be described as the product of the classical inertial sublayer stability function and a factor that is only a linear function of relative height in the roughness sublayer. This leads to the diabatic extension of Equation (3.14):

$$\frac{k(z-d)}{\theta_*}\frac{d\theta}{dz} = (1 - p_H + p_H \frac{(z-d)}{Z_R}) \; \phi_H(\zeta) \; ; \qquad \zeta < 0 \; . \tag{3.17}$$

With the roughness sublayer formulation of Equation (3.17) we are able to extrapolate the more realistic roughness sublayer profiles to the modified roughness length for heat $z_{S,H}$. This leads to:

$$\frac{k \; [\theta_R - \theta_s]}{\theta_*} = (1 - p_H) \left(\ln(\frac{Z_R}{z_{S,H}}) - \psi_H(\frac{Z_R}{L}) + \psi_H(\frac{z_{S,H}}{L}) \right) \\ + p_H \; \frac{2L}{\gamma Z_R} \left(\phi_H^{-1}(\frac{z_{S,H}}{L}) - \phi_H^{-1}(\frac{Z_R}{L}) \right) . \tag{3.18}$$

The last term is obtained because of the special form of ϕ_H (see Equation (3.9)). Note that for the limit $p_H \to 0$ the surface-layer limit, Equation (3.8), is recovered. In the neutral limit ($Z_R/L \to 0$) the last term on the r.h.s of Equation (3.18) approaches $p_H(1 - z_{S,H}/Z_R)$ and thus Equation (3.15) is recovered. Figure 3.4 shows the standard stability function at the top of the roughness sublayer (Equation (3.8)) and the modified formulation (Equation (3.18)) for the current location, i.e., with Z_R = 26.5 m, z_{0H} = 2.0 m and p_H = 0.6. It is observed that stability dependence is somewhat weaker in the modified formulation, and leads to significantly larger dimensionless temperature gradients in very unstable cases.

To test the two stability formulations, Equation (3.8) and Equation (3.18) are compared with the observed temperature difference between the surface and the 36-m height. Figure 3.5 shows the ratio of observed and modelled values as function of stability. Data are selected for wind direction within the range [45:125°] and classified into stability classes according to Z_R/L. For each class the average of the observed $-u_*(\theta_{36} - \theta_S)$ is calculated. Modelled values are derived from the r.h.s of the standard formulation (Equation (3.8)) and from the r.h.s of the modified formulation Equation (3.18), in either case multiplied by the observed $<w\theta>/k$. Also the calculation is performed for a wind-speed dependent roughness length for heat (var) and a constant roughness length for heat (fix). In all four variations of the model a wind-speed independent displacement height is used. Using a variable d gives only minor differences. Then, the ratio between average model values and average observed values within a stability class is calculated and, for each class,

66
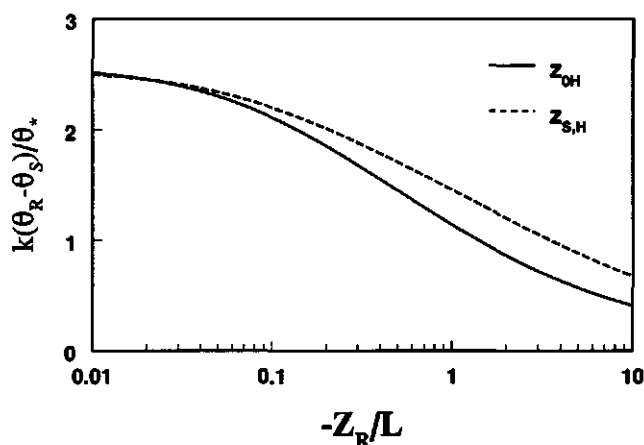
Figure 3.4. Standard and new formulation of the integrated stability function for temperature between the top of the roughness layer (θ_R) and the surface (θ_S) as function of stability.

standard errors of the mean are calculated from the members within a class. These are indicated for the model z_{0H} = fix, but are the same for the other models.

For unstable conditions it is seen that the modified formulation gives higher values for the dimensionless temperature difference between the top of the roughness sublayer and the surface, than the standard formulation. The modified formulation with a fixed $z_{S,H}$ describes the observations much better than the standard formulation with a fixed z_{0H}. By using a wind speed dependent roughness length (z_{0H} = var) the standard formulation can be brought in closer agreement with the observations. Thus, by using a realistic flux-profile function to extrapolate from the top of the roughness sublayer to the surface we find that a wind-speed independent roughness length for heat ($z_{S,H}$ = fix) matches the observations best.

In B97 it is shown that, for stable conditions, potential temperature gradients above the forest follow Monin-Obukhov similarity reasonably well, despite the large footprints and less then ideal fetch on the larger scale. It is found that the roughness-sublayer correction is merely an offset over the whole stability range. This leads to an extension of the dimensionless potential temperature gradient:

$$\frac{k(z - d)}{\theta_*}\frac{d\theta}{dz} = \phi_H(\zeta) - p_H + p_H\frac{(z - d)}{Z_R} ; \qquad \zeta > 0 . \qquad (3.19)$$

From this we derive the temperature difference over the stable roughness sublayer:

67
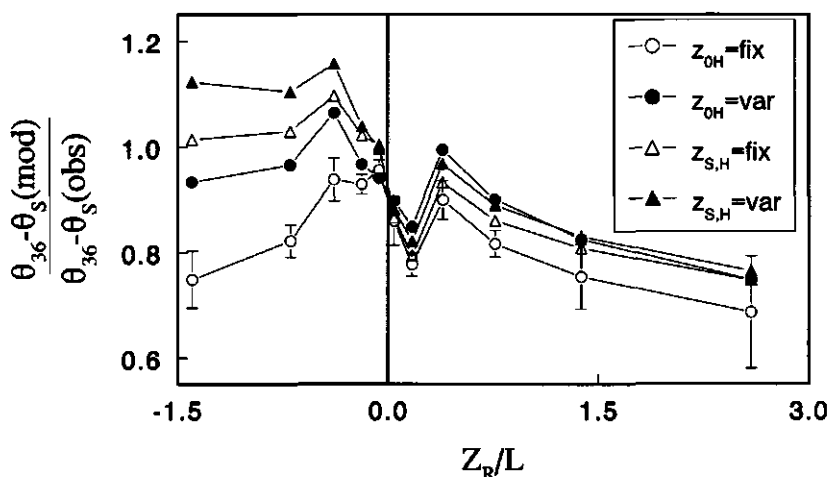
Figure 3.5. Modelled potential temperature difference between surface and 36 m divided by corresponding observed values per stability class. For explanation of the four model versions see text.

$$\frac{k\,[\theta_R - \theta_S]}{\theta_*} = (1 - p_H)\,\ln(\frac{Z_R}{z_{S,H}}) + p_H\,(1 - \frac{z_{S,H}}{Z_R}) - \psi_H(\frac{Z_R}{L}) - \psi_H(\frac{z_{S,H}}{L}) \; . \quad (3.20)$$

Contrary to the unstable case this form does not lead to a different functional form for the stability part of the equation as compared to the surface layer formulation Equation (3.8). In Figure 3.5, data with stable atmospheric stratification are also shown. For this stability range it is observed that all formulations give values substantially smaller than 1 for most of the stability range, which corresponds to an underestimation of the estimated temperature difference between 36 m and the surface. Apparently other factors are significant for stable conditions. Figure 3.6 shows individual hourly averaged temperature differences, with modelled values shown as a function of observed values; data are stratified into stability classes. It is observed that the deviation for the slightly stable case, which is apparent in Figure 3.5, is also found in the individual observations. However, deviations for these cases are small in an absolute sense and thus preclude definite conclusions. Perhaps the roughness sublayer parameterisation is inadequate here. For the very stable cases the figure shows that observed temperature differences at times exceed modelled values significantly.

68
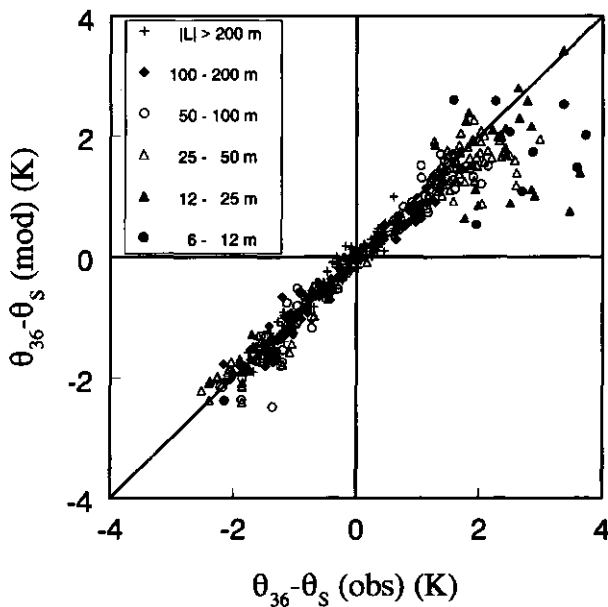
Figure 3.6. Modelled potential temperature difference between surface and 36 m as function of observed values. Data are stratified into stability classes. The model '$z_{S,H}$ = fix' is used.

3.7 The behaviour of forest trunk space air temperature during day time

Until now, we have found that during daytime there is a good correspondence between the radiative surface temperature and the aerodynamic surface temperature. In effect this means that we have found the relation between radiative surface temperature and the atmospheric conditions above the forest. Now the question arises as to how the temperature inside the forest relates to the atmospheric conditions above the forest. Surface storage temperature, i.e. the air temperature at the interface between soil/biomass and the air, is not measured. Forest trunk-space air temperature observed at 4-m height may serve as an acceptable substitute. This is the case, because the soil and most of the biomass is below the dense crown layer and little radiative energy enters the trunk space below the crown layer. During daytime heat is generated, by absorption of radiation, at the crown level where the highest temperatures are found. As long as air temperature rises, the biomass and soil are taking up heat from the forest trunk-space air. This results in a trunk-space air temperature that is, in general, lower than the air temperature above the forest. Figure 3.7 shows the potential temperature difference between forest trunk-space (z = 4 m) and the top of the roughness sublayer (z = 36 m) as a function of sensible heat flux for unstable conditions. Data are stratified into classes

69
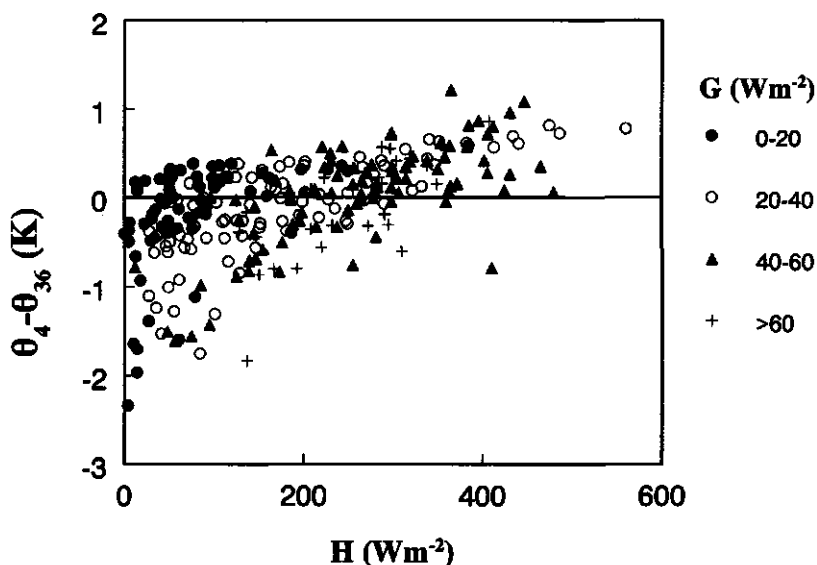
Figure 3.7. Potential air temperature of the forest trunk space relative to the 36-m level as a function of sensible heat flux. Data are stratified into storage heat flux classes.

of storage heat flux. It is indeed observed that trunk-space air temperature increases with increasing sensible heat flux and decreases with increasing storage heat flux.

Studies of Denmead and Bradley (1985), Gao et al. (1989) and Bergström and Högström (1989) show that the vertical transfer of momentum and heat from vegetation to the atmosphere is dominated by gusts that generate a large fraction of the flux in a small fraction of the time. Surface renewal analysis (Paw U et al., 1995; Katul et al., 1996; W.Chen et al., 1997) is successfully used in a number of studies to estimate surface fluxes from the characteristic ramp structure observed in high frequency temperature time series of gusts just above the vegetation. Here we use this concept to describe the trunk-space air temperature as a function of gusts penetrating the trunk space from above, and subsequent heat exchange with the soil and biomass. Raupach et al. (1996) argue that the roughness sublayer above dense vegetation behaves as a turbulent mixing layer that is characterised by the occurrence of an inflexion point in the wind profile. This hypothesis is supported by a number of turbulent characteristics that are typical for mixing layer turbulence found in laboratory studies.

According to Raupach et al. (1996) the characteristic length scale L_S associated with the gusts is related to the wind speed at canopy height U_h and to the shear at the canopy height U_h', and is $L_S = U_h/U_h'$. The spatial distance between

successive gusts Λ_S is found to be $\Lambda_S = 8L_S$ for a large variety of canopies, while the advection speed of the gusts is $U_A = 2U_h$. Thus the gust recurrence time is $T_X = 16L_S/U_h = 16/U_h'$. For the current forest we estimate the shear at canopy height from Equation (3.13) with $p_M = 0$ as found by B97. Thus we have $U_h' = u_*/(k[h - d])$ = $7.5u_*/h$, where $d = 2/3h$, and thus $T_X = 2.1h/u_*$.

When a gust penetrates the forest trunk-space it carries with it the temperature of air from above the forest. We model this temperature as $\theta_R + \alpha_H\theta_*$. Here, α_H incorporates two effects: the uncertainty of the effective height from which the air originates, and the effect of a temperature increase due to the exchange of heat at the crown level. Each gust exchanges a fraction f, the gust renewal fraction, of the trunk-space air of the forest. After penetration, the air inside the forest has time to exchange heat with the soil and the biomass, leading to a gradual temperature decrease. Thus a high sensible heat flux (H) acts to increase the forest trunk-space air temperature relative to the air above, and a high storage heat flux leads to a decrease of forest trunk-space air temperature. The total decrease in temperature will be proportional to the storage heat flux (G) and proportional to the time between successive gusts, which itself is inversely proportional to the wind speed.

On the basis of the preceding arguments we come to the following parameterisation for the forest trunk-space air temperature θ_i for daytime cases:

$$u_* \, (\theta_i - \theta_R) = \alpha_H\frac{H}{\rho C_p} - \alpha_G\frac{G}{\rho C_p} \, , \tag{3.21}$$

where ρ is the density of air, C_p is the specific heat capacity of air. α_H and α_G are parameters to be determined from the observations and α_G is related to f by:

$$\alpha_G = (\frac{1}{f} - \frac{1}{2})\frac{u_* T_X}{h} \, , \tag{3.22}$$

To evaluate Equation (3.21) with our data we take for θ_R the 36-m potential temperature and for θ_i the 4-m potential temperature. From 238 daytime hourly values for the wind direction range [45-125°] we find $\alpha_H = 2.8 \pm 0.3$ and $\alpha_G = 8.6 \pm 0.9$ with a correlation coefficient $R^2 = 0.62$. Though the sensible heat flux is, in general, much larger than the storage heat flux, the effects of the two opposing processes are of comparable size. By applying Equation (3.22) together with the values for α_G and T_X derived above, we find a gust renewal fraction of 0.2, which is a relatively low value if compared to the value 0.5 found by W.Chen et al. (1997). This suggests that the presence of a dense crown layer substantially inhibits gust penetration to the forest trunk space.

3.8   Discussion and conclusions

In the present study observations of surface radiation temperature are analysed for a very dense Douglas-fir forest with a closed crown level. It is investigated to what

71

4 Nighttime convection in the interior of a dense Douglas fir forest.[*]

Abstract

Infrared radiative surface temperatures as observed over a dense Douglas fir forest during stable atmospheric conditions are analysed. It is shown that the concept of a single surface temperature to describe both the thermal coupling and the radiative coupling between atmosphere and forest fails when longwave cooling is large and wind speeds are low. In such cases a decoupling of the radiative surface temperature from the air temperature aloft is observed. Conditions for decoupling are formulated in terms of an appropriate Richardson number. It is shown that a convective surface temperature comes into play that is coupled to the forest interior air temperature. Observed radiative surface temperature is then composed of this convective surface temperature and the aerodynamic surface temperature. Forest interior air temperature during nighttime is, in general, lower than air temperature above the canopy. A simple two layer canopy model is used to explain this phenomenon in terms of the distribution of atmospheric sensible heat flux and storage heat flux over the two canopy layers.

Key words: Forest, Surface temperature, Radiative surface temperature, Convection, Nighttime, Trunk space.

4.1 Introduction

Surface temperature plays a crucial role in the description of energy transfer between the earth's surface and the atmosphere. The temperature at the interface between the canopy/soil system and the atmospheric air is more or less variable in space, depending on atmospheric conditions. Surface temperature here is defined as a weighted average of the temperatures over this interface. Conceptually, at least three different surface temperatures may be distinguished; the radiative surface temperature, $T_{S,R}$, at which the surface emits longwave radiation; the aerodynamic surface temperature, $T_{S,A}$, that determines the sensible heat transfer from the surface to the atmosphere, and the storage surface temperature, $T_{S,G}$, that drives the heat content of the soil and biomass. Each of these temperatures will differ in their

large forested area is 1.5 km. Coordinates are 52° 15' N and 5° 41' W, 52 m above sea level. The stand has a tree density of 785 trees ha⁻¹. The firs were planted in 1962 and in 1989, the year the measurements were performed, the trees had reached a mean height of 18 m and a mean diameter at breast height of 0.21 m. The single sided leaf area index (LAI) varies between 8 and 11 m^2 m^{-2} throughout the year (Evers et al., 1991). The forest floor is covered with a needle layer of 3 to 5 cm thickness, while understorey vegetation is almost absent; the trunk space extends to approximately 10-m height without many branches and needles. The topography is slightly undulating with height variations of 10 to 20 m over distances of 1 km. The forest consists of stands with typical dimension of a few hectares. In the neighbourhood of the research site the dominant stand species are Douglas fir, Beech, Japanese Lark and Scotch Pine. Upwind from the research site in the wind direction sector 45 to 125° the forest stands have comparable geometry as the local stand. In the other directions differences are larger. In this study only observations within the wind direction sector 45 to 125° are used. Bosveld (1997) discussed fetch conditions in relation to a footprint analysis based on the work of Leclerc and Thurtell (1990) and Schmid (1994). The source area in the method of Schmid (1994) is the area, with equal contributions at points of the boundary (an ellipse-like shape), from which 50% of the flux at the sensor location is derived. For the 30 m observation level, the distance of the most upstream point is at 200 m for $L = \infty$, at 300 m for $L = 200$ m, and at 750 m for $L = 50$ m. Thus observed fluxes are effectively an average over a number of upwind stands. For even more stable conditions the upstream point may well reach over the edge of the forest area. The study of Bosveld (1997) also showed that well defined flux-profile relations for momentum and temperature exist up to stabilities of $z/L = 1.0$, which covers almost all cases used in this study. This suggests that continuous turbulence exists for almost all cases.

Temperature and wind speed measurements were performed along an open mast at 4, 18, 24, 30 and 36-m height as indicated in Figure 4.1. The lowest level was in the trunk space of the forest interior. The 18 m level was at the tree tops. Eddy-covariance fluxes of temperature and horizontal momentum were measured at 30 m. Continuous observations were obtained during the period April-December 1989. Data were sampled at a rate of 1 Hz and reduced to 10-minute values. After quality control, data were averaged to hourly values. Corrections on the eddy-covariances were performed related to streamline tilt, low frequency loss, moisture influence on sonic temperature, and wind influence on sonic temperature as described in Bosveld (1997). Estimation of high frequency loss due to line averaging over the sonic path and sensor seperation was done on the basis of surface-layer spectra described by Kaimal et al. (1972). Even at atmospheric stabilities of $z/L = 1$ this loss is expected to be less than 2% and was therefore neglected.

Storage heat flux was not measured directly, but obtained by using a force restore model driven by the forest interior air temperature. The model is tuned on energy balance measurements during a number of nights. The model is described in
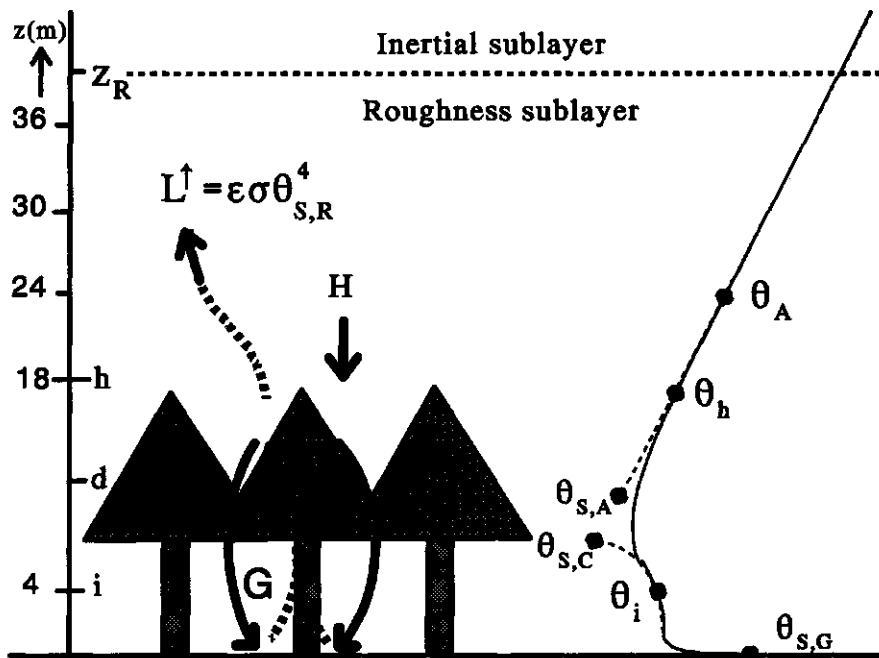
Figure 4.1. Conceptual graph and some defining quantities of the forest site. The indicated heights (z) refer to observation levels of temperature.

appendix 4.A.

Surface temperatures

Throughout this paper potential temperatures (θ) are used rather then temperatures (T). The reference pressure level is chosen at 12.5 m, which is the estimated effective source height of the infrared radiation. This height is just above the height where the crowns meet to form a closed cover. By choosing this reference level we are allowed to use the potential radiation temperature indiscriminately in radiation and in heat transfer calculations. In the following 'temperature' is understood to mean potential temperature unless otherwise stated.

Figure 4.1 shows the forest configuration. Four surface temperatures are indicated, namely $\theta_{S,R}$, $\theta_{S,A}$, $\theta_{S,C}$ and $\theta_{S,G}$, where $\theta_{S,R}$ is the observed radiative surface temperature, in the figure captured in the formula for longwave upward radiation ($L^\uparrow$), ε is emissivity and σ is the Boltzmann constant; $\theta_{S,A}$ is the aerodynamic surface temperature. This quantity is not measured but derived from extrapolation of the roughness sublayer air temperature profile to the displacement height (see below). As such it is a fictitious surface temperature. $\theta_{S,C}$ is the convective surface temperature. This, too, is a conceptual temperature and will also be defined below. Both conceptual surface temperatures are connected with, dashed indicated,

79
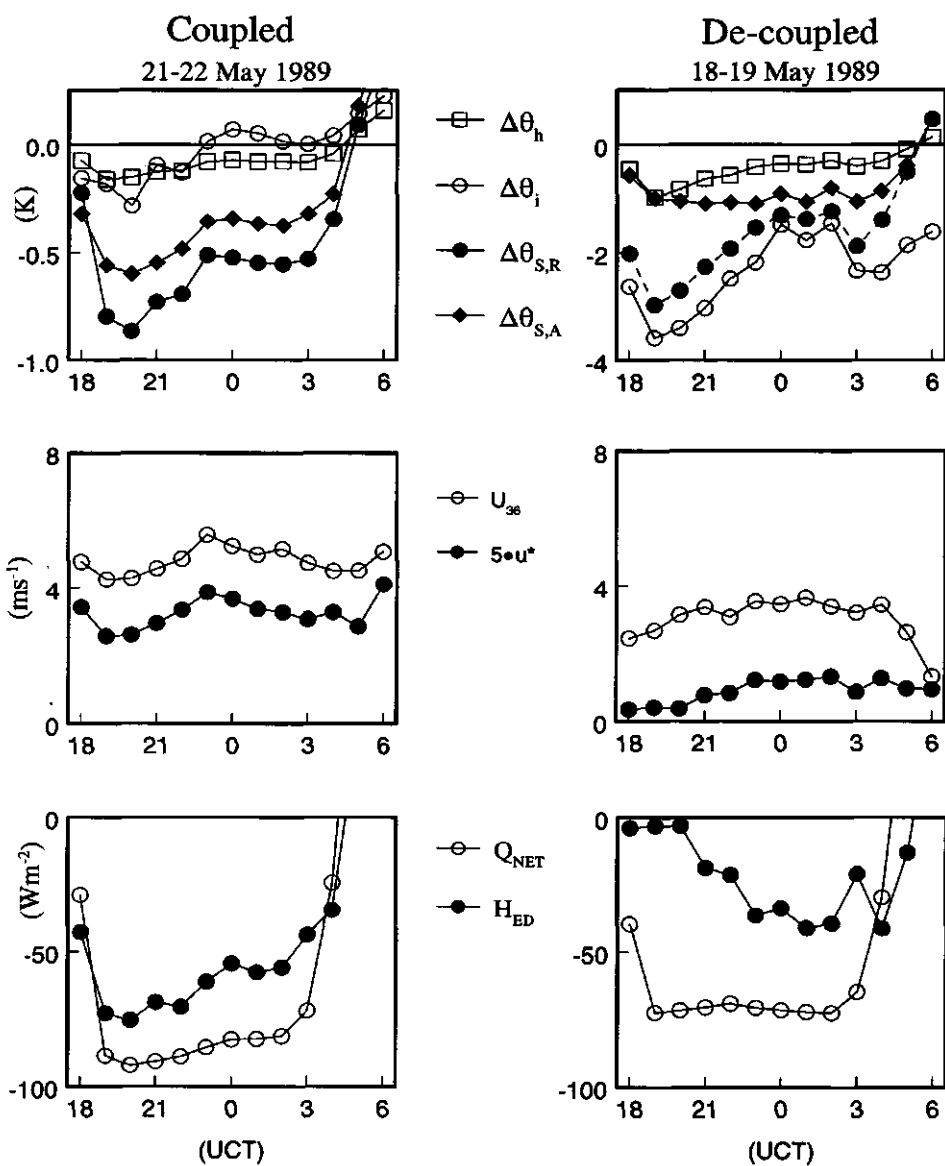
Figure 4.2. Potential temperature differences, wind speeds and surface fluxes for two clear nights. Left panels - high wind speed. Right panels - low wind speed.

82

that $\Delta\theta_{S,A}$ and $\Delta\theta_{S,R}$ agree within 0.3 K. We refer to this as a coupled case. Both u_* and H are relatively large and temperature differences are small indicating a good turbulent mixing in and above the forest. The right panels of Figure 4.2 show data for another clear night, net radiation is -75 Wm^{-2}, with low wind speed ($U_{36} = 3.5$ m s^{-1}). It is seen that θ_i starts to fall well below θ_h in the first few hours of the night. Note the difference in the ordinate scale between the coupled and the decoupled cases. $\theta_{S,R}$ follows θ_i, suggesting that there is good coupling between the forest trunk space and the crown level; $\theta_{S,A}$ follows θ_h. In this case $\theta_{S,R}$ is much lower than $\theta_{S,A}$. We refer to this as a decoupled case. Later in the night (2100 h) wind speed increases slightly. The result is that temperature differences become smaller and the pronounced decoupling disappears.
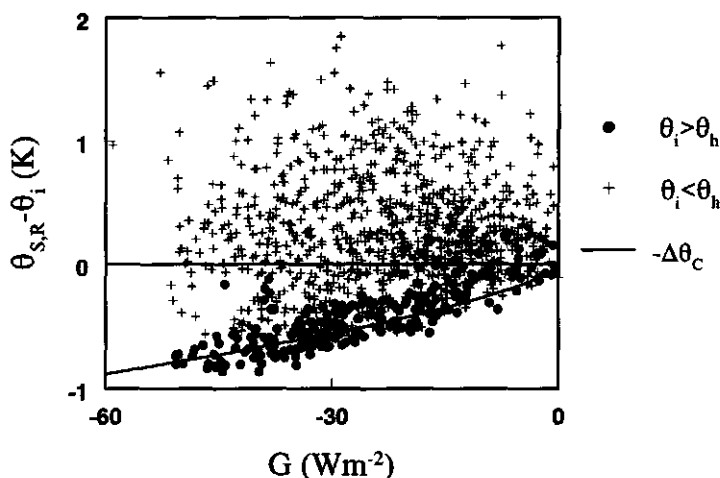
Figure 4.3. Difference between radiative ($\theta_{S,R}$) and forest interior (θ_i) temperature as a function of storage heat flux (G). Stability classification into temperature difference over the crown layer.

To investigate the relation between radiative surface temperature and forest interior air temperature, their difference ($\theta_{S,R}$-θ_i) is shown as a function of the storage heat flux, G (Figure 4.3). Hourly values with wind direction between 45 and 125° are shown. Data are stratified into stable ($\theta_i < \theta_h$) and unstable ($\theta_i > \theta_h$) forest interior air temperature relative to the air temperature at canopy height. There is a clear lower limit to the difference in radiative surface temperature and forest interior air temperature which is a function of the storage heat flux. The lower limit is approached when $\theta_i > \theta_h$. This suggests that, when the forest air is unstable relative
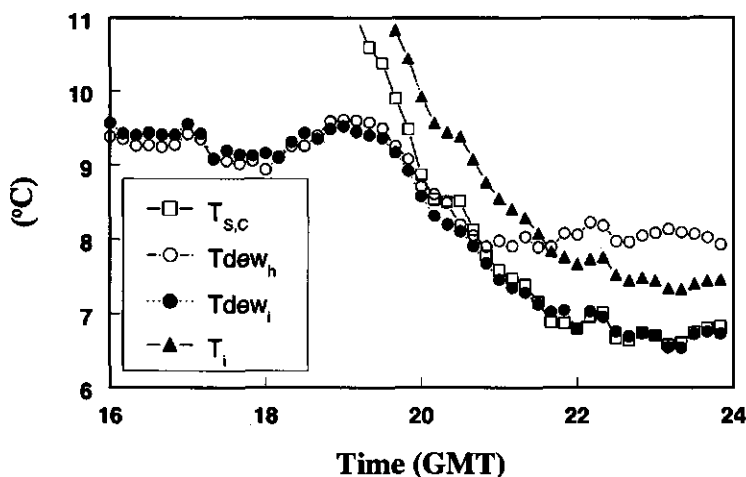
Figure 4.4. The impact of convective surface temperature on the dewpoint temperature in the forest interior during one night (3 May 1989).

stable stratification over the crown layer ($\theta_i < \theta_h$). Here we make use of the condensation properties of water vapour as detected by the wet bulb and dry bulb temperature sensors in and above the forest. Observations of dewpoints inside the forest ($Tdew_i$) and at the tree-top height ($Tdew_h$) are shown, together with air temperature inside the forest and convective surface temperature, for a night where air is close to saturation. Absolute temperature, instead of potential temperature, is used here to enable comparison with dewpoint temperatures. It is observed that air inside the forest does not become saturated despite continuously decreasing temperatures. The dew point inside the forest follows the convective surface temperature, leading eventually to a substantially lower dewpoint inside the forest than above the forest.

How can we explain this behaviour? Apparently air that is transported downward into the forest is cooled by parts of the crown. Simultaneously water vapour is condensed until the dewpoint is equal to the convective surface temperature. Thus it seems reasonable to assume that, also for a stable stratification over the crown layer ($\theta_i < \theta_h$), the convective surface temperature remains representative of the lower parts of the crowns. At least part of its behaviour is directly connected to radiative surface temperature. On the other hand, we might expect that the aerodynamic surface temperature, derived from the sensible heat flux from the atmosphere to the surface, is representative for the upper parts of the

86

crown, those parts that are in good aerodynamic contact with the air layer just above the forest.
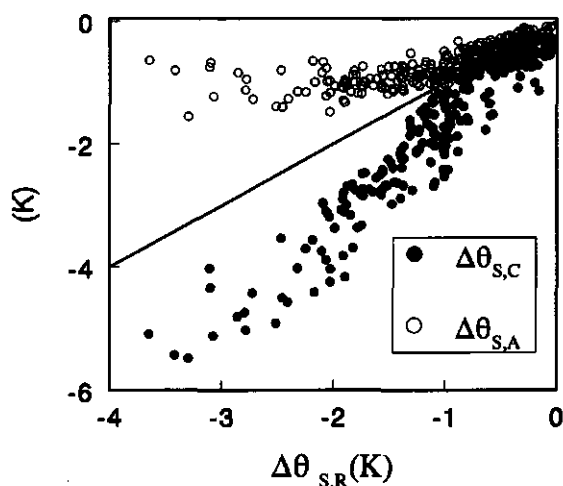
Figure 4.5. Aerodynamic ($\Delta\theta_{S,A}$) and convective temperature difference ($\Delta\theta_{S,C}$) as function of radiative surface temperature difference ($\Delta\theta_{S,R}$).

Figure 4.5 shows the aerodynamic surface temperature difference and the convective surface temperature difference as a function of radiative surface temperature difference. All temperatures are relative to the 24-m temperature. Only data with sufficient turbulence intensity ($u_* > 0.05$ m s^{-1}) are selected to ensure a well defined aerodynamic surface temperature. To ensure the absence of dewfall, which would increase the crown temperature, data are rejected with convective surface temperature less than 1 K higher than the dewpoint at the canopy top. From the figure it is seen that, for temperature differences smaller than 1 K, the three surface temperatures become approximately equal. These are the well mixed cases at higher wind speeds. For low wind speed and large longwave cooling the three temperatures diverge, and it can be inferred that the radiative surface temperature is approximately the average of the two other temperatures.

4.4 Towards an understanding of the exchange processes within the forest canopy.

Decoupling and convection

From the previous analysis it is clear that decoupling on clear nights preferably occurs at low wind speed. Decoupling can only occur if the forest interior air temperature is lower than the air temperature above the forest. This stable stratification then prevents mixing of the forest trunk space air with the air layers above the forest. This considerations leads to an aerodynamic Richardson number criterion for decoupling:

$$Ri_A = \frac{gh}{T} \cdot \frac{\theta_h - \theta_i}{u_*^2} \ , \tag{4.11}$$
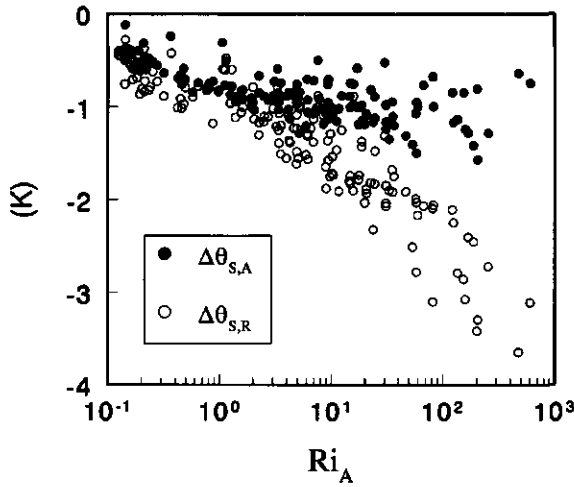
Figure 4.6. Aerodynamic ($\Delta\theta_{S,A}$) and radiative surface temperature difference ($\Delta\theta_{S,R}$) as a function of the aerodynamic Richardson number Ri_A.

where θ_h is temperature at canopy height and θ_i is forest interior air temperature. In Figure 4.6 radiative and aerodynamic surface temperaturea are shown as a function of this aerodynamic Richardson number. It is seen that decoupling occurs for $Ri_A \approx$ 2 and higher.

88

To predict the occurence of decoupling one would prefer a Richardson number Ri_{EXT} based upon external forcing parameters, i.e. wind speed at a reference height and longwave cooling. Ri_{EXT} would be expressed in terms of an effective radiation temperature difference between the surface and the clear sky. However, we found that Ri_{EXT} was less succesful in stratifying the data than Ri_A. This can be understood by realising that Ri_A is based upon parameters that describe conditions close to and inside the canopy. The critical value of Ri_{EXT} is found to be approximately 0.7; this corresponds with $Q_N \approx 5.5U_{36}^2$ where Q_N is expressed in W m^{-2} and U_{36} in m s^{-1}.

Nighttime longwave radiative cooling gives rise to stable stratification of the air layer above the forest. Gust generation is suppressed and other transport mechanisms must provide the coupling between the forest trunk space and the air layers aloft. At night the forest trunk space air was generally observed to be colder than the air above the forest. This is somewhat surprising since the trunk space air is close to the biomass and soil, which are the main sources of heat during night. Depending on the magnitude of the temperature jump over the crown layer, and depending on the wind speed just above the forest, smaller or larger parts of upper levels of the crown will be coupled to the aerodynamic surface temperature. On the other hand, depending on the convective velocity scale related to the convective process inside the forest, smaller or larger parts at the lower portion of the crowns will be coupled to the convective surface temperature. A convective Richardson number can be defined by:

$$Ri_C = \frac{gh}{T} \cdot \frac{\theta_h - \theta_i}{w_C^2} .$$
(4.12)

Here, w_C is the free convective velocity scale based on the storage heat flux, which is the flux that is transported through the trunk space:

$$w_C = \left(\frac{gh}{T} \frac{G}{\rho C_P} \right)^{1/3} .$$
(4.13)

To further explore the behaviour of the distinct temperatures, let us define a coefficient q that quantifies the relative contribution of the convective surface temperature and the aerodynamic surface temperature to the radiative surface temperature:

$$\theta_{S,R} = q\theta_{S,C} + (1 - q)\theta_{S,A} .$$
(4.14)

When these three temperatures are not too different it can be shown that a similar relation holds for the corresponding longwave radiative longwave fluxes. Thus, q can be interpreted as the surface fraction that radiates at the convective surface temperature. Conversely $1 - q$ is the surface fraction that radiates at the aerodynamic surface temperature.

We may expect that q is a function of atmospheric conditions. To explore

1.5

1.0

q

0.5

0.0

0   20   40   60

Ri_C

u_*/w_C

Δ   <0.5

+   0.5-1.2

●   >1.2

0.2
0.7
1.2
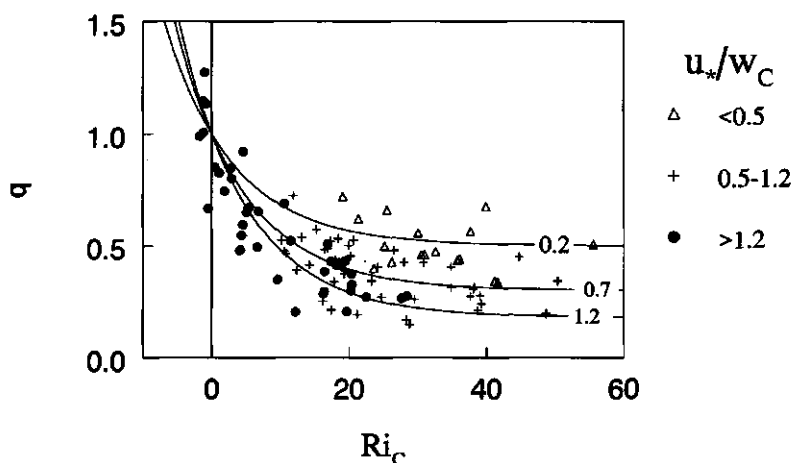
Figure 4.7. The surface fraction q as a function of convective Richardson number for different classes of u_*/w_C. Lines represent Equation (4.15).

this, Figure 4.7 shows q values as a function of the convective Richardson number Ri_C. Here, $\theta_{S,A}$ is derived from Equation (4.3), $\theta_{S,C}$ is derived from Equation (4.10) and $\theta_{S,R}$ is observed. A selection based on temperature differences larger than 0.3 K was made to reduce scatter due to uncertainties in the measurements. Data are stratified into classes of the ratio u_*/w_C, which is a measure of the dominance of the turbulence above the forest compared to the turbulence generated by convection inside the forest. Since the convective velocity scale is a rather weak function of heat flux inside the forest, Ri_C is dominated by the temperature jump over the crown layer. As such we observe that q shows a limiting behaviour for very stable stratification, with a limiting value q_∞ that is a function of u_*/w_C. When turbulence above the forest is dominant, q_∞ becomes small. This might be expected because turbulence above the forest will dominate in the crown layer, and thus the crown-layer temperature will be related to the air temperature above. For small values of Ri_C the value of q increases, an effect that is only fully observed in the data when turbulence intensity over the forest is high. These are typically the same cases as observed in Figure 4.3 for unstable stratification over the crown layer. It should be noted that temperature differences are small here (≈ 0.5 K), and likely the results are somewhat biased due to systematic calibration uncertainties for the different instruments. Nevertheless, if the convective eddies extend to the top of the trees or even higher, they are likely to disturb the temperature profile in a layer just above

the trees. This means that the extrapolation towards $\theta_{S,A}$ is in error. The disturbed layer will be cooler than assumed when calculating $\theta_{S,A}$ because of the influence of the convective surface temperature. When $\theta_{S,C}$ and $\theta_{S,R}$ are close to each other and deviate substantially from $\theta_{S,A}$ then q will approach 1 by definition.

It appears that q is well represented by:

$$q = q_\infty + (1-q_\infty) \, e^{-Ri_c/10}$$
$$q_\infty = 0.6 \, e^{-u_*/w_c} \tag{4.15}$$

Curves labelled with typical values for u_*/w_C, corresponding to the three classification classes are shown in Figure 4.7.

Nighttime energy balance of the canopy crown

As noted before q and $1 - q$ can be interpreted as surface fractions radiating at the convective surface temperature and aerodynamic surface temperature, respectively. Depending on the stratification and turbulence intensity above and below the crown level, a smaller or larger fraction q of the available energy is emitted as longwave radiation at the convective surface temperature coupled to the lower parts of the crown. A fraction $1 - q$ of the available energy is emitted as longwave radiation at the higher parts of the crowns at the aerodynamic surface temperature.

From the current analysis it is seen that, in general, the convective surface temperature is lower than the aerodynamic surface temperature. How is this to be explained? The assumption that only the storage heat flux is converted at the lower crown level, and the atmospheric sensible heat flux is converted at the top crown level leads to a contradiction for low wind speed situations where H approaches zero. In this case the crown tops would be in radiative balance with the downward longwave radiation of the sky and the upward longwave radiation of the lower crown layer. The aerodynamic surface temperature would fall perhaps 5 to 8 kelvin below the air temperature. This is clearly not observed. We therefore must assume that part of the storage heat flux is transported to the higher levels and probably part of the sensible heat flux is transported to the lower levels of the crown before being emitted as longwave radiation.

To estimate the degree of mixing of these fluxes we explore a simple two layer model outlined in Figure 4.8. The lowest layer, the convective crown layer, is at temperature $\theta_{S,C}$. The top layer, the aerodynamic crown layer, occupies a projected surface fraction $1 - q$ and is at temperature $\theta_{S,A}$. The sky is assumed to radiate downward with an effective temperature T_{sky}. Depending on the dominance of the convection from below, or the turbulence from above, the interface between the two layers shifts through the crown, changing the surface fraction q and thus the relative contribution of the two temperatures to the radiative surface temperature.

For both layers an energy balance equation can be given. Here the radiation terms are linearised and B is the derivative of the Stefan-Boltzmann blackbody emission with respect to temperature. The energy balance for the lowest layer is
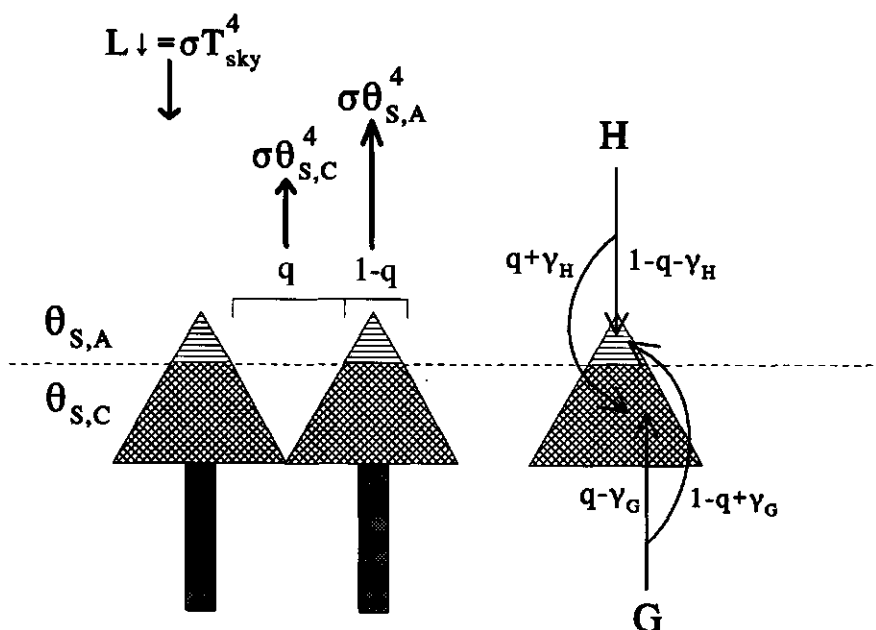
Figure 4.8. Two-layer model to explain temperature separation between forest interior and aerodynamic surface temperatures due to partitioning of sensible heat flux and storage heat flux.

given by:

$$B \cdot \left[qT_{sky} + (1-q)\theta_{S,A} - \theta_{S,C} \right] = (q - \gamma_G) \ G + (q + \gamma_H) \ H \ . \tag{4.16}$$

where the first two terms on the l.h.s. represent the longwave radiation received from the sky and the upper layer respectively. The third term on the l.h.s. is the loss due to longwave radiation. It is assumed that downward longwave radiation from this layer is in balance with the upward radiation from the soil and biomass. The terms on the r.h.s. represent the heat fluxes received from the soil/biomass system and the atmosphere, respectively (note that G and H are negative during nighttime). γ_G and γ_H are the coefficients of separation for G and H respectively. The coefficients are zero when both heat fluxes are distributed over the two layers proportional to their active radiative surface fractions q and $1 - q$ respectively. When $\gamma_G > 0$ this means that a larger fraction (i.e $1 - q + \gamma_G$) of G is released at the top layer. Similarly, $\gamma_H > 0$ means that a larger fraction (i.e. $q + \gamma_H$) of H is released at the lower layer. Here emissivity is taken 1, which seems reasonable for the current forest (see Bosveld et al., 1999a). For the top layer we find analogously:

$$B \left[(1-q)T_{sky} + (1-q)\theta_{S,C} - 2(1-q)\theta_{S,A} \right] = (1 - q + \gamma_G)G + (1 - q - \gamma_H)H \ . \tag{4.17}$$

Summing the Equations (4.16) and (4.17) leads to the energy balance

equation for the system as a whole. Eliminating T_{sky} leads to an expression for the temperature difference between the aerodynamic crown layer and the convective crown layer:

$$B \cdot (1 - q^2) \cdot (\theta_{S,A} - \theta_{S,C}) = -\gamma_G \, G + \gamma_H \, H \, . \tag{4.18}$$

In general, G is larger than H in an absolute sense and thus this simple model will give a positive temperature difference if $\gamma_G \geq \gamma_H \geq 0$. This means that a positive temperature difference can be explained if more than a fraction $1 - q$ of the generated storage heat flux is released at the top crown layer. Figure 4.9 shows the
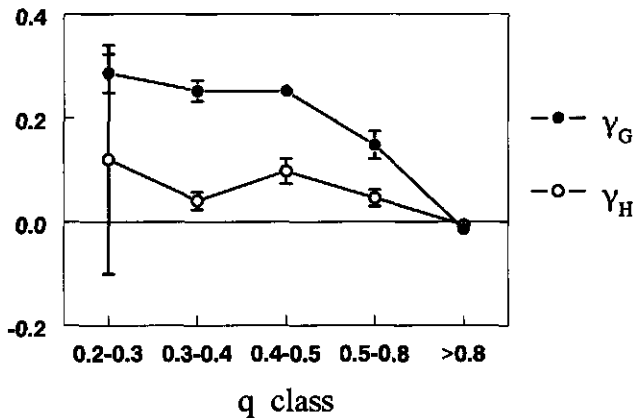
Figure 4.9. Separation coefficients (γ_G and γ_H) of the two layer model as a function of surface fraction q.

separation coefficients derived from a regression on Equation (4.18) for different classes of q. It is observed that γ_H deviates only slightly from zero. This means that sensible heat flux is distributed over the two canopy layers almost in proportion to their exposed surfaces. γ_G, however, is positive for most q classes. Thus, a more than proportional fraction of storage heat flux is transported to the top layers of the crown.

Figure 4.9 suggests that the relations between q and γ_H and between q and γ_G are both proportional to $(1 - q^2)$, the factor appearing in the l.h.s. of Equation (4.18). This means that the temperature difference can be rewritten in the form:

$$\theta_{S,A} - \theta_{S,C} = \frac{-0.3 \, G + 0.1 \, H}{B} \, , \tag{4.19}$$
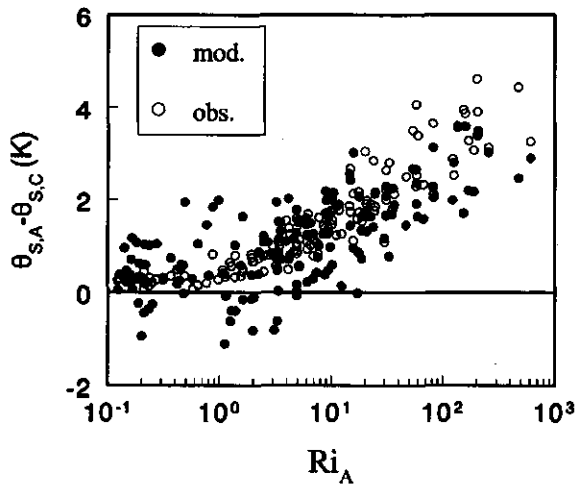
Figure 4.10. Difference of aerodynamic and convective surface temperature as a function of the aerodynamic Richardson number.

where the empirical factors 0.3 and 0.1 are estimated from Figure 4.9. Note that the values of $\gamma_G/(1 - q^2)$ and $\gamma_H/(1 - q^2)$ in Equation (4.19) are mainly based on decoupled cases ($q < 0.8$). For the coupled cases they are difficult to determine, since the flow regime inside the forest will be different and thus different values for the empirical factors are likely to apply. In Figure 4.10 the differences between aerodynamic and convective surface temperature are shown as a function of the aerodynamic Richardson number. Observed values are derived from the measurements by applying Equations (4.3) and (4.10), model values are calculated from Equation (4.19). It is seen that values compare reasonably well. For $Ri_A < 2$, the coupled cases, the modelled data become scattered but not in contradiction with the observations. However, an estimate with less scatter for coupled cases is found by simply taking the temperature difference to be zero. Interestingly, the relation $G = H/3$, which is obtained from Equation (4.19) for coupled cases with zero temperature difference, is the same as found by Berkowicz and Prahm (1982) for low vegetation.

94

4.5   Conclusions

In this study we investigated the behaviour of radiative surface temperature in relation to other temperatures for a very dense Douglas-fir forest. A description of energy exchange with a single surface temperature breaks down when wind speed is low and longwave cooling is large, i.e. clear sky conditions. This decoupling of the radiative surface temperature from the aerodynamic surface temperature is governed by an aerodynamic Richardson number based on the turbulence intensity above the forest and the vertical temperature difference over the crown layer. Using a Richardson number based on external forcing parameters, longwave cooling and wind speed at 36 m, a poorer stratification of the data is obtained. Nevertheless a critical value can be defined.

To explain the observed radiative surface temperatures, a third surface temperature needs to be introduced. This 'convective' surface temperature is related to the process of mixing in the forest trunk space driven by radiative cooling of the crowns. It is related to the forest interior air temperature through a convective temperature difference based on the storage heat flux. The radiative surface temperature is a combination of the aerodynamic surface temperature and the convective surface temperature.

The analysis suggests that the aerodynamic surface temperature is coupled to the top crown layer whereas the convective surface temperature is coupled to the lower crown layer. Depending on the turbulence intensity above the forest, the convective turbulence intensity in the trunk space and the temperature difference over the crown layer, the relative contribution of both surface temperatures to the radiative surface temperature changes. This suggests that the vertical position of the interface between the two layers changes, resulting in changing surface fractions.

Based on these considerations a simple two-layer radiation/energy model is constructed. This model allows for a distribution of atmospheric sensible heat and storage heat over the two layers. The top layer is termed the aerodynamic crown layer and the lowest layer is termed the convective crown layer. The observation that forest interior air temperature is, in general, lower than the air temperature above the forest can be explained by the model if it is assumed that a large fraction of the storage heat flux is released in the aerodynamic crown layer.

This takes us back to Figure 4.1 where arrows through the crown layer are drawn to illustrate the redistribution of heat between the layers inside the forest. Since cooling of the convective layer will mainly occur in the gaps of the aerodynamic crown layer, downdraughts will occur through these gaps. The updraughts that have taken up storage heat will penetrate through the centre of the trees directly into the aerodynamic crown layer. Since these organised movements are tied to the geometry of the forest they are unlikely to be fully captured by point measurements inside the forest.

From the material presented in this paper it is clear that modelling of the interaction between the canopy and the atmosphere under stable atmospheric conditions is not at all straightforward. The radiative flux, the soil heat flux and

atmospheric fluxes are all of the same order of magnitude under such conditions. Moreover, the exchange efficiency of the atmosphere is very sensitive to slight changes in these fluxes. This study shows that the process of canopy convection has a clear impact on the radiation and energy balance and therefore is expected to be relevant in the description of nighttime canopy/atmosphere interaction in numerical weather prediction and climate models for regions where forest dominate.

4.A   Modelling heat storage in biomass and soil

In this study the biomass and soil heat flux are modelled by a heat storage model that is forced by the 4 m air temperature in the trunk space of the forest. The bio-geometrical measurements (Jans et al., 1994) show that almost all the biomass is concentrated in the tree stems. Most of the biomass is below the level at which the crowns touch. Below this level the solar irradiation is low and the net longwave radiation will be low as well. This justifies the use of the air temperature at 4 m as the forcing temperature for the biomass and soil heat flux.

Following Meester and Vugts (1996), we represent the trees by homogeneous cylinders with height h and radius r. Searching for exponential damped solutions of the heat conduction equation forced by a temperature T_0, we arrive at a series of differential equations, indexed by n, for the storage heat flux

$$\frac{dG_n}{dt} = -\frac{G_n}{\tau_n} - \frac{2\lambda}{r}\frac{dT_0}{dt} ,$$ (4.20)

where λ is the thermal conductivity and the damping times are given by

$$\tau_n = \frac{r^2}{ax_n} ,$$ (4.21)

where a is the kinematic diffusivity and x_n is the nth zero point of the zero order Bessel function of the first kind. The biomass heat flux is obtained by summing Equation (4.20) over n.

For the soil heat flux we have to solve the temperature diffusion equation for a half infinite medium. This problem is less straightforward to solve because the damping times now form a continuum. If we, however, realise that our interest is only in time scales of one day or less, we can solve for a finite layer of soil that has a thickness substantially larger then the penetration depth of the diurnal temperature wave into the soil. If we define, now, r to be the depth of the soil layer and apply a zero-flux lower boundary condition we arrive at exactly the same equations as for the cylindrical case except that now x_n are the zero points of the cosine function.

In our situation we are interested in expressing the time averaged storage heat flux in terms of the storage heat flux at the previous time step and the temperature difference between the current and the previous average temperature. -

By applying a Laplace transform to the differential equations we obtain explicit forms of the storage heat flux components. By averaging these equations over the time step interval we arrive at:

$$<G_n>(t+T)=<G_n>(t)\ e^{-T/\tau_n}\ +\ \frac{2\lambda}{r}\frac{1-e^{-T/\tau_n}}{T/\tau_n}(<T>(t+T)-<T>(t))\qquad(4.22)$$

The second factor in the second term at the rhs reflects the effect of averaging. It acts as a low pass filter for variations in the temperature.

The storage heat fluxes thus calculated are for unit area of heat transporting surface. Here we are interested in heat flux per unit horizontal area. This means that for the biomass heat flux a factor of 0.8 has to be applied. From soil characterisations (Tiktak and Bouten, 1990) and wood characterisation (De Korte, 1990), and using the method of De Vries (1966) for estimating soil heat conductivity from soil classification, we arrive at the following thermal parameters for the current forest: $C_h(\text{soil}) = 1.85$ MJ m^{-3} K^{-1}, $C_h(\text{biomass}) = 2.71$ MJ m^{-3} K^{-1}, $\lambda(\text{soil}) = 1.0$ W m^{-1} K^{-1} and $\lambda(\text{biomass}) = 0.38$ W m^{-1} K^{-1}.
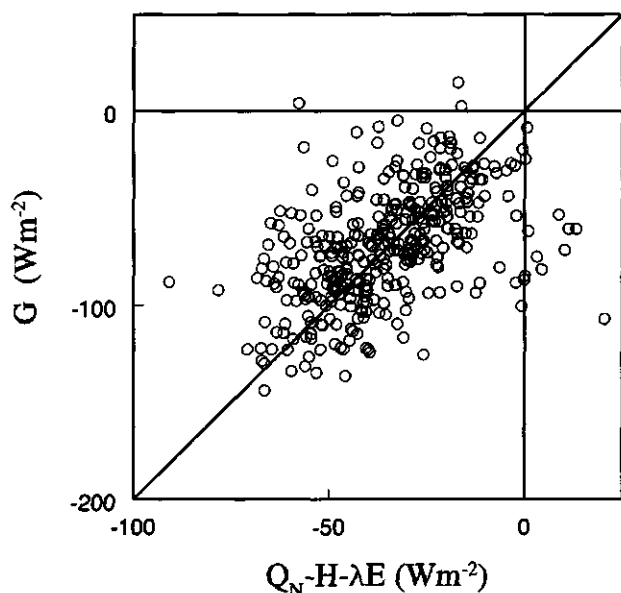
Figure 4.11. Modelled storage heat flux as function of observed residual in the surface energy fluxes for nighttime conditions.

The actual temperature at the soil and biomass surface may be different due to the presence of a litter layer on the soil and the bark around the stems and because of an aerodynamic resistance between the free trunk air space and the surfaces. All these factors lead to an overestimation of the actual storage heat flux

97

by the model. Moreover soil thermal parameters vary with soil water content. The model was compared with nighttime observations of the residual of the energy components, $Q_N - H - \lambda E$, where Q_N is net radiation and λE is latent heat flux. Forty-two dry days were selected. Daytime cases are excluded because the storage heat flux is, in general, much smaller than the other fluxes and thus residuals show large scatter. It was found that the model overestimates storage heat flux by a factor of two. The model was adapted accordingly. Figure 4.11 shows the adapted modelled storage heat flux as a function of the nighttime energy balance residuals.

5   Evaluation of transpiration models with observations over a Douglas fir forest.[*]

Abstract

Hourly observations of eddy-correlation water vapour fluxes obtained over a Douglas-fir forest are used to evaluate three transpiration models. The models are 1) a modified Priestley-Taylor formula, 2) the Penman-Monteith model with a Jarvis type of formulation for the canopy resistance, including an explicit function for water vapour deficit and 3) the Penman-Monteith model in which the water vapour deficit response is replaced by a response to transpiration rate itself as described by Monteith (1995). Model parameters are optimised against the observations of 41 dry days spread over the growing season of the forest. Root mean square values of the residuals are approximately 21 W m^{-2}. This is to be compared with a lower bound of 17 W m^{-2} estimated from the atmospheric statistics of the eddy-correlation observations. Distinct responses to the water vapour deficit, solar radiation, soil water potential and shoot growth are found. No temperature response was found. The response to soil water potential seems to disappear after day number 203, probably as a result of adaptation of the root system. The response of transpiration to an increase of leaf area index during shoot growth suggests that the transpiration from new shoots is twice as high as that from older shoots. However, other physiological changes at the start of the growing season may play a role as well. Systematic differences between model and observed transpiration could be related to specific wind directions. These deviations correspond with deviations found in the observed energy balance for the same wind directions. An analysis of residuals shows that the Jarvis model gives good results for all conditions encountered. It is shown that the Monteith model can be formulated such that it is almost equal to the Jarvis model for this aerodynamically rough forest. Despite its simple formulation a modified Priestley-Taylor formula (including LAI and soil water potential response) gives reasonable results, although at moderate irradiation and high water vapour deficit deviations are significant. A comparison with results from another coniferous forest (Thetford forest) shows that transpiration rates are approximately the same despite large differences in *LAI*.

Keywords: *transpiration, Douglas fir trees, eddy correlation, Penman-Monteith equation, energy balance.*

5.1   Introduction

Quantitative information on the response of forest transpiration to changing environmental factors is relevant for forestry, water management, air pollution research and climate research. Transpiration of forests depends on external factors such as atmospheric conditions and soil water status and on internal factors such as tree physiological and biometrical conditions. Stomatal response is the main mechanism through which a tree can regulate CO_2 and H_2O exchange with the ambient atmosphere. Assimilation is driven by solar radiation, whereas transpiration is mainly driven by water vapour deficit. Since these two quantities are positively correlated the tree will have difficulty in assimilating CO_2 while keeping water loss within acceptable bounds.

Forest transpiration is often modelled in terms of the single big leaf approach based on the Penman-Monteith equation (Monteith, 1965). The use of such an approach has been very successful (Raupach and Finnigan, 1988). Formulations of such models differ in the way canopy resistance is described as function of the external conditions. One way is to parametrise canopy conductance by a product of response functions as suggested by Jarvis (1976), an approach commonly used in various forms nowadays. Monteith (1995) introduced a direct coupling between canopy resistance and the rate of water transport through the plant. This eliminates the necessity to prescribe a moisture deficit response function for which there seems to be no plant physiological basis (Monteith, 1995; Mott and Parkhurst, 1991). For large scale climate models these formulations have the disadvantage that one has to know a large number of parameters for each species. A model with less parameters is based on the Priestley-Taylor formula (Priestley and Taylor, 1972). De Bruin and Holtslag (1982) show that with certain approximations the Penman-Monteith equation leads to a modified version of the Priestley-Taylor equation.

The aim of the present study is to evaluate the performance of the transpiration models of Jarvis (1976), Monteith (1995) and Priestley and Taylor (1972). This is done on the basis of 43 dry days of eddy-correlation transpiration measurements taken over a moderately homogeneous coniferous forest. Emphasis is on the diurnal variation as well as on the seasonal variation of transpiration.

5.2   Materials and methods

Research site

The research was carried out in a 2.5 ha Douglas fir plantation, located within a large forested area in the Netherlands. Climate is maritime with rain throughout the year. Yearly rainfall is typically 800 mm. The stand has a tree density of 785 trees

ha^{-1}. The firs were planted in 1962. In 1989, the year that the measurements were performed, the trees had reached a mean height of 18 m and a mean diameter at breast height of 0.21 m. The leaf area index amounts to 11 (Evers et al., 1991). The average fine root length amounts to 19.10^6 m ha^{-1} of which almost 90% is situated in the topsoil to a depth of 0.4 m (Olsthoorn, 1991). The soils are classified as Typic Distocrepts on ice-pushed sandy loam and loamy sand textured river sediments. The soils are well drained with a ground water table at a depth of 40 m (Tiktak and Bouten, 1994).

The topography is slightly undulating with height variation of 10 to 20 m over distances of 1 km. The area is divided in stands with typical dimension of a few hectares. In the neighbourhood the dominant stand species are Douglas fir, Beech, Japanese Larch and Scotch Pine. A small clearing is situated just North of the mast. Larger clearings are situated 1 km to the south east of the mast and at more than 2 km South West of the mast. The edge of a large heather area is at a distance of 1.5 km to the East. In all other directions the forest extends for more than 3 km.

In a study on the relation between fluxes and profiles for this site, Bosveld (1997) shows that footprints for eddy correlation measurements performed at 20 m above the displacement height reach well over the borders of the local stand except for the most unstable conditions and Easterly wind direction. Thus, the site must be considered as inhomogeneous with respect to tree species.

The measurements

Measurements were performed continuously during the period April-September 1989. The micro-meteorological measurements were performed on a 36 m high guyed mast. Sensible heat flux was measured with a sonic anemometer-thermometer system (DAT-300, Probe TR61A, Kaijo Denky Co., Tokyo, Japan) at 30 m above the forest floor. Configuration and corrections are described in Bosveld (1997). Eddy correlation latent heat fluxes were derived from a fast response Ly-α hygrometer (BLR, Electro Magnetic Research Corporation, Rockville, USA) mounted approximately 30 cm below the sensor volume of the sonic anemometer. Calibration was performed in a climate chamber. Calibration before and after the measuring campaign differed from 5-10% depending on the specific humidity of the air. An in-situ calibration curve was derived by comparing psychrometer measurements, which were performed during the whole campaign at 31 m height, with Ly-α hygrometer output. It was found that this curve more closely resembled the latest laboratory calibration. It was decided to use this latest laboratory calibration for the whole period. Latent heat flux observations were corrected for temperature flux (Webb et al., 1980). Corrections for high and low frequency losses in the latent heat flux measurements are performed analogously to the sensible heat flux corrections described in Bosveld (1997). Latent heat flux is corrected for water vapour storage between the crown level and the observation height.

Profiles of wind, temperature and humidity are measured at 4, 18, 24, 31 and

101

36 m height. Temperature and humidity were measured with ventilated and shielded dry bulb and wet bulb sensors manufactured at KNMI (Slob, 1978). Wind speed was measured with three-cup anemometers developed at the Agricultural University of Wageningen. Rain amounts were obtained at a nearby clearing. A rain indicator was operated at the top of the mast.

Short wave incoming radiation was measured with a pyranometer (CM11, Kipp en Zonen, Delft, the Netherlands). Net radiation was measured with a net pyrradiometer (Funk CN1, Middleton Instruments, Australia). The instrument was mounted on a 2.5 m long boom extending outside the mast at 36 m above the forest floor. To keep temperature differences over the instrument low and to prevent dew formation on the domes the instrument was ventilated. Short wave calibration of both the Kipp instrument and Funk instrument is performed regularly at KNMI. The long wave calibration factor for the net radiometer is assumed to be the same as the short wave calibration factor. It was discovered afterwards that the net radiation instrument was tilted approximately 4 degrees during the measuring campaign. Measurements were corrected on the basis of estimated direct solar radiation. Direct solar radiation was estimated from 10 minute average total short wave incoming radiation measurements.

Instruments were inspected and cleaned at least every week. Signals were sampled at 1 Hz. Data reduction to 10 minute averages, standard deviations and covariances were performed on-line. These values were screened by means of graphical presentations. Finally hourly mean values were calculated.

Soil water potential was derived from a combination of soil water measurements and the soil hydrological model SWIF (Tiktak and Bouten, 1992 and 1994). The measurements were performed with time domain reflectometry (Heimovaara and Bouten, 1990), tensiometer readings and neutron probe. The soil hydrological model was used to assimilate the measurements, to generalise the measurements to stand average values and to interpolate in time. To obtain a soil water potential which is representative for the root zone of the forest, vertical profiles (logarithmic values) were weighted with the root density profile as given by Olsthoorn (1991).

Direct measurements of the storage heat flux into the biomass and soil are lacking. Bosveld et al. (1999) describe a storage heat flux model which is forced by the forest interior air temperature. The thermal parameters in the model are estimated from nighttime energy balance measurements.

In total 43 dry days are selected for which all relevant quantities are available for the whole day. Small gaps were filled by interpolation or by using redundancy in the data. The detection of dryness was done on the basis of rain indicator observations. In Figure 5.1 soil water pressure heads and daily rain amounts are shown for the period DOY = 90-270. Below the x-axis of the rain panel the selected dry days are indicated.

Energy balance
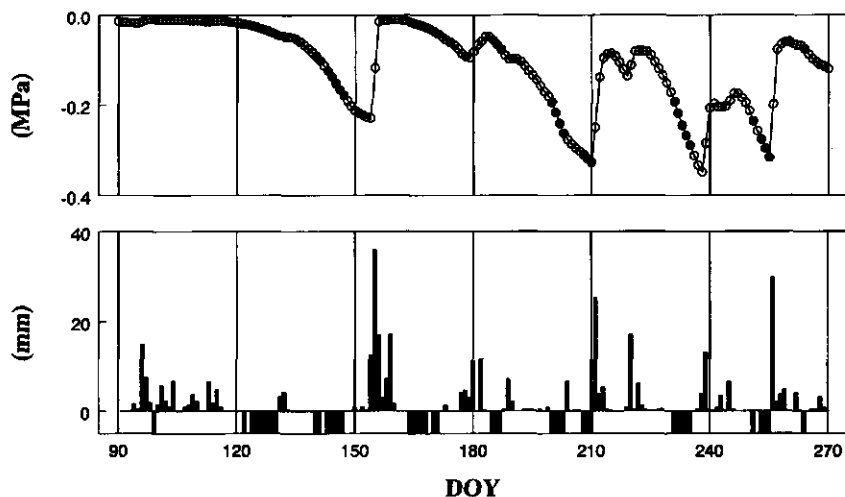
Figure 5.1. Daily soil water pressure heads and rain amounts. The 43 selected days are indicated in the upper panel by solid dots and in the lower panel below the rain x-axis.

To test the quality of the observations the energy balance is analysed. Figure 5.2 shows the daily average available energy and the average total turbulent heat flux for the 43 selected days. Successive periods are labelled with their start day number of the year (*DOY*). Remarkably high turbulent heat flux are found for *DOY* = 128 and 234. These are days when wind direction was between 240 and 270°. This suggests that advection effects related to horizontal inhomogeneities leads, at times, to deviations from a zero energy balance. These two days are deleted from the data set. Systematic different biasses occur in spring and fall as compared to the summer observations. For the remaining 41 days, available energy is on average 1% lower than total heat flux. From the observed CO_2 fluxes by Vermetten et al.(1994) for the same location and year we find that net CO_2 exchange consumes another 2% of the available energy. This leaves us with an imbalance of 3% in the surface energy, a value comparable to estimated accuracy of the measuring system. Overall accuracy is influenced by instrumental properties like calibration accuracy, drift of Ly-α calibration and behaviour of net radiometer at high irradiation. Advection as well as different footprints of the net radiation sensor and the eddy correlation system may play a role as well.
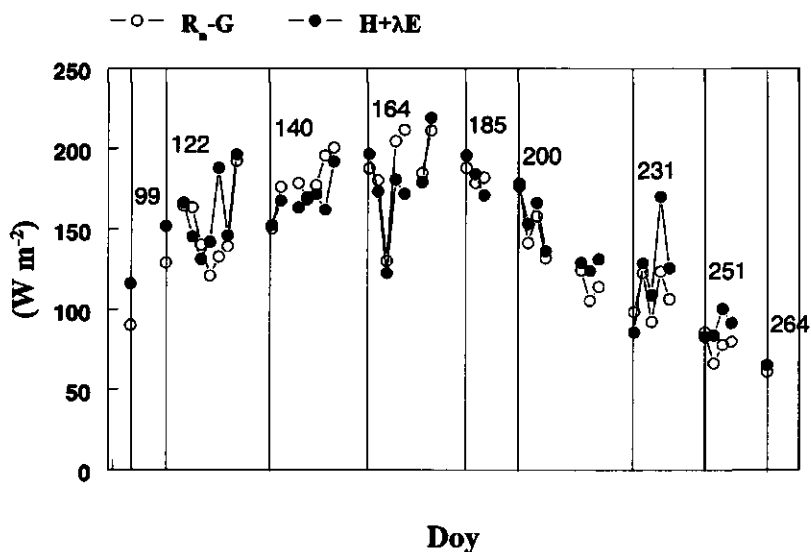
Figure 5.2. Daily average values of the available energy R_n-G and the total turbulent heat flux $H+\lambda E$ as function of day of the year for the 43 selected days.

5.3   Canopy transpiration models

Modelling plant transpiration rates involves the prescription of parameters. Parameters depend on vegetation type and even for the same plant species these parameters may depend on climate regime and soil type. Preferably the parameters should have a clear plant physiological meaning to make generalisations possible. To be of practical use, one has to compromise with the necessity to minimise the number of parameters.

The Penman-Monteith equation gives a framework in which the influences of atmosphere and the plant/soil system on transpiration are clearly separated. Originally the Penman equation was derived to model the evaporation of open water (Penman, 1948). To apply the equation for vegetation Monteith (1965) modified it by introducing the canopy resistance. This equation serves as a starting point for many formulations of transpiration. It reads:

$$\lambda E = \frac{s(R_n - G) + \rho C_p D g_a}{s + \gamma (1 + g_a/g_s)} \tag{5.1}$$

where λE is latent heat flux, s the derivative of the saturated water vapour curve, $\mathbf{R}_n$ the net radiation, G the storage heat flux, ρ the density of air, C_p the specific heat capacity of air, D the specific water vapour deficit at the reference level, γ the

psychrometric constant and g_S the surface conductance for water vapour. g_a is the aerodynamic conductance from the canopy to the reference level for scalar quantities. Here it is assumed that the g_a's for temperature and moisture are equal.

The surface conductance for dry cases is composed of the stand scale canopy conductance g_C and a conductance g_0 which remains when the stomata are closed:

$$g_S = g_C + g_0 \tag{5.2}$$

g_0 is related to cuticular transport of water vapour and to forest floor evaporation.

The Jarvis-model

Tan and Black (1976) have shown that the stand scale canopy conductance of a Douglas fir forest is to a large extent determined by the stomatal conductance of the needles. Hence, the stand scale stomatal conductance depends on the same variables as needle stomatal conductance. This stomatal conductance is often modelled as a product of response functions f_i (Jarvis, 1976; Stewart, 1988). In the present study g_C is assumed to be determined by leaf area index *LAI*, modelled as a function of day of the year, by specific water vapour deficit D, by solar radiation R_s, by air temperature T and by soil water potential ψ according to:

$$g_C = g_{C,ref}\, f_L(DOY)\, f_D(D)\, f_R(R_s)\, f_T(T)\, f_\psi(\psi) \tag{5.3}$$

where the f_i are response function which attain a value of 1 at a certain reference value of the argument and $g_{C,ref}$ is a free parameter to be optimised, representing the canopy conductance at reference conditions.

The Monteith-model

Monteith (1995) introduced a direct coupling between stomatal conductance and the transpiration flux instead of prescribing a dependence on water vapour deficit. On the basis of studies on leaf level resistances of a variety of species he arrives at a particularly simple relation:

$$\frac{g_C}{g_m} = 1 - \frac{\lambda E}{\lambda E_m} \tag{5.4}$$

where g_m is an asymptotic conductance when no transpiration occurs, i.e when $D = 0$. λE_m is an asymptotic maximum latent heat flux occurring when atmospheric demand is maximal. The relation may breakdown at large atmospheric demand when soil is too dry to sustain a reasonable rate of transpiration or it may break down at low atmospheric demand when stomatal opening has reached its maximum value. This formulation makes the Penman-Monteith equation an implicit equation, quadratic in the latent heat flux. At this stage it is not clear how the response functions should be distributed over the parameters g_m and λE_m. This is explored in the next section. In principle λE in Equation (5.4) refers to the transpiration through

stomata. The residual latent heat flux through cuticula and from forest floor evaporation is modelled with the Penman-Monteith equation and a surface resistance g_0. The two fluxes are simply added, a procedure which is legitimate as long as aerodynamic transport resistances and temperature differences in the forest are small.

The modified Priestley-Taylor equation

Although conceptually attractive, the Penman-Monteith equation has a disadvantage from the perspective of atmospheric modellers who look at grid box averaged fluxes and their interaction with the boundary layer. First a strong dependence of latent heat flux on moisture deficit is introduced with the ventilation term, and then this strong reaction is damped by the response of the stomatal conductance. In the Jarvis-model this response is explicitly described; in the Monteith-model it is implicitly present through the response to transpiration. In many practical situations where soil water is not limiting, transpiration is a rather conservative quantity which seems to be primarily determined by the available energy. This is expressed by Priestley and Taylor (1972) in what has become known as the Priestley-Taylor equation. In a modified form introduced by De Bruin and Holtslag (1982) it reads:

$$\lambda E = \alpha \left(\frac{s}{s + \gamma} (R_n - G) + \beta_C \right) \tag{5.5}$$

where α is a parameter which depends on species and on the soil water availability and β_C is a constant transpiration flux accounting for the observation that transpiration proceeds, even when available energy becomes zero. A refinement is given in Van Ulden and Holtslag (1985) who model the latter effect by accounting for the ventilation by dry air. Here we combine the two approaches in the form

$$\lambda E = \alpha_m f_L(DOY) f_\psi(\psi) \left(\frac{s}{s + \gamma} (R_n - G) + \beta_V \rho \lambda D_d u_* + \beta_C \right) \tag{5.6}$$

where α_m is the maximum value of α when soil water is not limiting, β_V is the ventilation coefficient, u_* is friction velocity and D_d is the portion of the specific moisture deficit that is not-correlated with the available energy.

Specification of the response functions

Due to shoot growth and needle fall, the *LAI* changes throughout the year. From in-situ observation and from micro-wave transmission measurements (Tiktak et al., 1990) it was observed that shoot growth starts around day number 130 and ends around day number 180. New needles may have different stomatal conductance than older needles. Here we assume a piece-wise linear form for the growth curve:

$$f_L(DOY) = 1 - \Delta L \ (DOY + 185)/315 \qquad 0 \leq DOY < 130$$
$$f_L(DOY) = 1 - \Delta L \ (180 - DOY)/50 \qquad 130 \leq DOY \leq 180 \qquad (5.7)$$
$$f_L(DOY) = 1 - \Delta L \ (DOY - 180)/315 \qquad 180 \leq DOY \leq 365$$

where ΔL, a free parameter of the model, is the relative amplitude of the LAI response. The function is 1 when LAI is at its maximum at $DOY = 180$.

Figure 5.3 shows average g_S values as a function of water vapour deficit obtained by inverting the Penman-Monteith equation. Each point represents the average over data within a water vapour deficit interval. The values are plotted at their average water vapour deficit. The bars indicate the standard deviation in the mean value. When bars are missing only one observation was present in that class. Data are stratified into short wave downward radiation classes. The figure shows that the conductance follows approximately hyperbolic curves and that g_S increases with increasing R_s. For very low water vapour deficits ($D < 1$ g kg^{-1}) g_S may deviate from this curves. For the current 41 dry days these conditions are seldom reached and are therefore not considered here. The following response function is chosen:

$$f_D(D) = \frac{1}{1 + a_D(D - D_r)} \qquad (5.8)$$

where a_D is a free parameter and D_r is a reference water vapour deficit at which f_D becomes 1, here chosen as 3 g kg^{-1}. For $D < 1$ g kg^{-1} the response function is set to $f_D(D = 1$ g kg$^{-1})$. When $a_D = 1/D_r$ the function becomes inversely proportional to D. For smaller values of a_D the response becomes weaker. The functional form is equivalent to those used by Lindroth (1985) and Lohammar (1980). Slightly different forms are given by Jarvis et al. (1976) for Sitka spruce and Stewart and De Bruin (1985) for Scots pine and Corsican pine.

In Figure 5.4 average values of g_S are shown as a function of incoming short wave radiation classes. Each point represents the average over data within a R_s interval. The values are plotted at the average R_s value of that interval. The error bars indicate standard error in the mean. Data are stratified into classes of specific humidity deficit. It is observed that g_S increases with increasing R_s and that the dependency is strongest at low R_s values. We describe the light response with the function:

$$f_R(R_s) = \frac{R_s \ (R_{max} - R_{1/2})}{R_s \ (R_{max} - 2R_{1/2}) + R_{1/2} \ R_{max}} \qquad (5.9)$$

where R_{max} is the radiation level where f_R is 1, here fixed at 1000 W m^{-2}, and $R_{1/2}$ is a free parameter that describes the R_s value where the response is 0.5. The light response function used in this study is the same as given by Jarvis (1976) and Stewart (1988) who used a rearranged form of equation (5.9).

An attempt to isolate the temperature response in an analogous way to the light response, did not show a significant result. For the temperature response Jarvis (1976) used a function that is forced to zero at $T = 0$ and 40°C and the optimum
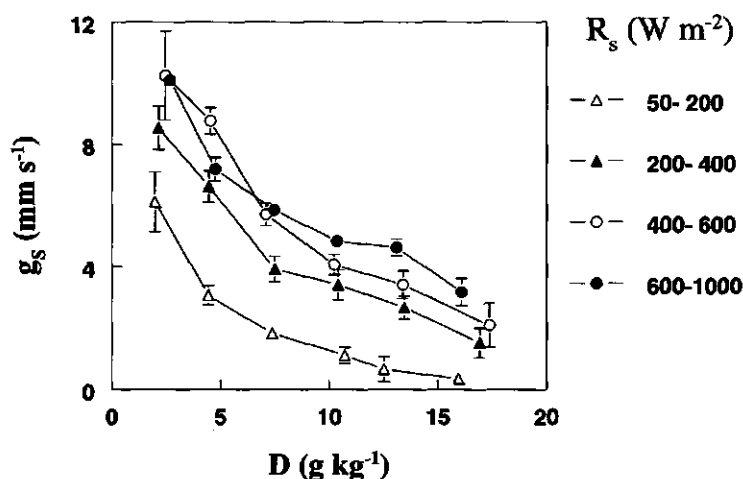
Figure 5.3. Observed surface conductance as a function of specific water vapour deficit stratified into classes of short wave downward radiation.

temperature as a free parameter. This form has the disadvantage that the parameter cannot be set to 'no temperature response'. Here we prescribe the optimum temperature (T_{OPT} = 25°C) and let the response at the edge of the range [0,40°C] be a free parameter:

$$f_T(T) = 1 - \eta_T + \eta_T \cdot (\frac{40 - T}{40 - T_{OPT}})^{2 - T_{opt}/20} \cdot (\frac{T}{T_{OPT}})^{T_{opt}/20} \quad ; \quad 0 \leq T \leq 40°C$$

$$f_T(T) = 1 - \eta_T \qquad \qquad ; \quad T < 0, T > 40°C$$

(5.10)

where η_T is a free parameter. Outside the range [0,40°C] the function is set to $1-\eta_T$. Day time air temperature never came close to these range limits.

Black (1979) found a significant influence of soil water on transpiration of Douglas fir. Soil water potential is a measure of the specific energy consumption of the root system to extract water from the soil. Therefore, prescribing reduction in terms of soil water potential is probably less obscured by the variation in soil type than a prescription in terms of soil water deficit. Soil water reduction is described as:

$$f_\psi(\psi) = 1 \qquad \qquad ; \quad \psi \geq \psi_r$$

$$f_\psi(\psi) = 1 - \beta_\psi (\psi_r - \psi) \quad ; \quad \psi < \psi_r$$

(5.11)

108
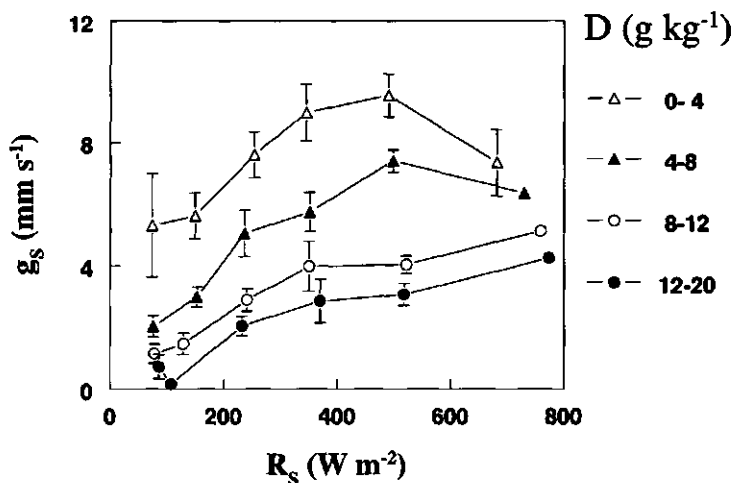
Figure 5.4. Observed surface conductance as a function of short wave downward radiation stratified into classes of specific water vapour deficit.

where β_ψ is a free parameter that describes the steepness of the response and ψ_r represents the reduction point, here taken as -0.06 MPa.

Until now we have not specified how the response functions in the Monteith formulation should be distributed over the two parameters g_m and λE_m defined in Equation (5.4). As a guide line we may look for a formulation which is equivalent to the Jarvis formulation. To this end we take the limit of infinite aerodynamic conductance of the Penman-Monteith equation (Equation (5.1)) to arrive at the relation:

$$\lambda E = \rho\lambda g_c D \tag{5.12}$$

Here we ignore the residual conductance g_0. For the current forest this limit is approached during day time conditions with dry air, when surface conductance is much smaller than aerodynamic conductance. With this relation we can rewrite Equation (5.4) in terms of moisture deficit:

$$g_c = \frac{g_m}{1 + \rho\lambda g_m D/\lambda E_m} \tag{5.13}$$

Comparing this with the Jarvis formulation of g_c (Equation (5.3)), with the moisture deficit function taken from Equation (5.8), we see that the two expressions become functionally equivalent if we choose:

109

$$\lambda E_m = \lambda E_+ \, f_L \, f_R \, f_T \, f_\psi \qquad (5.14)$$

where λE_+ is the maximum transpiration when other factors are not limiting and if we choose:

$$g_m = g_+ \, f_L \, f_R \, f_T \, f_\psi \qquad (5.15)$$

where g_+ is the maximum conductance when no transpiration occurs and when other factors are not limiting. Simple relations can be found between the Jarvis parameters $g_{C,ref}$ and a_D and the Monteith parameters g_m and λE_m. For finite aerodynamic conductance deviations occur. In fact when g_a approaches zero, while other parameters stay the same, the evaporation approaches the equilibrium evaporation which is often larger than the actual evaporation of the forest. This means that the surface conductance in the Monteith formulation decreases, whereas the surface conductance in the Jarvis formulation stays the same.

Parameter optimisation

Optimisation is done by minimising the sum of squares of the residuals of the latent heat fluxes:

$$S^2(a) = \sum_{i=1}^{N} \left(y_i - y_m(a,x_i) \right)^2 \qquad (5.16)$$

where y_i is the i'th measurement, y_m is the corresponding model value, a stands for the model parameters and x_i for the input data of the i'th model value. Minimisation of S^2 is carried out by varying a with the Levenberg-Marquart method as described in Press et al. (1986). The root mean square error (RMSE) is given by:

$$\sigma_y = \sqrt{\frac{S^2(a_0)}{N - v}} \qquad (5.17)$$

where a_0 is the parameter set for which $S^2(a)$ is at the minimum and v is the number of free parameters. Standard errors for the parameters are derived from the diagonal elements of the covariance matrix.

5.4   Results

In this section the results of optimisations for the various transpiration models are presented. Model values are calculated by using observations at 30 m above the forest floor. The aerodynamic conductance g_a is derived from observed wind speed, friction velocity and sensible heat flux. Flux profile relations for the forest roughness layer are taken from Bosveld (1997) and a modified roughness length for heat of 0.23 m is taken from Bosveld et al. (1998). Here it is assumed that the roughness length for water vapour is the same as for sensible heat. For the residual

110

conductance when stomata are closed we estimate a mean value of 1 mm s^{-1} from night time eddy correlation measurements.

The Jarvis-model serves as a reference since it performs best as will be shown. In Table 5.a the results of these parameter optimisations are given in three

Jarvis

	N	RMSE(W m^{-2})	g$_{c,ref}$(mm s^{-1})	ΔL	a$_0$(kg g^{-1})	R$_{v2}$(W m^{-2})	β$_v$(MPa^{-1})
Z	984	24.5	15.8±0.7	0.40±0.02	0.26±0.01	260±20	0.4±0.2
A	984	20.9	17.9±0.8	0.41±0.02	0.27±0.01	290±20	2.8±0.2
Ev	504	19.2	18.0±1.2	0.39±0.03	0.28±0.02	310±30	2.8±0.3
Od	480	22.4	18.0±1.1	0.43±0.03	0.26±0.02	280±20	2.9±0.3
FF	984	21.2	18.0±0.9	0.47±0.02	0.31±0.02	320±20	3.0±0.2
Ly	984	19.4	17.5±0.8	0.54±0.02	0.29±0.02	280±20	2.9±0.2

Monteith

	N	RMSE(W m^{-2})	g$_s$(mm s^{-1})	ΔL	λE$_0$(W m^{-2})	R$_{v2}$(W m^{-2})	β$_v$(MPa^{-1})
A	984	21.1	181±71	0.38±0.02	221±5	370±15	2.7±0.2
B	984	21.2	113±59	0.40±0.02	228±7	390±15	2.7±0.2
C	984	24.1	415±606	0.71±0.04	168±5	940±80	3.1±0.2

Modified Priestley-Taylor

	N	RMSE(W m^{-2})	α	ΔL	β$_v$(×10^{-3})	β$_c$(W m^{-2})	β$_v$(MPa^{-1})
A	984	23.9	0.52±0.01	0.28±0.02	4.3±0.4	31±3	2.1±0.1
B	984	25.6	0.56±0.01	0.31±0.02	[0.0]	43±2	2.2±0.1
C	984	26.3	0.54±0.01	0.25±0.02	6.5±0.4	[0.0]	2.1±0.1

Table 5.a. The results of various optimalisations for the three models. For explanation see text.

sections corresponding to the three models. For all models various optimisations are obtained by fixing parameters at different values. It was found that the temperature response parameter (η_T) in the Jarvis and Monteith model was not significant different from 0. This parameter was therefore fixed at 0 in the present analysis.

Optimisation of the Jarvis model

The Jarvis model is optimised against the hourly latent heat flux values of the 41 selected dry days (Run Z). Before discussing parameter values we concentrate on Figure 5.5 where daily average latent heat fluxes are shown for the Jarvis model and the observations. Here again successive periods are indicated with the *DOY* of the first day. Model overestimation occurs for the period 143-147. Soil water potential dynamics shows that this period is in the first drying phase (Figure 5.1). Overestimation occurs also in the period 200-203. This period falls in the second drying phase. For the period 208-210 no overestimation is found though soil water potential is still decreasing. A rainfall event of 7 mm at day 204 seems to have not much impact on the soil water potential. Water contents increase in the top 10 cm of the soil whereas soil water in deeper layers continues to decrease. In the period 253-255 soil water potential is low again, here the model underestimates transpiration.

This analysis suggests that the response of the forest to soil water availability is different before and after *DOY* = 204. The forest root system may have adapted to the dry situation. The findings of Olsthoorn and Tiktak (1991) on root growth for this period are not conclusive since they show that root amount increases during May, June and July and starts to decrease by the end of July (*DOY* = 210) for the top soil levels. Root amounts at deeper soil layers stay approximately constant. To account for this apparently changing response, the soil water potential response function is adapted to allow for different response before and after *DOY* = 204. A new optimisation is performed on the Jarvis-model (Jarvis run A in Table 5.a) which shows that the RMSE-value of the residuals has decreased significantly. Explained variance is 91%. Now a significant response to soil water pressure head before *DOY* = 204 is found. After *DOY* = 204 the soil water reduction parameter is not significant different from 0 and is therefore fixed at 0 for this period.

The a_D value of 0.27 kg g^{-1} indicates that stomatal conductance is almost inversely proportional to water vapour deficit. Light response is gradual as indicated by the parameter value $R_{1/2}$ = 290 W m^{-2}. A significant response in terms of the LAI function is found. The conductance at reference conditions of 18 mm s^{-1} indicates that at favourable conditions canopy resistance can go below 100 s m^{-1}.

Optimisation of the Monteith model

For the Monteith model optimisation results for the 41 days are shown in the second part of Table 5.a, labelled run A. The RMSE-value is only slightly larger than the Jarvis run A. This is to be expected because the two formulations are

112
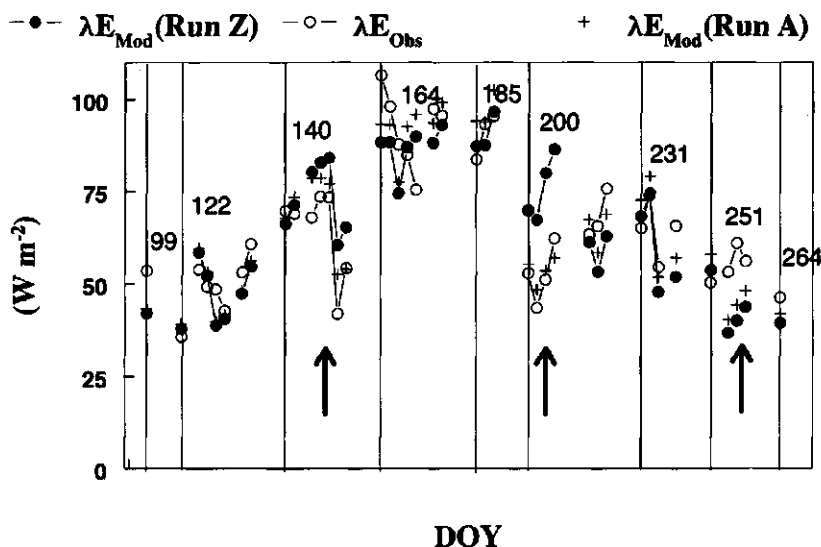
Figure 5.5. Daily average observed latent heat flux and model values for the 41 selected dry days. (•) Jarvis Run Z, (+) Jarvis Run A. Periods with large deviations for Run Z are marked.

forced to be approximately equivalent. The maximum transpiration flux (λE_+=221 W m^{-2}) obtained for the Monteith model (run A) is a realistic value since it is close to the largest observed values, typically 200 W m^{-2}. The parameters for *LAI* response (ΔL), soil water potential response before *DOY* < 204 (β_ψ) are of comparable magnitude to those obtained for the Jarvis formulation. The light response parameter ($R_{1/2}$) is somewhat larger.

We can calculate the equivalent moisture deficit parameters for infinite g_a. These are $g_{C,ref}$ = 21.6 mm s^{-1} and a_D = 0.293. This is comparable to the Jarvis (run A) values. Canopy conductances calculated with these equivalent parameters are somewhat higher than when using the Jarvis parameters. This is to compensate for the effect of finite g_a.

Other ways of distributing the response functions over λE_m and g_m than described in Equation (5.14) and Equation (5.15) respectively, could lead to a different performance of the Monteith formulation. In run B the response functions in the formulation of g_m are removed, whereas the response function in λE_m are retained. The RMSE-value of run B is only slightly larger than of run A. In run C the response functions in the formulation of λE_m are removed except for the soil water response, and all response functions in g_m are retained except for soil water response. Now the RMSE-value is significantly larger than of run A. Moreover the

113

$R_{1/2}$-value has become unrealistically large. This suggest that the model tries to compensate for deviations by adapting the light response function.

Optimisation of the Priestley-Taylor model

For the Priestley-Taylor model optimisation results are shown in the third part of Table 5.a. The part of specific humidity deficit decorrelated from net radiation (D_d) is estimated from the current data set as D -0.01*(R_n-G). Run A shows the result with all parameters free. A definite soil water response and *LAI* response are found but the corresponding parameters are somewhat smaller than in the Jarvis formulation. This is to be expected, because here the response functions are linearly related with latent heat flux. In the Penman-Monteith formulation the responses are damped through the action of a finite g_a. The α-parameter is 0.5 which is significantly lower than the value of 1 found for well watered grassland by Beljaars and Bosveld (1997). This shows that this forest has a significantly lower transpiration rate than grassland even when soil water is not limiting. In run B of the modified Priestley-Taylor model the parameter $β_V$, related to the ventilation term, is fixed at zero. Run C gives the result with $β_C$, representing the offset flux, fixed at zero. Both optimisations give significantly larger RMSE-values.

Analysis of the residuals

In terms of RMSE-values the Jarvis model performs best. The Monteith model performs almost equally well provided the approximate equivalent formulation is used (Run A). Here we try to identify the conditions where the three models deviate from the observations. In Figure 5.6 a,b and c residuals are stratified into classes of D, R_s and Time of day respectively. The Jarvis and the Monteith models show little deviation from the observations. The modified Priestley-Taylor model underestimates considerably in the first few hours after sunrise, at times when moisture deficit is lower than in the afternoon. Here we see clearly the action of stomatal regulation which distorts the correlation between available energy and evaporation.

In Figure 5.7 the Jarvis-model residuals are classified into wind direction classes of 30°. Also displayed is the bias in the energy balance. In both cases fractional deviations are shown. Both the energy balance and the latent heat flux are positively biased for the wind direction between 240° and 300°. These are the wind directions which dominated for DOY 128 and 234, days which were already excluded because of an imbalance of the surface fluxes. In this directions more deciduous trees are present upwind and aerodynamic roughness is larger than in the other directions (see Bosveld, 1997). For the wind direction between -30° and +30° both biasses are negative. This is the direction of the small clearing. Observations in this sector are less reliable because of tower interference. For wind directions between 30° and 240° biasses are small both in evaporation as in the energy balance.

114
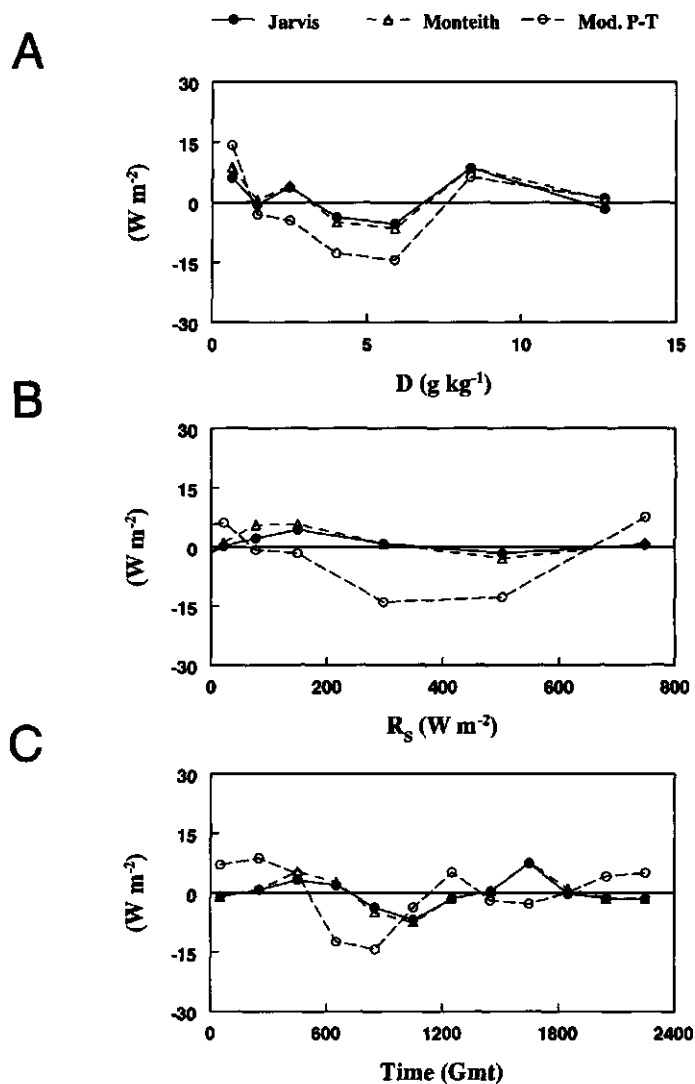
Figure 5.6. Average model biases as function of A) moisture deficit (daytime), B) Short wave incoming radiation (daytime) and C) time of the day.

115
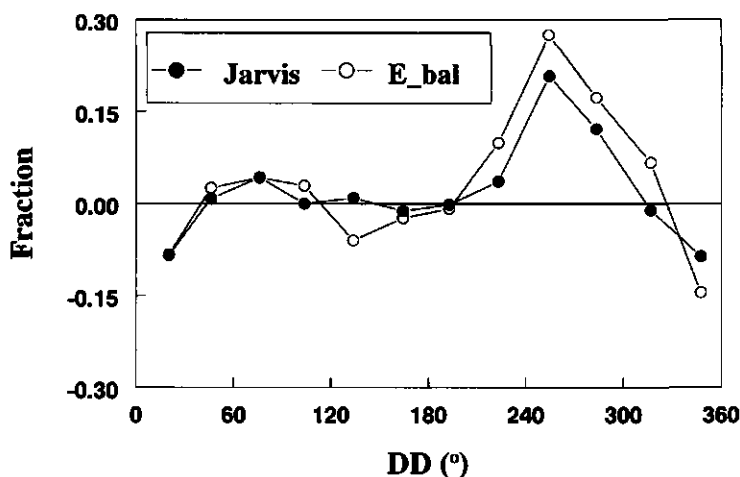
Figure 5.7. Hourly residuals of energy balance and of Jarvis model as function of wind direction.

Figure 5.8 shows daily averaged Jarvis-model values as function of the daily averaged observed values (open dots). It is observed that at days with high evaporation the model tends to overestimate. At days with low evaporation the model underestimates. Optimising the Jarvis formulation on daily averaged residuals show a significant better agreement between model and observations on a daily basis (closed dots). Especially the light response parameter is significantly lower for the latter optimisation. Of course this new optimisation gives worse results when looking at the diurnal cycle. The result suggests that the forest has difficulty to maintain evaporation at high rates, probably due to soilwater depletion around the roots during the day.

Behaviour of the models

In Figure 5.9 iso-lines of model transpiration fluxes are shown as a function of short wave incoming radiation and water vapour deficit for the three models. The models are fed with a constant aerodynamic resistance of 5 s m^{-1}, and a friction velocity of 0.6 m s^{-1}. These values are typical for daytime conditions. Available energy is parameterised as 0.73 times short wave incoming radiation (an approximate relation derived from the current data set). A maximum LAI was taken and an unstressed soil water potential value. If we take the Jarvis model (run A) as

116
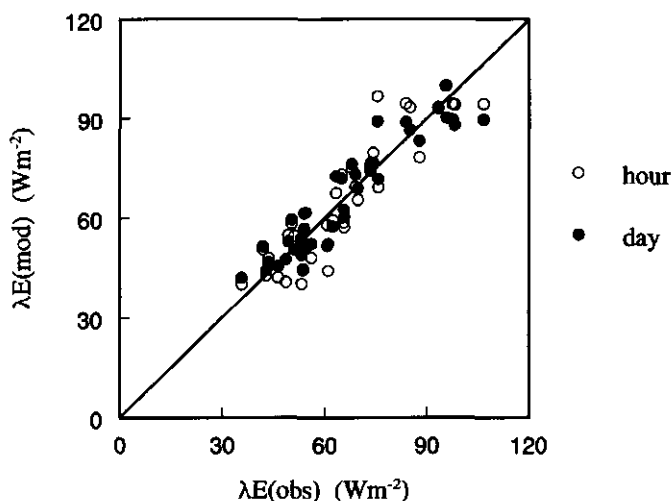
Figure 5.8. Daily averaged Jarvis-model transpiration as function of observed transpiration, optimized on (○) hourly residuals and (•) daily averaged residuals.

a reference than we observe that the Monteith model (run A) differs only at high irradiation and low water vapour deficit. These cases are virtually absent in the data set. They are typically the conditions where the assumption fails, that the ventilation term dominates over the energy term in the Penman-Monteith equation, and thus where the equivalence between the Jarvis model and the Monteith model breaks down. The modified Priestley-Taylor model (run A) including the decorrelated water vapour deficit term shows to be a comparable function of D and R_s as the Jarvis model. Only for low D values a different behaviour is observed. The original Priestley-Taylor form with a constant term would give horizontal lines and thus cannot account for the slight increase of transpiration with increasing water vapour deficit found from the Jarvis optimisation.

5.5 Sensitivities and statistical considerations

Sensitivity of the parameter estimates

To investigate the reliability of the estimated parameters a number of sensitivity tests were performed. To show that the parameter values are not sensitive to the

117
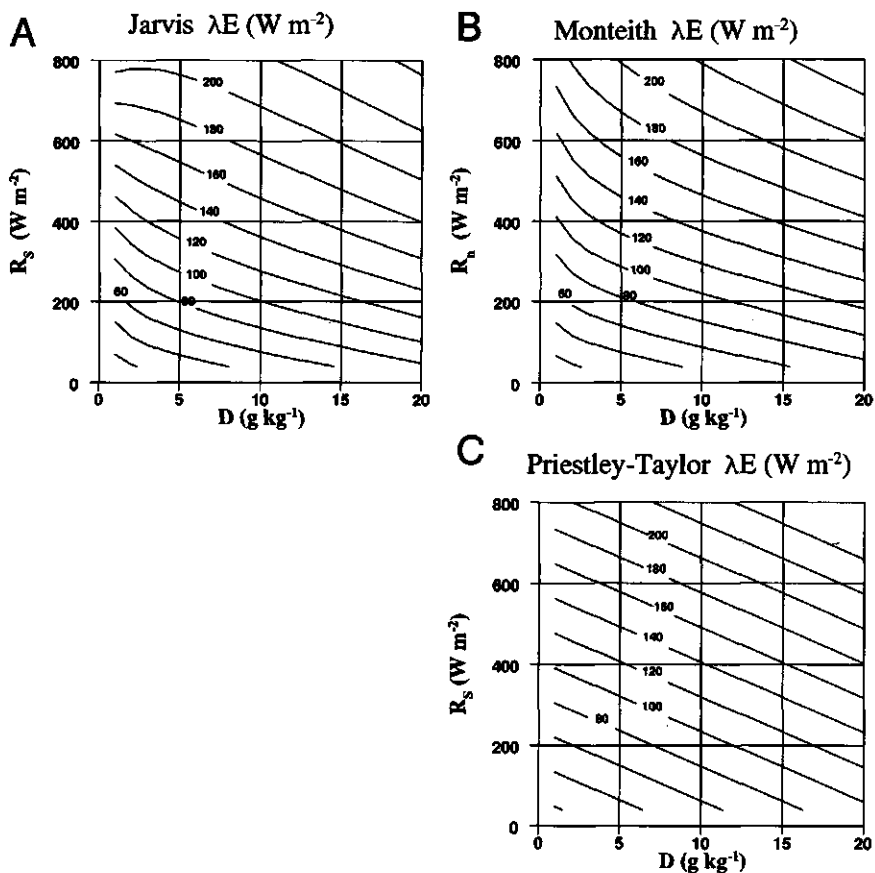
Figure 5.9. Iso-latent heat flux lines as function of short wave incoming radiation and moisture deficit for A) Jarvis-model, B) Monteith model and C) Modified Priestley-Taylor-model.

118

particular days selected, at least when properly distributed over the year, two new optimisations of the Jarvis model are performed for the even and odd days respectively (Run Ev and Od in Table 5.a). It is observed that variations of the parameters are small and within the error bounds.

The sensitivity of the parameter estimate for the presence of forest floor evaporation was investigated by using the model of Schaap and Bouten (1997), based on the Penman-Monteith approach and optimised for the same Douglas fir site. It uses forest trunk space meteorological data (temperature, specific humidity, wind speed and available energy) and litter layer water content as input variables. Schaap and Bouten (1997) show that for this dense forest the ventilation term of the model dominates, therefore we neglect the energy term. Meteorological data are taken from hourly observations at 4 m height and litter water content is taken from TDR observations and the soil hydrological model SWIF in the same way as described above for soil water pressure head. The observed latent heat flux consists of transpiration of the crowns and a presumably smaller part of evaporation from the forest floor. Schaap and Bouten (1997) show for the current Douglas fir stand that forest floor conductance ranges from 0.3 to 1 mm s^{-1} for a dry litter layer. This is consistent to the mean night time bulk conductance of 1 mm s^{-1} found from the current observations which include cuticular conductance. For the wet litter layer conductances can be much higher. At this stage it is not clear which fraction of the forest floor evaporation is actually observed in the measurements, since horizontal advection in the trunk space below the crown layer will likely occur. A new optimisation result is presented as run FF for the Jarvis model in Table 5.a. For this run we subtract the modelled forest floor transpiration from the observed latent heat flux. At the same time the forest floor evaporation is omitted from the model by reducing quit arbitrarily the residual conductance g_o in the model from 1.0 to 0.5 mm s^{-1}. It is observed that changes in the parameters are small.

As noted in a previous section there is some uncertainty in the calibration of the Ly-α hygrometer. As a sensitivity test the eddy-correlation fluxes were recalculated with a calibration which is a linear interpolation in time of the calibration before and after the measuring campaign. Re-optimisation showed that only the parameter ΔL increases significantly in value. This shows that parameters related with a long term change in the behaviour of the forest are sensitive to slow but prolonged instrumental drift.

Comparison with another forest site

Stewart (1988) describes a model for the transpiration rate of Thetford forest. Thetford forest consists also of conifers (Corsican pine and Scots pine) and has a comparable maritime climate as the present forest. Here we look how well the model for Thetford forest describes the transpiration rates of the current forest. Here we take the most advanced scheme investigated by Stewart (1988). This scheme has the same structure as the current Jarvis-model, although response functions differ slightly. The model is run with the meteorological forcing variables of the current

data set. The relative leaf area index function and the optimised parameters for Thetford forest are taken. Leaf area index for Thetford forest ranged from 1.8 to 2.8 during the year, much lower than the variation of 8 to 11 found at the current location. Soil water response in the Stewart model is formulated in terms of soil water deficit in the top 1 m of the soil. For the current location these values were obtained from a combination of the soil hydrological model data and observations in the same way as soil water potential was derived. The maximum soil water deficit at the current location is 110 mm, somewhat larger than the value of 83 mm found for the Thetford forest. The soil water response parameter is adapted such that response as a function of fractional soil water deficit is the same for both locations. The Stewart model underestimates by 25%, with an RMSE-value of 40 W m^{-2}. By introducing the residual surface conductance in the Stewart model bias was only 1% and the RMSE-value decreased to 35 W m^{-2} which is still considerably larger than the 21 W m^{-2} found for the optimised Jarvis model. Largest deviations occur because the model and the current forest differ in soil water response after $DOY = 203$, differ in LAI-function and because they differ in light response curve, light response being more gradual at the current location.

RMSE-values and parameter error bounds

The variance in the residuals (MSE) of the optimised Jarvis model is 440 W^2 m^{-4}. We may wonder which error sources contribute to this value. An important contribution to the MSE-value comes from the inherent stochastic nature of turbulence which leads to a random error in the turbulent latent heat flux measurements (Lumley and Panofsky, 1964). We estimate the contribution of this source by looking at the six 10 minutes observations from which the hourly values are derived. This is done by performing a linear regression in time for each six 10 minutes observation within an hour. Then the mean-square of the six residuals around the regression line is calculated. This gives an unbiased estimate of four times the variance in the hourly value. The factor four comes from six minus the number of freedoms in the regression. From this we derive that over the 41 days the MSE introduced by atmospheric statistics is 290 W^2 m^{-4}. Still 35% of the MSE cannot be explained by atmospheric statistics.

Stratification of the residuals into classes of water vapour deficit, short wave incoming radiation and time show that the models are not perfect. However, none of these classifications contribute significantly to the MSE-value of the Jarvis model. Stratification into wind direction classes shows a small but significant contribution of 25 W^2 m^{-4}. If we look at the daily average values a more significant contribution is found of 60 W^2 m^{-4}. Thus wind direction cannot explain the contribution to MSE of a stratification in days. This shows that the model misses systematic longterm processes that determine forest transpiration.

The error bounds given for the parameter estimates are based on the assumption that the model is perfect and that the errors in the individual observations are independent and Gaussian distributed. The independency of

residuals can be studied by averaging observed and modelled transpiration over subsequent longer periods. When the data were independent, the variance of the residuals should be inversely proportional to the averaging period. In Figure 5.10 the variance of the residuals minus the atmospheric variance are shown for averaging periods (T_{avg}) ranging from 1 to 24 hours. The random error in hourly mean values induced by atmospheric noise is uncorrelated in time since the integral length scale of the transporting eddies in the surface layer is much smaller than 1 hour. Here it is assumed that the atmospheric noise is not correlated to any other process that has impact on the total variance in the residuals. Also displayed are the theoretical lines that would be obtained when hourly residuals were independent and for a stochastic process with exponential decaying correlation function with a correlation time of 18 h. This analysis suggest that statistical nature of the residuals can be described by the sum of two random processes, one with MSE = 290 W^2 m^{-4} and uncorrelated in time and one with MSE = 150 W^2 m^{-4} and a correlation time of 18 h. From a statistical point of view this means that the effective number of independent observations is less than the 984 used in this study. For such statistical conditions the error bounds on the parameters are approximately a factor 3 larger than those given in Table 5.a.

5.6   Discussion and conclusions

On the basis of the Penman-Monteith formulation, surface conductances of a Douglas-fir forest are derived from measured transpiration rates. Most of the time, observed surface conductance is lower than 10 mm s^{-1}. Due to the very rough nature of the forest, the aerodynamical conductance between the surface and a suitable reference height above the forest is often larger than 100 mm s^{-1} for neutral and unstable atmospheric conditions. Consequently the ventilation term in the Penman-Monteith equation (Equation (5.1)) generally dominates over the energy term. Following McNaughton and Jarvis (1983) we conclude that the coupling between forest transpiration and the conditions of the free atmosphere is very strong. For such conditions the forest is expected to have a significant stomatal response to water vapour deficit to limit transpiration.

Indeed, from an optimisation of the Jarvis model it is found that canopy conductance is approximately inversely proportional to water vapour deficit, whereas for example Beljaars and Bosveld (1997) found a much weaker response for grassland. This means that, when other factors are constant, the water vapour deficit response acts to keep transpiration within small bounds over a large range of water vapour deficit values.

No temperature response was found. However, the range of daytime temperatures is small in the current data set. A clear light response is found which is much more gradual than light response of individual needles. This behaviour suggests that more stomata located deeper in the forest become light saturated when light intensity increases. Transpiration is 40% lower before shoot growth than after
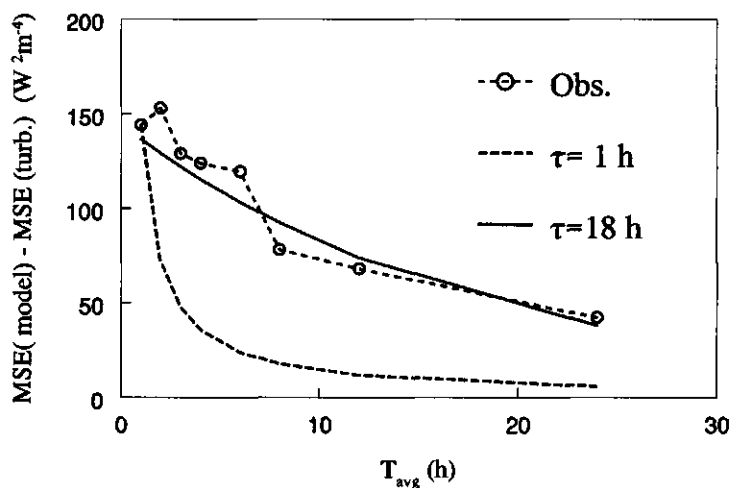
Figure 5.10. Observed variance of residuals minus atmospheric variance as function of averaging time. Model lines are for correlation times 1 and 18 h.

shoot growth in early summer. This is to be compared with a 20% lower crown biomass before shoot growth, found from direct observations and from micro wave transmission observations (Tiktak et al. 1990). This suggests that the new shoots have a stomatal conductance which is higher than the conductance of older needle year-classes, an effect that has been reported for conifers by Running (1976). But also other factors related to changing plant physiology at the start of the growing season can be of importance here.

A significant response to soil water potential is found for the first half of the year. After day number 203 soil water stress reduction seems to disappear, probably as a result of adaptation of the root system to the dry conditions.

On a daily averaged basis the model overestimates at high evaporation rates. It is suggested that in reality soil water depletion around the roots limits transpiration for such days.

Data were stratified into wind direction classes. The residuals of the Jarvis model show the same pattern as the deviations in the energy balance. This suggest that for some wind directions advection is important. For wind directions between 30 and 240° residuals in transpiration were small, indicating that inhomogeneities in the upwind terrain are of minor importance. Other uncertainties like forest floor evaporation and the calibration of the Ly-α were investigated. None of them have an important effect on the parameter estimates.

A comparison with the results of Stewart (1988) for Thetford forest shows that the average latent heat flux is almost equal for both sites over the 41 selected dry days. However systematic differences occur both on the seasonal scale related to soil water and LAI-development, as well as on the diurnal time related to light response. The explained variance increases from 72% for the a-priori estimate based on Stewart (1988) to 91% for the current Jarvis model optimised against local observations. LAI for both locations differ by a factor of 4, which suggests that a large fraction of the needles is not active at the current location.

Residuals between modelled and observed latent heat flux, apart from the uncorrelated atmospheric noise, are correlated on the average over periods of approximately a day. At times, consecutive days show systematic biases. This poses doubts on the confidence limits given for the parameter estimates. It is suggested that they should be increased with a factor of 3.

Recently Lhomme et al. (1998) show that the Monteith model is equivalent to the Jarvis model if a response to leaf water potential is used instead of water vapour deficit. Here we show that the Monteith model is approximately equivalent to the Jarvis model for this aerodynamically rough forest if the response functions are incorporated in both g_m and E_m. Especially the incorporation of the response functions in E_m proved to be important to obtain a good fit to the observations. The reason is that changes in g_m have only effect on cases with low moisture deficit, whereas changes in E_m have an effect over the whole range of atmospheric conditions. It would be more satisfactory if we could relate the both parameters to distinct physiological processes. At this stage however, the plant physiological interpretation of the two parameters g_m and E_m remains unclear.

The Priestley-Taylor model, modified according to De Bruin and Holtslag (1982) and Van Ulden and Holtslag (1985) and adapted in this study to incorporate the effect of soil water stress and the yearly cycle of LAI, performed reasonably well on the hourly basis, given the fact that no explicit plant reaction is taken into account on the diurnal time scale. The model was shown to work well for grassland by De Bruin and Holtslag (1982), a situation where the coupling of the vegetation to the atmosphere is relatively small and thus the transpiration is mainly driven by the available energy. For this forest however, the coupling between atmosphere and vegetation is strong. It seems that the strong reaction of the canopy conductance to changes in water vapour deficit acts to keep the correlation between available energy and transpiration high. The modified Priestley-Taylor model underestimates transpiration during moderate irradiation and moderate water vapour deficit. The replacement of the constant β_C by the ventilation term (with β_V) seems less satisfactory, but a combination of the two terms gives the best results. With respect to a priori parameter estimates it is encouraging to note that in run B the product $\alpha \cdot \beta_C$ (=24 W m^{-2}) is almost equal to the value of 20 W m^{-2} found for the well watered grassland by De Bruin and Holtslag (1982).

123

5.7 Acknowledgments

6 Evaporation and transpiration reduction of a partially wet Douglas-fir forest.[*]

Abstract

The Penman-Monteith equation is extended to describe evaporation of intercepted rain, transpiration and the interaction between both processes for a partially wet forest canopy. This single layer model simulates the effects of energy consumption, stomatal blocking and changed moisture deficit close to the canopy as a function of canopy water storage. The evaporation part of the model needs input parameters related to the distribution of water over the canopy and the transport of energy between the wet and dry fractions of the needles. The transpiration part of the model needs parameter values related to the dry canopy surface resistance which is described with a Jarvis-type response formulation. The explicit expressions obtained for the water vapour fluxes facilitates a straight forward identification of the various processes. Observations of canopy water storage amounts and xylem sapflow during drying episodes after rainfall are used to evaluate the model for a dense Douglas-fir forest. First, the evaporation part of the model is optimised against the rate of change of observed canopy water storage for 15 well defined drying episodes. The sensitivity of the evaporation parameters to variations in transpiration and various instrumental uncertainties is analysed. Second, the parameters related to dry canopy surface resistance are estimated from 61 dry days of sapflow observations. With these surface resistance parameters and the optimised parameters for evaporation, there is only one parameter remaining, i.e. maximum fractional blocking of the stomata (f_s). Finally, this parameter is estimated from the sapflow observations during 44 wet days. The impact of uncertainties in the observed sapflow measurements on the estimated f_s is discussed. The analysis suggests that most of the transpiration reduction comes from energy competition and micro-climate influence. The remaining difference between observed and modelled transpiration reduction can be described by assuming that $1/3^{rd}$ of the stomata are blocked by water during maximum canopy storage.

6.1 Introduction

When water is present in the forest crown layer due to the interception of rain, the total rate of water loss from the forest includes both evaporation and transpiration. This paper deals with the analysis and modelling of evaporation and transpiration of

125

a partially wet forest canopy and the interaction between these two processes.

The evaporation of a completely wet vegetation is often modelled as the potential evaporation, by using the Penman-Monteith equation (Monteith, 1965) with a zero surface resistance for the transport of water vapour (Dolman and Gregory, 1992; Beljaars and Viterbo, 1994). For dry low vegetation the rate of transpiration is close to the potential rate when soil water is not limiting (Stewart and Rouse, 1977), thus a discrimination in terms of canopy wetness is of limited importance for such canopies when describing the total evapotranspiration flux. For forest the situation is different. Due to the high aerodynamic roughness and due to a relatively high stomatal resistance a large difference in magnitude may exist between evapotranspiration of a wet forest and transpiration of a dry forest. For a pine forest, Stewart (1977) showed that the partially wet forest evaporates at a rate somewhere between this potential evaporation and the transpiration rate when the canopy would be dry. Monteith (1977) explains this behaviour by arguing that heat fluxes between the wet and dry parts of the canopy experience a finite aerodynamic resistance. Had this resistance been zero, as would be the case if the water was homogeneously dispersed over the canopy in very small drips, then evaporation would continue at the potential rate (Shuttleworth, 1976). Using the product of potential evaporation and the fractional amount of intercepted water Bouten et al. (1996) obtained good results in a four layer model for the current Douglas-fir forest, to simulate the dynamics of vertical profiles of canopy water storage amounts.

The Penman-Monteith equation also provides a framework for modelling transpiration rates. Surface resistance is then described as a function of environmental factors like short wave incoming radiation, moisture deficit of the air, temperature and soil water content (Jarvis, 1976). The presence of water in the crown layer reduces the transpiration rate of the canopy. The two most obvious mechanisms of transpiration reduction are blocking of the stomata by a water layer and energy consumption by the process of evaporation, energy that otherwise would have been available for transpiration. A more subtle influence concerns the heat fluxes from and to the evaporating water, influencing the moisture deficit at the transpiring surface and consequently the transpiration flux. Conversely, the transpiration of the forest may influence the evaporation, especially at the end of a drying period when the transpiration flux may be high while the evaporation is low.

In this study we concentrate on the description of the latent heat exchange between the canopy and the free atmosphere. Thus, we are not focused on the details of in-canopy exchange processes nor on the behaviour of the last fractions of free water in the lower layers of the canopy. The latter is treated in models to estimate surface wetness durations (Butler, 1986; Barr and Gillespie, 1987; Huber and Itier, 1990). Vertical structured models are thus to complex for our purpose and the use of them would involve the prescription of a large amount of parameters, for which often not enough information is available. The single big leaf approach has shown to be a successful and relatively simple framework for modelling water vapour exchange fluxes between vegetation and the atmosphere (Raupach and Finnigan, 1988). Thus in the following, we will develop an extension of the

126

Penman-Monteith model which is still single layered, but which allows for energy exchange between a wet and dry surface fraction and which allows for a prescribed degree of stomatal blocking.

The model is compared with observations obtained over a Douglas-fir forest. Estimates of evaporation rate and canopy wetness are derived from observations of canopy water storage amounts by means of micro-wave attenuation (Bouten et al., 1990; Bouten and Bosveld, 1991). Estimates of transpiration rates during wet episodes are obtained from xylem sapflow heat pulse velocity (HPV) measurements. A single big leaf model described by Bosveld and Bouten (1999a) and optimised on 61 dry days of sapflow observations is used as a reference transpiration to assess transpiration reduction during wet episodes.

In the next section, the research site and the observations are described. In section 6.3 the model is derived. In section 6.4 parameters related to evaporation and transpiration reduction are derived from the measurements. In Section 6.5 a discussion on parameter constraints is given and a sensitivity analysis is presented. In section 6.6 a discussion of the results is given and conclusions are drawn. The calibration procedure for sap flow measurements is described in appendix 6.A. Appendix 6.B gives algebraic details about the derivation of the model.

6.2   Research site and observations

The research site

The research was carried out in a 2.5 ha Douglas fir plantation, located within a large forested area in the Netherlands. The stand has a tree density of 785 trees ha^{-1}. The firs were planted in 1962. In 1989, the year that the measurements were performed, the trees had reached a mean height of 18 m and a mean diameter at breast height of 0.21 m. The leaf area index amounts to 11 m^2 m^{-2} (Evers et al., 1991). More information is given in Bosveld (1997) which also gives a fetch analysis and an assessment of the aerodynamic roughness.

Canopy water storage measurements

The micro-wave transmission technique enables the measurement of canopy water storage amount with high temporal and vertical resolution (Bouten et al., 1990). Sensor and receiver were 15 m apart and tracked in the vertical from forest floor to tree tops every 5 minutes. The scanned vertical surface cuts through a number of tree crowns. Calibration to stand average water amounts was done on the basis of night time throughfall measurements at low wind speeds and low evaporation rates. A further comment on the calibration method can be found in Bouten and Bosveld (1991). Canopy storage capacity (2.5 mm) was derived from night time observations when drainage from intercepted water has ceased. Measurements were performed

127

from May until November 1989.

Sap flow measurements

Sapflow velocities were measured in 12 trees at two sides by means of heat pulse velocity (HPV). The HPV technique (Marshal, 1985) is based on the hourly application of a 10 Joules heat pulse through a heating wire wrapped around a thin pin, which is horizontally driven into the sapwood of a tree. The heat pulse is convected with the sapflow. Dissipation of the heat pulse takes place by conduction in both upward and downward directions. Two Pt100 sensors, located about 1 cm above and below the heating wire, are used to measure the time lags of the heat pulse. From the difference the contribution of convection to the heat pulse velocity and the sap flow velocity are calculated. Hourly measurements were made in the period June till October 1989.

For each sensor, the convective heat pulse velocity is linearly related to the xylem sap velocity (Swanson and Whitfield, 1981; Cohen et al., 1985). However, the absolute values registered by individual sensors should be treated with great care. Effects of installation, light exposure of trees, emboly, or non-uniformness of tracheids can cause large differences between sensors. Comparing with eddy correlation transpiration rates shows that sapflow responds rather quickly upon changes in external conditions during daytime, whereas at nighttime sapflow proceeds for many hours at high levels while transpiration ceases quickly upon sunset. To obtain transpiration rates from these measurements 7 sensors were selected which show good behaviour throughout the observation period. To convert HPV observations to transpiration the method needs calibration. Calibration is performed on the basis of eddy correlation water vapour flux measurements and on the basis of soil water balance observations. The procedure is described in appendix A. Time delays between sapflow and transpiration due to water buffering in the tree has been reported by Schulze et al. (1985) and Granier et al. (1990). Therefore only daily averages are used in this study.

Meteorological observations

Profiles of dry-bulb and wet-bulb temperature as well as wind are observed along a 36 m open structured tower at 4, 18, 24, 31 and 36 m height. The observations at the 31 m level are used as forcing variables for the model. The aerodynamic resistance from this reference level to the canopy is derived from a flux-profile scheme representative for the roughness sublayer of the current forest described in Bosveld (1997) and from the scalar excess resistance found in Bosveld et al. (1999a). The meteorological instruments are described in Bosveld (1997) and Bosveld and Bouten (1999a). Here we will concentrate on the performance of the instruments shortly after wet conditions. The Funk-type net radiometer was ventilated to avoid large temperature differences over the instrument. This also served a rapid evaporation of drops from the domes which otherwise would

128

influence the measurements. Accurate observations of water vapour deficit is crucial for properly analysing evaporation data. Water vapour deficit is measured with psychrometers. They were strongly ventilated which stimulates water drops being dragged away or evaporated from the dry bulb sensor.

6.3   Extension of the Penman-Monteith model for partially wet conditions

The concept of a single big leaf assumes a horizontal homogeneous surface in which no horizontal length scale is present. As soon as we introduce wet patches on the big leaf we are forced to specify a horizontal length scale, related to the distance between the wet and dry parts. This length is inevitably related to the strength of the interaction between the dry and wet parts, either through the air or through the canopy tissue. In a real wet canopy separation between wet and dry vegetation parts occur at various length scales. On the smallest scales we have drops forming on needles surrounded by dry parts. Also the upper side of a needle may be wet, whereas the lower side remains dry. Bouten et al. (1996) show that after a rain event the top of the vegetation dries out first, resulting in an increasing separation distance between dry and wet canopy parts. With respect to transpiration, needles in the top of the vegetation that dries out first have the lowest stomatal conductance because they are well exposed to light. In our approach we ignore all these complexities and assume that the energy exchange between wet and dry parts of the canopy is governed by only one effective separation length scale. Moreover, we assume that at any instant all needles which are not blocked by intercepted water have the same effective stomatal conductance.

Surface fractions

The single big leaf concept is extended by including surface fractions having different resistances with respect to moisture transport. Figure 6.1 schematically shows the compartimentation of a unit area of the idealised leaf. When the canopy is dry, we allow for two surface types with their respectivic surface fraction: w_S, the fraction of the surface with stomata and $w_D = 1 - w_S$, the fraction of the surface without stomata. The stomata-free surface fraction is introduced to allow for water at the big leaf without blocking of the stomata. Both surface types can be covered with water each to its own maximal fraction f_S and f_D respectively, indicated by the dotted lines. Thus the maximum wettable surface fraction is $w_2^+ = w_S f_S + w_D f_D$. This maximum value is reached when during rain, the amount of intercepted water has reached the canopy water storage capacity. Canopy water storage capacity is defined as the maximum canopy water storage after dripping has ceased. In Figure 6.1 a situation is shown where the wetted surface area is 2/3rd of the maximum value.

We now seek expressions for the stomatal surface fraction not covered by water (w_0), the non stomatal fraction not covered by water (w_1) and the wet fraction (w_2) as functions of the surface area covered by water. For the three surface
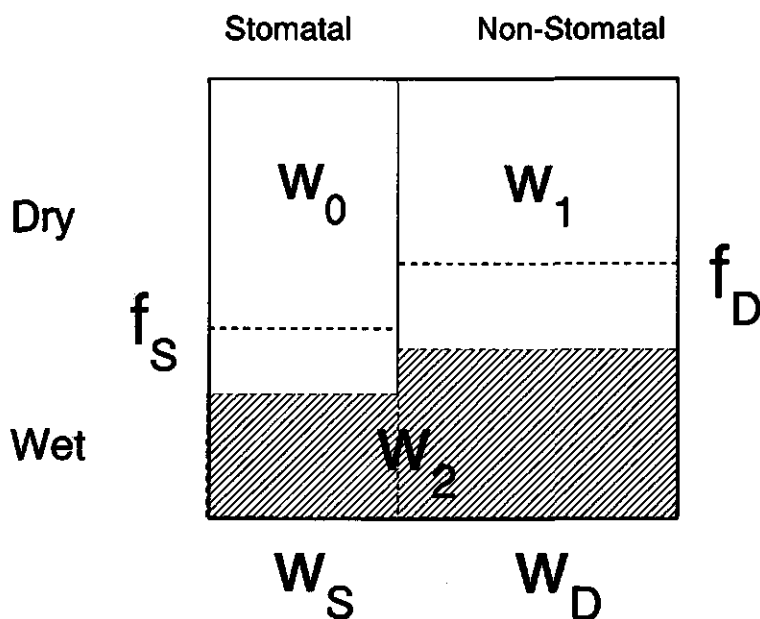
Figure 6.1. Compartimentation of the single big leaf in: (w_0) stomatal, (w_1) non-stomatal and (w_2) wet fraction, at $2/3^{rd}$ of maximum wetness. Other parameters are explained in the text.

fractions we have:

$$
\begin{aligned}
w_0 &= w_S \, (1 - f_S \, g_w) \\
w_1 &= w_D \, (1 - f_D \, g_w) \\
w_2 &= w_2^+ \, g_w
\end{aligned}
\qquad (6.1)
$$

where g_w is the fraction of wet surface area relative to its maximum value (w_2^+). The three surface fractions are constrained by:

$$
\Sigma \, w_i = 1 \qquad (6.2)
$$

g_w is, in general, not measured, but canopy water storage amount is accessible for observation. Fractional canopy storage x is defined as the ratio between actual canopy water storage and the canopy water storage capacity. It is assumed that fractional wet surface area is uniquely related to fractional storage through wetting function $g_w = g_w(x)$. Note that $g_w(1) = 1$ and $g_w(0) = 0$. From Huber and Itier (1990) we take $g_w(x) = x^v$, where v defines the curvature of the wetting function. It is a free parameter of the model.

The fluxes of temperature $\langle wt \rangle_i$ and specific humidity $\langle wq \rangle_i$ are defined per unit area of the corresponding surface fraction. Thus the total fluxes of temperature $\langle wt \rangle$ and specific humidity $\langle wq \rangle$ are given by:

$$<wt> = \Sigma \ w_i <wt>_i$$
$$<wq> = \Sigma \ w_i <wq>_i$$

(6.3)
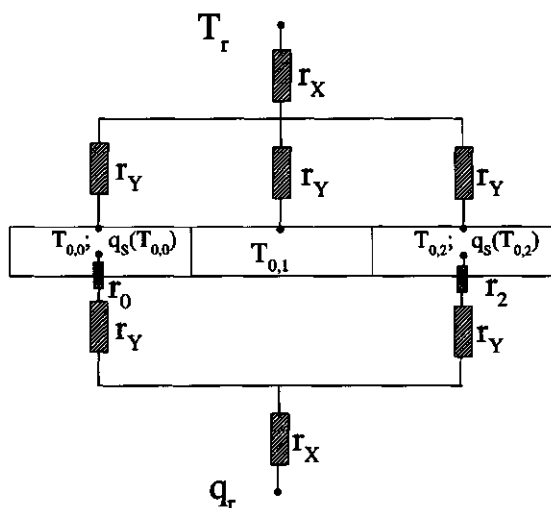
Figure 6.2. Resistances between reference level and the three surface fractions, both for temperature and moisture. Symbols are explained in the text.

Aerodynamic resistance

By following Monteith (1977) and as indicated in Figure 6.2, the aerodynamic resistance between the reference level and the surface r_a is split into two parts; r_x is the common resistance for all surface types from the reference level to a merging level closer to the canopy; r_y is the resistance from this merging level to each surface type. Here it is assumed that the aerodynamic resistances for water vapour and temperature are equal. Surface resistance for fraction 0, r_0, and for fraction 2, r_2 are introduced. For the stomatal free dry part surface resistance is infinite and therefor ignored in the figure. Analogous to the derivation of the Penman-Monteith equation we write down the temperature differences and specific humidity differences over the paths from the different parts of the leaf to the reference level and assume that the specific humidity inside the surfaces are at saturation:

$$r_x \cdot <wt> + (r_y \quad) \cdot <wt>_i = T_{0,i} - T_r$$
$$r_x \cdot <wq> + (r_y + r_i) \cdot <wq>_i = q_{sat}(T_{0,i}) - q_r \qquad (6.4)$$

where $T_{0,i}$ is the temperature at the i'th surface, $q_{sat}(T_{0,i})$ is the saturated specific humidity at the surface temperature. r_i is the surface resistance for the i'th surface. Note again that $r_l = \infty$ in our case.

Using Taylor expansion for the specific humidity difference around the reference temperature T_r we arrive at:

$$q_{sat}(T_{0,i}) - q_r = D_r + S \cdot (T_{0,i} - T_r) \qquad (6.5)$$

where D_r is the specific humidity deficit at the reference level and S is the derivative of the specific humidity at saturation to the temperature. By combining Equation (6.4) and Equation (6.5) the unknown surface values of temperature and specific humidity can be eliminated, in much the same way as is done in the derivation of the original Penman-Monteith equation:

$$-S \cdot (r_y <wt>_i + r_x <wt>) + (r_y + r_i) \cdot <wq>_i + r_x <wq> = D_r \qquad (6.6)$$

Energy budget

For each surface of the single big leaf the radiation balance equation can be written down. The net radiation of the i'th surface type Q_i is given by:

$$Q_i = (1 - \alpha) \cdot K\!\downarrow + L\!\downarrow - \varepsilon \sigma T_{0,i}^4 \qquad (6.7)$$

where $K\!\downarrow$ is shortwave incoming radiation, $L\!\downarrow$ is longwave incoming radiation, α is albedo and ε is emissivity. Here we assume that all surface types experience the same radiation forcing from above and that the albedo and emissivity is the same for all surface types. To relate the net radiation to the energy balance of each surface type we assume that the soil and biomass storage heat flux G is distributed over the three surface types in proportion to their corresponding surface fractions. It is assumed that heat is conducted from the hotter surface types to the cooler surface types proportional to the temperature difference between the surface types. We then have for the available energy flux per unit area of surface type i:

$$A_i = \rho C_p <wt>_i + \rho \lambda <wq>_i + \rho C_p \sum_{j \neq i} w_j \cdot c_{ij} \cdot (T_{0,i} - T_{0,j}) \qquad (6.8)$$

where $A_i = Q_i - G$, ρ is the density of air, C_p the specific heat of air and λ is the specific latent heat of water. c_{ij} is the temperature conduction coefficient between surface j and i. The first term on the r.h.s. of Equation (6.8) represents the sensible heat flux from the i'th surface fraction (H_i). The second term on the r.h.s. represents the latent heat flux from the i'th surface fraction (λE_i). Taking the areal weighted sum of Equation (6.8) gives the total available energy flux per unit big leaf:

132

$$A = \sum_i w_i(\rho C_p \langle wt \rangle_i + \rho\lambda\langle wq \rangle_i) + \rho C_p \sum_i \sum_{j\neq i} w_i w_j \cdot c_{ij} \cdot (T_{0,i} - T_{0,j}) \qquad (6.9)$$

The heat conduction terms have to cancel which leads to the condition that c_{ij} is symmetric. By taking the difference of Equation (6.8) for index i and j we get:

$$\begin{aligned} -\varepsilon\sigma \cdot (T_{0,i}^4 - T_{0,j}^4) &= \rho C_p \ (\langle wt \rangle_i - \langle wt \rangle_j) + \rho\lambda(\langle wq \rangle_i - \langle wq \rangle_j) \\ &+ \rho C_p \left(\sum_{k\neq i} w_k \cdot c_{ik} \cdot (T_{0,i} - T_{0,k}) - \sum_{k\neq j} w_k \cdot c_{jk}(T_{0,j} - T_{0,k}) \right) \end{aligned} \qquad (6.10)$$

By virtue of Equation (6.4), the temperature differences can be expressed as a product of resistances and temperature fluxes which gives for Equation (6.10):

$$\rho C_p \ (1 + r_y(g_L + c)) \cdot (\langle wt \rangle_i - \langle wt \rangle_j) + \rho\lambda(\langle wq \rangle_i - \langle wq \rangle_j) = 0 \qquad (6.11)$$

where $g_L = \varepsilon\sigma T_r^3/(\rho C_p)$, the differential longwave radiative conductance which arises from the linearisation of the radiation term around the reference temperature. Here it is assumed that the c_{ij} all have the same value c. Equation (6.11) expresses that a difference in latent heat flux of two surface types is always compensated by an opposing difference in sensible heat flux between the two surface types, to keep the energy balance closed. The same equations also show that the differential sensible heat flux through the atmosphere is always accompanied by proportional amounts of heat conduction and differential longwave heating. Note that Equation (6.11) is the only place where the processes of heat conduction and differential longwave heating appear, and they appear only through the factor $1 + r_y(g_L + c)$, which is mathematically equivalent to ignoring conduction and longwave radiation and increasing the heat capacity of the air. Only two of the six components of Equation (6.11) are independent, here we choose $\{ij\} = \{01\}$ and $\{ij\} = \{21\}$.

The general solution for the latent heat fluxes

Thus the Equations (6.6), (6.9) and (6.11) constitute six independent equations with six unknown fluxes. Solving the model equations to explicit expressions for the fluxes is rather complicated. It is therefore advantageous to introduce at this stage the condition that surface fraction 1 is non-transpiring ($r_1 = $ inf) as is already anticipated in Figure 6.2. The water vapour flux of surface 1 becomes zero and component $i = 1$ of Equation (6.6) can be omitted. Thus the problem is reduced to a five variable problem. Setting $r_2 = 0$, as is done to simulate the effect of a water surface fraction, doesn't reduce the number of equations. It is even advantageous to keep r_2 as a free parameter, for the time being, because then the problem remains symmetric in 0 and 2, a property which makes solving the equations more easy and which can be exploited to check the calculations. Appendix B shows the important algebraic steps in the derivation of explicit expressions. For the latent heat flux from surface fraction 0, per unit area of the big leaf, we arrive at:

$$w_0 \lambda E_0 = \frac{\beta A + \rho \lambda D / r_a}{\beta + 1 + \hat{\eta}_0}$$

$$\hat{\eta}_0 = \frac{1}{w_0} \left\{ \eta_0 + (1 - w_0)(1 + \frac{\beta}{\mu})\delta_y + w_2 \frac{(1 + \frac{\beta}{\mu})\delta_y + \eta_0}{(1 + \frac{\beta}{\mu})\delta_y + \eta_2} (1 + \beta - (1 + \frac{\beta}{\mu})\delta_y) \right\} \tag{6.12}$$

where $\beta = S/\gamma$, $\mu = 1 + r_y(g_L + c)$, $\delta_y = r_y/r_a$, $\eta_0 = r_0/r_a$ and $\eta_2 = r_2/r_a$. Here the equation is cast in the usual Penman-Monteith form in which an apparent dimensionless surface resistance $\hat{\eta}_0$ for the water vapour flux from surface fraction 0 arises. The latter appears to be a function of the fractional areas and resistances of the different surface fractions. The third term in brackets in the expression for $\hat{\eta}_0$ represents the interaction between the two evaporating surface fractions. Note that this interaction term disappears when $\mu = 1$ (no leaf conduction and no differential longwave cooling) and $\delta_y = 1$ (the merging level at the reference level). It turns out that the fractional aerodynamic resistance δ_y always occurs in combination with $(1 + \beta/\mu)$. As such it is convenient to define a parameter p by:

$$p = (1 + \beta/\mu)\delta_y \tag{6.13}$$

Remember that p is a function of atmospheric resistance through μ. In the following we will apply the general solution of Equation (6.12) to derive expressions for transpiration and evaporation separately.

Application for transpiration

Transpiration in the presence of free liquid water is derived from Equation (6.12) by taking $\eta_2 = 0$. In that case η_0 is the surface resistance of the stomatal fraction. For the dry case, $w_2 = 0$, we have $w_0 = w_s$ and we demand that the original one component Penman-Monteith equation is recovered. Thus, the apparent dimensionless surface resistance $\hat{\eta}_0$ should be equal to the bulk dimensionless stomatal resistance η_S defined by $\eta_S = r_s/r_a$, where r_s is the bulk stomatal resistance. This leads to a relation between the surface resistance of surface fraction 0 and the bulk stomatal resistance:

$$\eta_0 = w_s \eta_s - (1 - w_s)p \tag{6.14}$$

Substituting this expression into Equation (6.12) for the general wet case gives:

$$Tr(\text{mod}) = w_0 \lambda E_0 = \frac{\beta A + \rho \lambda D_r / r_a}{\beta + 1 + \hat{\eta}_0}$$

$$\hat{\eta}_0 = \frac{w_s}{w_0} \left\{ \eta_s + (1 - \frac{w_0}{w_s}) p + w_2 (1 + \frac{\eta_s}{p})(1 + \beta - p) \right\}$$

(6.15)

The introduction of η_s makes the formulation for the dry case independent of w_s by definition. Equation (6.15) shows that for the wet case only the ratio of w_0 and w_s appears. This means that the value of the stomatal fraction (w_s) itself has no influence on the model transpiration. For the non-blocking case ($w_0 = w_s$) we have:

$$\hat{\eta}_0 = \eta_s + w_2 (1 + \frac{\eta_s}{p})(1 + \beta - p) \tag{6.16}$$

This shows that the resistance for transpiration increases in the presence of free liquid water. This is to be expected because the consumption of energy by evaporation and the moistening of the air close to the vegetation suppresses the capability to transpire.

Application for Evaporation

The evaporation from the free liquid fraction of the surface can be found by taking the solution given by Equation (6.12), interchange 0 and 2, put $\eta_2 = 0$ and substitute Equation (6.14):

$$Ev(\text{mod}) = w_2 \lambda E_2 = \frac{\beta A + \rho \lambda D_r / r_a}{\beta + 1 + \hat{\eta}_2}$$

$$\hat{\eta}_2 = \frac{1}{w_2} \left\{ (1 - w_2)p + \frac{w_0}{w_s} \frac{(1 + \beta - p)}{(1 + \eta_s/p)} \right\}$$

(6.17)

This shows that the presence of a non-evaporating surface fraction results in a finite resistance for evaporation. This resistance emerges from the resistance encountered by the compensating heat flux flowing between the dry and the wet fraction in order to keep the energy balance closed. As for the transpiration case it is seen that w_0 and w_s appear only as their ratio.

For $w_2 = 1$, i.e. total coverage with free liquid water and thus $w_0 = 1$, we recover the potential evaporation formula with zero surface resistance. Also for $p = 0$ the potential evaporation is recovered. This corresponds to the fine dispersed droplets case (Shuttleworth, 1976; Monteith, 1977).

For $\delta_y = 1$ and no leaf conduction and no differential long wave cooling the dry and wet parts become independent. For this case $p = 1 + \beta$ and the evaporation becomes:

135

$$Ev(\text{mod}) = w_2 \lambda E_{pot} \tag{6.18}$$

where λE_{pot} is the potential evaporation derived from the Penman-Monteith equation.

The role of the stomatal fraction

Equations (6.15) and (6.17) show that the dependency of the transpiration and evaporation on w_0, the stomatal surface fraction not covered with water, comes only in the ratio to w_S, the stomatal surface fraction. This shows that the model has superfluous degree of freedom. In principle we can take the limit $w_S \rightarrow 0$ and retain the ratio f_S which still determines the fraction of maximal stomatal blocking. In this limit the surface resistance of the stomatal fraction goes to zero as well. From Equation (6.1) it is found that $w_2^+ = f_D + w_S(f_S - f_D)$. By taking the limit $w_S \rightarrow 0$ we find that $w_2^+ = f_D$ and thus w_2^+ and f_S become independent parameters.

6.4   Results

We have defined the model and derived expressions for evaporation and transpiration from the coupled set of algebraic equations. Evaporation and transpiration are expressed in terms of meteorological forcing variables and in terms of a number of parameters which relates to the details of the two processes and their interaction. In this chapter we use observations to estimate the model parameters. First the parameters related to evaporation are derived from canopy water storage measurements and then the only remaining parameter, f_S, related to stomatal blocking is estimated from sapflow measurements.

Parameters are found by constructing a normalised sum of squared residuals between observed and modelled evaporation fluxes (χ^2). Normalisation is based on the standard deviation of the individual observations (σ_y^2). The optimal parameters are obtained by minimising χ^2. The minimum of χ^2 is denoted by χ_0^2. By absence of an independent estimate of σ_y^2 the value χ_0^2/N is chosen, where N is the number of observations. Standard statistical theory states that confidence limits on the parameter estimates can be calculated by varying the parameters such that $\Delta\chi^2 = \chi^2 - \chi_0^2$ is less than approximately the number of free parameters. Bosveld and Bouten (1999a) discuss the consequences if assumptions on statistical independence of the residuals and perfectness of the model are not fulfilled. They suggest that for their eddy-covariance transpiration observations during dry days, the confidence limit on $\Delta\chi^2$ should be increased perhaps by a factor 2 to 3.

Analysis of evaporation observations

From the micro-wave interception observations 15 periods after rain events were selected during which no rain or drainage of intercepted water occurred, and during

136

which significant drying of crown water occurred. The evaporation flux for the current half hour was derived by taking the difference between the next and the previous half hour average canopy water storage amount. As defined previously fractional storage (x) was calculated from observed canopy water storage amounts divided by the canopy water storage capacity. The micro-wave attenuation measurements depends on free liquid water as well as water that resides in the biomass tissue. During dry episodes there is still some variation in the background attenuation which can be attributed to processes like dew fall, water storage change in the biomass and shoot growth. An accurate determination of the background value is of importance to interpret evaporation especially at the end of drying episodes. The background value was checked for each drying episodes and corrections with an estimated accuracy of 0.02 mm were applied where necessary.

To present the data in an interpretable way we use a reference evaporation according to:

$$Ev(ref) = x\lambda E_{pot} \qquad (6.19)$$

which is derived from the approximation presented in Equation (6.18) by putting $w_2^+ = 1$ and $v = 1$. Note that Ev(ref) is a rather arbitrary reference evaporation, because λE_{pot} generally depends on the reference height. Figure 6.3 shows half hourly values of observed evaporation as a function of reference evaporation for the selected 15 drying episodes. The data are stratified into three classes of fractional storage. It is observed that at high storage fractions the evaporation tends to be lower than the reference evaporation. Here the stomatal conductance formulation for transpiration of Bosveld and Bouten (1999a) was chosen with their parameter values, which were estimated on the basis of hourly eddy-correlation measurements. The maximum stomatal blocking was fixed to $f_S = 0.0$.

The evaporation model is optimised against the observations of the 15 selected drying episodes. To cope with interdependencies between the parameters, the parameter w_2^+ is fixed at 0.3. This choice will be discussed in the next section.

Run	N	Rms (W m^{-2})	v	w_2^+	f_S	δ_y	c
A	551	38.6	1.13±0.05	[0.3]	[0.0]	0.48±0.08	0.40±0.24
B	551	39.6	1.17±0.04	[0.3]	[0.0]	0.67±0.04	[∞]
C	551	40.4	1.14±0.04	[0.3]	[0.0]	0.25±0.02	[0.0]
D	551	38.6	1.22±0.04	[0.3]	[0.0]	0.48±0.08	0.41±0.25
E	551	38.9	1.06±0.04	[0.3]	[0.0]	0.57±0.09	0.36±0.21

Table 6.a. The results of various optimalisations for the evaporation part of the model. Differences between the runs are explained in the text,
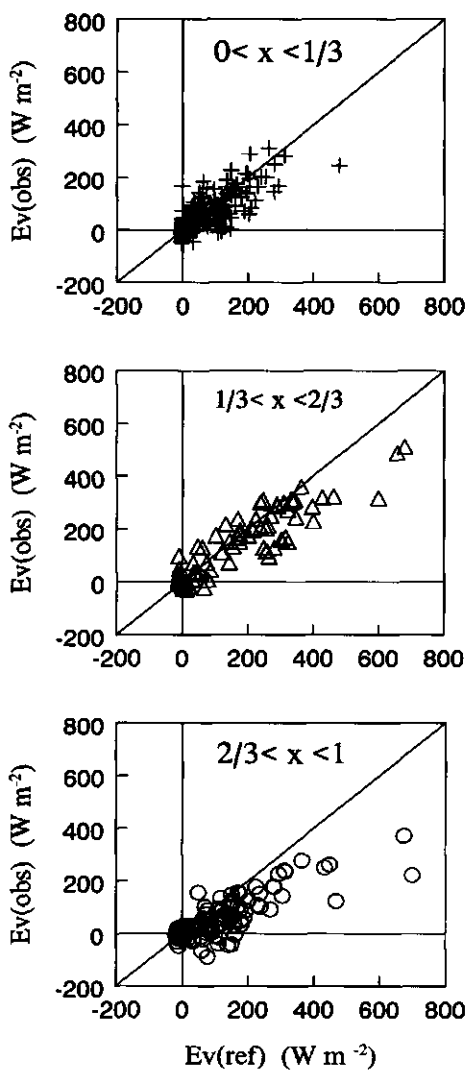
Figure 6.3. Observed evaporation as function of storage fraction times potential evaporation for 15 selected episodes. Data are classified into fractional storage classes.
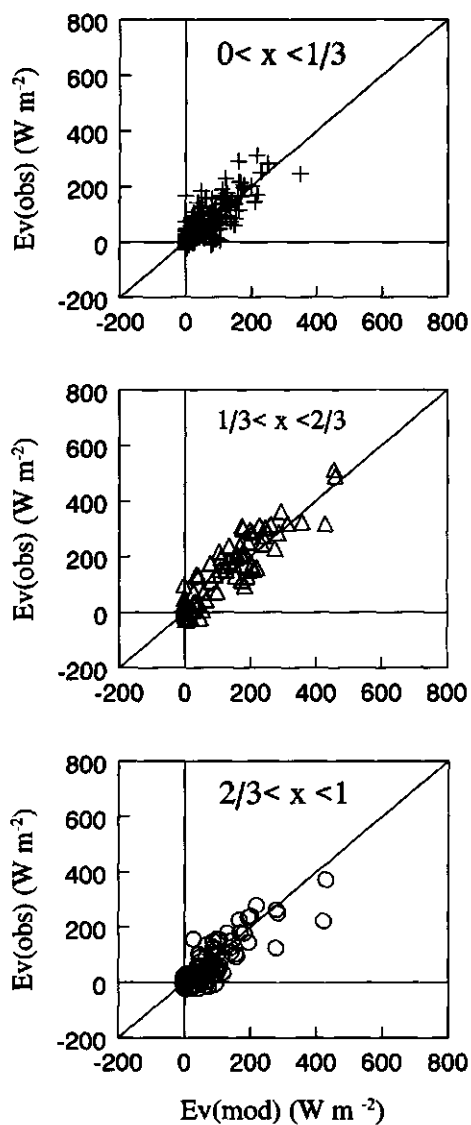
Figure 6.4. Same as figure 6.3 but now as function of optimized evaporation model.

between the optimised model evaporation and the measured evaporation. Again data are stratified into three wetted fraction classes. Much of the difference between the classes has disappeared and the model is capable of describing the measurements rather well.

The effect of transpiration on the evaporation is investigated. To this end the evaporation model was run with the optimised parameters fixed at the values of Table 6.a Run A, but with two different transpiration settings: 1) $f_s = 1$ (maximal blocking) and 2) $\eta_s = \infty$ (no transpiration). For the selected periods model evaporation is enhanced with 5% and 10% respectively over the 15 days period. In practice this would result in a quicker drying of the wet canopy after a rain event.

Analysis of transpiration reduction

In this section we investigate the impact of evaporation of intercepted crown water on transpiration. Transpiration is derived from sapflow measurements which were calibrated on eddy covariance measurements and soil water balance measurements, as described in Appendix 6.A. A single big leaf model (Bosveld and Bouten, 1999a), optimised against 61 dry days of sapflow measurements, was used to calculate the reference transpiration, Tr(ref), against which transpiration reduction can be evaluated. The model was run with time steps of one hour, but daily average values were used to optimise the model parameters. This was done because storage effects in the plant tissue result in a diurnal sapflow pattern that can differ from the diurnal variation of transpiration. In Table 6.b run A the optimisation result is

Run	N	Rms. W m^{-2}	$g_{s,ref}$ mm s^{-1}	a_D kg g^{-1}	$K_{1/2}$ W m^{-2}	β_ψ (<204) MPa^{-1}	β_ψ (>204) MPa^{-1}
A	61	4.4	14.8±0.1	0.30±0.02	70±22	1.7±0.2	1.3±0.1
B	61	7.4	20.2±0.2	[0.28]	[303]	1.7±0.2	0.8±0.1

Table 6.b. Two optimalisations for the transpiration model against dry-case sapflow values. Run A with $K_{1/2}$ and a_D free. In run B they are fixed at values optimizing for the diurnal change.

given. Here $g_{s,ref}$ is the stomatal conductance at a reference value for specific humidity deficit ($D_r = 3$ g kg^{-1}), a_D is related to the response to specific humidity deficit. $K_{1/2}$ represents the short wave incoming radiation at which light response is 50%, the β_ψ's relate to the soil water response before and after $DOY = 204$. For the functional forms we refer to Bosveld and Bouten (1999).

Now the parameter values optimised on the 61 dry days of sapflow observations are used to give model values of transpiration for the 44 selected wet days. In this respect the model serves as a reference transpiration against which
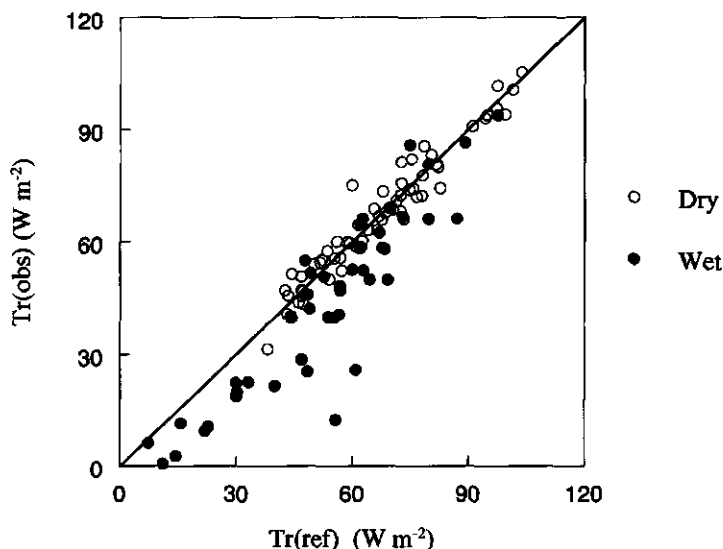
Figure 6.5. Daily averaged observed transpiration against reference transpiration. Data are stratified into dry and wet days.

transpiration reduction during wet periods can be estimated. Figure 6.5 shows the observed daily sapflow values as a function of reference transpiration. A stratification into wet and dry days is made. Values for dry days spread along a 1:1 line due to the optimisation process. The figure shows that measured sapflow is lower than the modelled reference transpiration for wet days. This indicates that transpiration reduction indeed occurs when the canopy is wet.

We are now in a position to use the evapo/transpiration model and see if it is capable of describing the observed transpiration reduction. Parameters for the evaporation part of the model are taken from Table 6.a, Run A. Parameters for the transpiration part are set according to the reference transpiration (Table 6.b, Run A). The only remaining parameter is f_s which describes the amount of blocking of stomata. It is found that average transpiration rates of model and observations become equal when $fs = 0.36 \pm 0.13$ is chosen. The confidence interval is based on the standard deviation between daily model values and observations of transpiration. This leads to an estimate of the uncertainty in the average transpiration over the 44 selected days from which the confidence range for f_s is derived. Figure 6.6 shows for the same data as in Figure 6.5 observed daily transpiration (sapflow), but now against transpiration according to the evapo/transpiration model with $f_s = 0.36$. It shows that transpiration reduction for the wet days is described well by the model, although scatter is somewhat larger than for the dry days. Table 6.c lists the
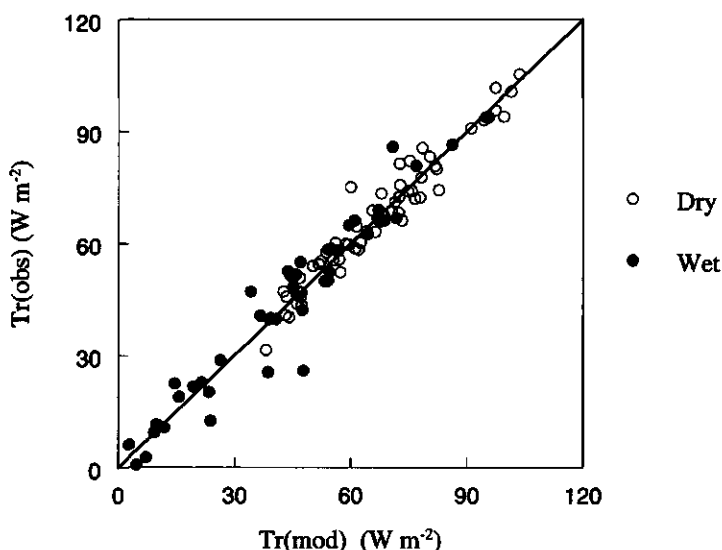
Figure 6.6. Daily averaged observed transpiration against modelled transpiration with wet/dry interaction and $f_S = 0.36$.

	(W m^{-2})	(W m^{-2})
Observed	43.8	Difference
Reference	53.0	+9.2
f_S=0.0	46.4	+2.6
f_S=1.0	38.7	-5.1

Table 6.c. Comparison of averaged transpiration rates. Observed versus various model runs.

observed transpiration rates averaged over the 44 wet days. Also listed are model values for three different interactions with evaporation. They are, 1) the reference transpiration based on the dry days optimalisation, 2) interaction with evaporation, but no stomatal blocking ($f_S = 0$) and 3) interaction with complete stomatal blocking at maximum wetting ($f_S = 1$). It is found that transpiration reduction amounts to 17% of the reference transpiration for the current 44 wet days. the largest part

(12%) of the reduction is explained by energy consumption and micro-climate change. The remaining reduction of 5% can be explained by assuming a maximum blocking of 1/3rd of the stomata.

6.5   Interpretation of the parameter estimates

In the previous section we have showed that the processes of evaporation and transpiration reduction can be described by the current evapo/transpiration model. In this chapter we turn to the interpretation of the parameter values. This involves an investigation of interdependencies of the model parameter and an analysis of the sensitivity of the model parameters with respect to uncertainties in the measurements and assumptions.

Interdependencies and parameter constraints

When different parameter combinations lead to the same evaporative flux, they are said to be interdependent. In such a case the measurements contain no information on the individual parameters, but often information is present that defines a relation between the dependent parameters. The evaporation equation (6.17) shows that the minimum surface resistance for evaporation occurs at maximum wetting, this is most clearly demonstrated by taking $\eta_{ls} = \infty$, i.e. ignoring transpiration. This suggests that the same evaporation rate can be obtained at a small maximum wet fraction (w_2^+) and a small value of p as at a larger maximum wet fraction and a large value of p. Thus p and w_2^+ are highly interdependent.

We note, however, that p is not a parameter of the model, but is a function of aerodynamic resistance and the model parameters c and δ_y through Equations (6.12) and (6.13). c and δ_y both relate to the resistance for heat flow between the surface fractions. In fact for $c = 0$ and $c = \infty$ corresponding δ_y values can be found with the same p value, which leads to the same modelled fluxes. In these extreme situations the dependence of p on the aerodynamic resistance disappears. Thus an intermediate value of c serves to introduce some aerodynamic resistance dependency in the formulation of p. Optimalisations are performed with c fixed at 0 and ∞ respectively. Table 6.a, run B and C show that δ_y is indeed quit sensitive to this variation in c. Both runs also show that eliminating the aerodynamic effect in p leads to a significant increase of the Rms.-value of the residuals.

The previous analysis suggest that w_2^+, c and δ_y are all to some extend interdependent and thus, we cannot expect that all parameters can be derived by optimising the model against evaporation observations. To find the individual parameter values one has to turn to other sources of information. In this paragraph independent estimates of the model parameters are sought for.

An estimate for c is obtained by assuming that the dry and wet fraction is dived in a chessboard pattern. Let l be the distance between the centres of the squares. This is the horizontal length scale, already noted in the section on model

expected because the increment in storage amounts has greatest influence at the end of drying periods. This is where model performance is especially sensitive to the wetting exponent.

At the start of drying episodes when storage amounts are high the comparison between model and observations rely heavily on the accuracy of the moisture deficit observations of which limitations has already been discussed in a previous section. Table 6.a run E shows the optimised parameters when specific humidity is decreased by 0.2 g kg^{-1}. The effect is to increase the moisture deficit and consequently of potential evaporation. The change in parameter values leads to an increased apparent surface resistance. The change in parameter estimates is within the confidence limits

In the evaporation part of the model we fixed the parameter w_2^+ at 0.3. This was necessary due to the interdependency of the model parameters. By repeating the whole parameter optimisation procedure for w_2^+ values between 0.2 and 0.4, values for f_S between 0.28 and 0.42 were found.

The behaviour of stomatal conductance at low moisture deficit is not well determined from the analysis of dry days because these conditions hardly occur. For wet days low moisture deficits are more common. Here we investigate the sensitivity of f_S to a change in stomatal conductance for the moisture deficit range 0 $< D_r < 1$ g kg^{-1}. Instead of a constant moisture deficit response for this range which is used in the original formulation, we let the stomatal conductance increase linearly with a factor 2 when decreasing D_r from 1 to 0 g kg^{-1}. Optimising the transpiration model for dry days with such a moisture deficit response for almost saturated cases did not show an influence on the other parameters related to stomatal conductance of the transpiration model. As expected, for the wet days this new reference transpiration leads to somewhat higher transpiration rates at low moisture deficit. This results in a somewhat higher f_S value of 0.41, compared to 0.36, needed to get the same modelled transpiration reduction as is observed.

Daily sapflow measurements were used to derive surface conductance parameters for the reference transpiration. The resulting value for $K_{1/2}$ (70 W m^{-2}) differs significantly from the value found by Bosveld and Bouten (1999a), $K_{1/2} = 300$ W m^{-2}, based on hourly eddy-covariance measurements. This means that the reference transpiration is not very accurate in resolving the diurnal cycle. Table 6.b run B show the result of a new optimisation where the parameters $K_{1/2}$ and a_D are fixed at the values found in Bosveld and Bouten (1999). It shows that the Rms.-value of the residuals is significantly higher than in run A. Figure 6.8 shows daily averages for both optimisations against observed daily averaged sapflow flux. It is observed that the model with fixed $K_{1/2}$ and a_D tends to underestimate daily averages at low transpiration rates and to overestimate at high transpiration fluxes. This suggest that the influence of short wave radiation, which is strongly correlated with available energy, is not completely described by the current model formulation of transpiration. At cloudy days with low irradiation the forest can sustain higher transpiration rates than the model (run B) predicts. At clear days with high irradiation the forest cannot sustain the high transpiration rates described by the

146

120

90

Tr(mod) (Wm^{-2})

60

30

0

0   30   60   90   120

Tr(obs) (Wm^{-2})
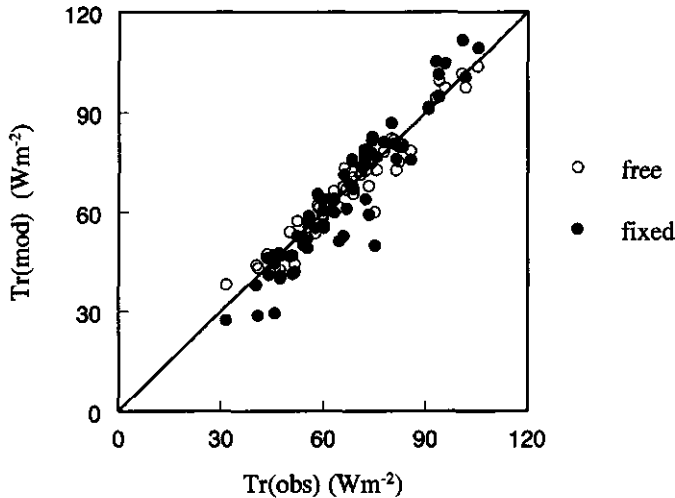
o   free

•   fixed

Figure 6.8. Simulated transpiration as function of observed daily sapflow for two optimalisations. (o) free $K_{1/2}$ and a_D, (•) fixed $K_{1/2}$ and a_D.

model. This may be the result of a larger soil water depletion around the roots during days when atmospheric demand is high. This depletion may disappear during the night through soil water transport. Another explanation may be the deeper penetration into the canopy of diffusive sunlight as compared to direct sun light. This would lead to more needles deeper in the crown becoming photosynthetically active with a lower stomatal conductance as a result. Bosveld and Bouten (1999) found the same result based on their eddy-covariance transpiration measurements when optimising the transpiration model on daily transpiration amounts. This then is the rational to use run A as the reference transpiration in the current analysis. Using run B as a reference transpiration leads to no transpiration reduction at all for the 44 wet days, this seems physically unrealistic.

6.6   Discussion and conclusions

A straightforward generalisation of the Penman-Monteith combination equation is obtained for a single big leaf, partly covered with water. Three surface fractions are discriminated; a stomatal fraction, a non-stomatal fraction and a wet fraction. The model allows for a consistent description of the interaction between evaporation and

147

transpiration. Explicit expressions are obtained for the rate of transpiration and evaporation as function of stored canopy water. It is shown that the processes of aerodynamic heat conduction between the surface fractions, heat conduction through the needle tissue and differential longwave radiative exchange can be condensed into one model variable (p).

Apart from stored canopy water the following parameters govern the evaporation part of the model: 1) maximum wettable fraction, 2) leaf heat conductance, 3) curvature of the wetting function and 4) fractional aerodynamic resistance to the merging level of dry- and wet surface fraction. The transpiration part of the model is governed by: 1) maximum fractional blocking, describing the physical blocking of stomata by liquid water on the needles and 2) Surface conductance, described by a Jarvis type of response functions with corresponding parameters.

The transpiration part of the model is formulated in such a way that the original Penman-Monteith formulation is recovered in the dry limit. By introducing the bulk stomatal resistance, the model becomes independent of the stomatal fraction in the dry limit. A surprising result of the model is that the same holds in the presence of water. This leads to an important simplification of the model by taking the limit to vanishing stomatal fraction while keeping bulk stomatal resistance constant.

Formulations for evaporation found in the literature like, potential evaporation or wetted surface fraction times potential evaporation can all be derived from the current model by taking appropriate limits. By applying the full model, significant better agreement between model and measurements is found, than by using these limiting formulations

Modelled transpiration reduction is compared with observations of sapflow during wet days and a reference transpiration derived for dry days. It is found that the observed transpiration reduction can, to a large extend, be explained by the processes of energy consumption, and by the change of the micro-environment, both due to the presence of the evaporating wet fraction. Together with these two processes, some stomatal blocking is needed to explain the total observed transpiration reduction. Estimated stomatal blocking is only $1/3^{rd}$ at maximum canopy wetness, which is in concord with in situ observations which shows that the lower sides of the Douglas-fir needles are only partly covered with water during wet episodes. This is the side where stomata are situated. A consequence is that dry-deposition of hazardous trace gases may continue at high rates when the canopy is wet.

In this study the moisture deficit observations at reference height are used as a forcing variable of the model. In this way we don't have to deal with feedback of the vegetation on the atmosphere. As pointed out by McNaughton and Jarvis (1983) moisture deficit close to a wet forest is intimately linked to the evaporation process. It is the combination of available energy and the stabilisation of the atmospheric profile when evaporation rate is high that determines the resulting moisture deficit. This leads to the concept of equilibrium evaporation, which is potential evaporation

148
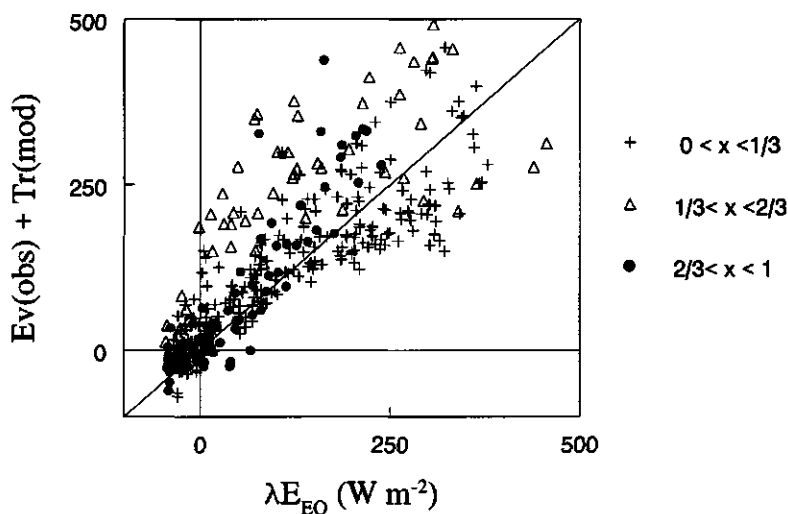
Figure 6.9. Half hourly values of the sum of observed evaporation and modelled transpiration against equilibrium transpiration. Data are stratified into fractional storage classes.

at zero water vapour deficit, as a limiting value for evaporation if advection is not important. In Figure 6.9 the observed evaporation fluxes are compared with the equilibrium evaporation. Data are stratified into classes of fractional storage. Although scatter is large it shows that most of the observations are larger than equilibrium evaporation especially when $x > 1/3$. This suggests that advection plays a role at the current location. This is to be expected because the current forest stand has very high LAI compared to neighbouring stands. Moreover the forest area is also of limited extend (scale of 5 km) and surrounded by low vegetation.

Figure 6.10 displays a time series of measured evaporation (Ev(obs)) and sapflow (Tr(obs)). Also shown are the modelled evaporation (Ev(mod)), reference transpiration (Tr(ref)) and reduced transpiration (Tr(mod)). The reduced transpiration follows sapflow very well till the end of the afternoon, after which the already noted night time deviations occur.

The use of a single level model in contrast to a vertical structured model leads to simplifications. The distribution of dry and wet surface changes during the drying process in a more complex way than described by the current model. Canopy convection from the level where intens evaporation takes place, may lead to transport of cool and moist air into the deeper layers of the forest. Canopy convection is shown to exist for the current forest during clear nighttime conditions
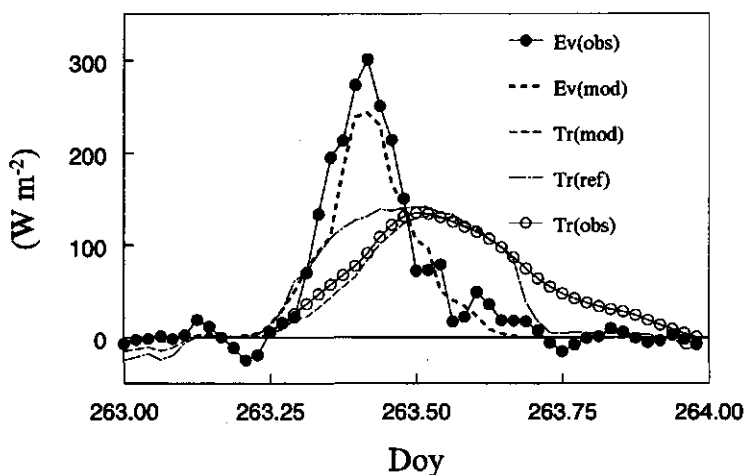
Figure 6.10. Evaporation and transpiration both observed and modelled for one day with a drying episode. Also shown is the reference transpiration. Sapflow deviates at night.

(Bosveld et al., 1999b). This may lead to an evaporation front evolving down into the canopy, explaining the success of the four layer model of Bouten et al. (1996) which was used to describe the whole cycle of interception, drainage and evaporation. The consequence of such a drying front is that needles in the top layer, well exposed to solar irradiation and thus high stomatal conductance, are the first to become active in terms of transpiration. This might suppress the importance of transpiration reduction.

All these simplifications hamper physical interpretation of the model parameters. It is likely that a model parameter, introduced to describe one process, is adapted to mimic a process not captured in the model. However, the range of parameter combination estimated from auxiliary information of the forest location is broadly in line with the estimates obtained from the optimalisation analysis.

6.7   Acknowledgment

6.A   Calibration of sapflow measurements

For the current study two methods were available to quantify the forest transpiration: (1) eddy correlation measurements at 30 m above the forest floor and (2) soil water balance calculations based on Time Domain Reflectometry (TDR), neutron scattering and tensiometer measurements. Here it is described how xylem sap flux calculations, based on the measurement of Heat Pulse Velocities (HPV) are calibrated against the two quantitative methods to arrive at transpiration fluxes representative for the current forest stand.

All three methods are carried out at different temporal and spatial scales. Transpiration amounts calculated from soil water balances were obtained on a daily basis, whereas hourly rates were determined with the other techniques. The eddy correlation measurements are described in Bosveld and Bouten (1999a). They produce a spatially averaged value over a region reaching well over the edge of the current stand. In the same study it is shown that impact of inhomogeneities in upwind directions on observed transpiration rates are limited. The soil water measurements are described in Tiktak and Bouten (1994). They are carried out in the root zones of about 40 trees spread over 9 sites within the stand. Sap flow was measured in 12 trees on 2 sites within the stand.

In order to compare transpiration estimates obtained by soil water balance calculations and by eddy correlation measurements, 21 measuring periods with no rain and with negligible drainage were selected. The lengths of these periods range from 1 day to 2.5 days, amounting to a total length of 30 days. Transpiration amounts were calculated from the differences in soil water content between the start and end of these periods, and from measured water vapour flux densities integrated over time. The correlation between the two estimates is rather poor ($R^2 = 0.52$) due to the relatively large errors in each type of estimate. Summed over all periods, a total of 85.1 mm was calculated for soil water balance and 78.0 mm for eddy correlation. These amounts are within the estimated error bounds. It was concluded, therefore, that the estimates of both techniques could be used to calibrate the HPV dynamics and to translate the results into a mean sap flux density for the total stand.

Seven sensors were selected which showed good coverage over the observing period. Direct averaging is not recommended since HPV amplitudes show a large variation among sensors. As heat pulse velocities lower than 1.1 cm hr^{-1} could not be measured, all sensors show missing values at different points, especially during night-time. Actually, the minimum sap flux density that can be measured differs for each sensor because of their characteristic sensitivity. If the missing values are set to zero, transpiration is underestimated. If they are omitted transpiration is overestimated because sensors with high HPV-values will dominate.

As an alternative, the time series of each sensor was scaled by fitting sine-functions through the measured HPV values for all dry days within the measuring period. The fit was obtained by minimising the sum of squares of the differences between the measured values obtained from individual sensors and a sinusoidal model described by:

$$HPV_{mod,i} = C_{1,i} + C_{2,i} \sin(2\pi[t - C_{3,i}])$$ (6.21)

Here, $C_{1,i}$, $C_{2,i}$ and $C_{3,i}$ are fitting parameters for sensor i, representing mean value, maximum amplitude and time lag, respectively; t is time [days]. The scaled HPV dynamics (*ScHPV*) of the various sensors were then calculated according to:

$$ScHPV_i = \frac{HPV_i - C_{1,i}}{C_{2,i}}$$ (6.22)

where HPV_i is the measured HPV of sensor *i*. In this way, all the HPV data are transformed such that they have the same mean value over the whole observing period (mean value = 0), and also the same mean of the daily maximum amplitude (mean value = 1). $C_{3,i}$ values were not incorporated in this scaling as all the sensors yielded the same value. After scaling the time series of all the sensors in this way, they exhibit comparable dynamics, making it possible to calculate arithmetic means of the scaled heat pulse velocity (*MScHPV*).
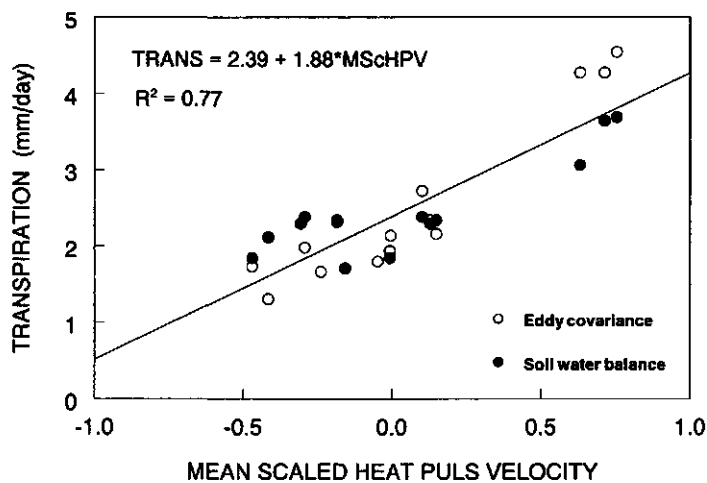
Figure 6.11. Regression of mean transpiration rates, estimated from eddy-correlation measurements and soil water balance calculations, with the mean scaled HPV, integrated over the same time intervals.

These mean scaled heat pulse velocities can be converted to sap flux densities (*SFD*), defined as vertical water flux within the trunk per unit soil surface, using the absolute transpiration values from eddy correlation and soil water balance calculations. Thirteen periods overlapping with eddy correlation measurements, and

152

fifteen periods overlapping with soil water balance measurements, ranging from 1 to 2.5 days, were available for estimating sap flux densities. Figure 6.11 shows the integrated *ScHPV* as function of the integrated amounts based on eddy-correlation (full squares) and soil water balance (open squares). If plant tissue storage differences are assumed to be negligible over time intervals of one day or longer, transpiration amounts derived from eddy correlation or soil water balances can be set equal to the sap flux density integrated over the same time interval. Since the sap flux density is assumed to be linearly related to the *MScHPV*, a regression of the mean transpiration rates against the integrated *MScHPV* produces estimates of the linear coefficient and the constant, also shown in Figure 6.11. From this the mean sap flux density can be calculated.

Theoretically, effects of installation and emboly around sensors cause an additional heat pulse delay which does not depend on the convective flow velocity: the higher the convective velocity, the larger the relative effect of this delay and thus the larger the effect on the measured heat pulse velocity. A curved relationship between sap flux density and HPV is, therefore, to be expected. As the data do not allow the estimation of another parameter, a linear relation was chosen to translate HPV into sap flux densities.

In order to check the assumption that one set of parameters for each sensor can be used throughout the growing season, the annual trend of each sensor was compared with the mean trend for all sensors. No systematic deviations were found. To check for a systematic deviation by all sensors in parallel the data have also been analysed as a function of time. No indication could be found that the parameters varied throughout the measuring period.

6.B Derivation of the model fluxes

We start with the Equations (6.6), (6.9) and (6.11), and set $r_1 = \infty$, which results in 5 equations with 5 fluxes. We introduce the dimensionless aerodynamic resistances:
$$\delta_x = r_x/r_a \ , \ \delta_y = r_y/r_a$$
the dimensionless surface resistances of surface fractions 0 and 2:
$$\eta_0 = r_0/r_a \ , \ \eta_2 = r_2/r_a$$
and the thermodynamic parameters:
$$\beta = S/\gamma \ , \ \mu = 1 + r_y(g_L + c)$$
Then we rearrange the two remaining components of Equation (6.6) into a difference and sum equation. We then arrive at the matrix equation:

$$\begin{pmatrix} w_0 & w_0 & w_1 & w_2 & w_2 \\ -\beta(\tfrac{1}{2}\delta_y + w_0\delta_x) & \tfrac{1}{2}\eta_0 + \tfrac{1}{2}\delta_y + w_0\delta_x & -\beta w_1\delta_x & -\beta(\tfrac{1}{2}\delta_y + w_2\delta_x) & \tfrac{1}{2}\eta_2 + \tfrac{1}{2}\delta_y + w_2\delta_x \\ -\beta\delta_y & \eta_0 + \delta_y & 0 & \beta\delta_y & -(\eta_2 + \delta_y) \\ \mu & 1 & -\mu & 0 & 0 \\ 0 & 0 & -\mu & \mu & 1 \end{pmatrix}$$

$$\times \begin{pmatrix} H_0 \\ \lambda E_0 \\ H_1 \\ H_2 \\ \lambda E_2 \end{pmatrix} = \begin{pmatrix} Q^* \\ \rho\lambda D_f/r_a \\ 0 \\ 0 \\ 0 \end{pmatrix} \qquad (6.23)$$

We now solve for λE_0. The numerator is $\mu[\beta\delta_y + \mu(\eta_2 + \delta_y)](\beta Q^* + \rho\lambda D_f/r_a)$. We recognise in the last factor the usual numerator of the single component Penman-Monteith equation. Thus as a guidance for calculating the denumerator, i.e. the determinant of the 5×5 matrix in Equation (6.23), we try to obtain the first two factors of the numerator expression explicitly.

We introduce

$K_0 = \beta\delta_y + \mu(\eta_0 + \delta_y)$

$K_2 = \beta\delta_y + \mu(\eta_2 + \delta_y)$

and performing the following column additions:

C1 + C3 + C4	is substituted in C3,
-C1 + μC2	is substituted in C2,
-C4 + μC5	is substituted in C5,

where Cx represents the x'th column from the matrix.

The determinant then is:

$$Det = \frac{1}{\mu^2} \cdot \begin{vmatrix} w_0 & (\mu-1)w_0 & 1 & w_2 & (\mu-1)w_2 \\ -\beta(\tfrac{1}{2}\delta_y + w_0\delta_x) & \tfrac{1}{2}K_0 + (\mu+\beta)w_0\delta_x & -\beta & -\beta(\tfrac{1}{2}\delta_y + w_2\delta_x) & \tfrac{1}{2}K_2 + (\mu+\beta)w_2\delta_x \\ -\beta\delta_y & K_0 & 0 & \beta\delta_y & -K_2 \\ \mu & 0 & 0 & 0 & 0 \\ 0 & 0 & 0 & \mu & 0 \end{vmatrix} \quad (6.24)$$

which can be evaluated to:

$$
\begin{aligned}
Det = \quad & K_2\ w_0\ (\beta\ (\mu\ -\ 1)\ +\ (\mu\ +\ \beta)\ \delta_x) \\
+& K_0\ w_2\ (\beta\ (\mu\ -\ 1)\ +\ (\mu\ +\ \beta)\ \delta_x) \\
+& K_0\ K_2
\end{aligned}
\tag{6.25}
$$

We observe the desired symmetry in index 0 and 2. With some algebraic manipulation we arrive at Equation (6.12).

7   Perspectives

The subject of this thesis is formulated in Chapter 1 as the scientific question:

-       What processes are relevant in controlling the exchange fluxes between the
        forest and the atmosphere and how can this control be quantified?

Answering this question leads to useful information for research on effects of air
pollution, weather and climate and remote sensing. Here we summarise the results
of the thesis and discuss to what extend we are now in a position to predict forest
response. In relation to this we also look at the generality of the results by
comparing characteristics of the current forest with information from the literature.

Results

We used the resistance concept with which atmospheric forcing variables at the
reference height are related to the corresponding fluxes. The aerodynamic resistance
in the roughness sublayer of the forest is described by extending the traditional
surface layer flux-gradient relations. The excess resistance is found on the basis of
infrared surface temperature measurements. The influence of the roughness layer on
the derived excess resistance is investigated. At night time the equivalence between
aerodynamic and radiation surface temperature breaks down due to canopy
convection. A model is developed to describe this process. The surface resistance
for transpiration is described in terms of the Penman-Monteith model and a Jarvis-
type formulation for the surface resistance. For wet conditions interaction occurs
between evaporation and transpiration. A generalised Penman-Monteith equation is
derived which describes evaporation and transpiration reduction as a function of the
external forcing variables and the fractional amount of intercepted canopy water.

Related studies

A number of other studies which are related to this study have been performed for
the current site. They form a valuable extension to this thesis. Here we summarise
in short the results of these studies. Schaap and Bouten (1997) studied forest floor
evaporation on the basis of lysimeter measurements. A combination equation is
developed which describes forest floor evaporation as a function of atmospheric
forcing and water content of the needle layer. Forest floor evaporation for the
current site, turns out to be 5 to 10% of the total evaporation. In addition, Bouten et
al. (1996) use throughfall measurements and interception measurements to optimise
a four layer model that describes interception capacity, drainage rate and

evaporation efficiency. Given the atmospheric conditions including precipitation with sufficient time resolution the partitioning in interception and throughfall can be estimated. Tiktak and Bouten (1990) use the soil hydrological model Soil Water In Forested ecosystems (SWIF) to assimilate various soil hydrological measurements at the site. The model describes soil water development given the atmospheric forcings and the distribution of precipitation over interception and throughfall. In Tiktak and Bouten (1994) long term water balances are estimated for the site from synoptical weather observations.

The results of chapter 2 on flux profile relations, are applied in a number of studies to assess the deposition load on the forest of sulphurdioxide (Vermetten et al., 1992) and ammonia (Duyzer et al. 1992; Duyzer et al. 1994). Vermetten et al. (1994) use the same relations to derive monthly mean CO_2 fluxes.

Forest characteristics and their generality.

In this section we recapitulate the forest characteristics found in this study and compare them with results from other studies. Let us start with the albedo which has not been measured in the context of this thesis, but in a later stage. The value for albedo is 0.11, in line with other dense coniferous forest (Jarvis, 1976). Leaf area index (*LAI*) equals 10, but varies with season. This value is very high, most forests have a *LAI* below 5. Average height of the dominating trees, (*h*) equals 18 m. The roughness length for momentum (z_{0M}) is typically 2 m, but varies with wind direction and increases with increasing wind speed. The displacement height (*d*) is estimated as 70% of vegetation height, which equals 12.5 m. This is consistent with observed flux gradients relations for temperature and wind at the top of the roughness layer. *d* decreases with increasing wind speed. These values are in concorde with typical relations found in the literature for the roughness length for momentum, $z_{0M} = 1/3 (h - d)$, see Shaw and Pereira (1982). Even the variations with wind speed seems to adhere to this relations. Wind speed dependence of z_{0M} and *d* for forest is not often reported. Monteith (1973) shows an example of a Douglas fir in a wind tunnel.

The roughness layer coefficient for enhanced exchange of heat, $p_H = 0.6$. The roughness layer coefficient for enhanced exchange of momentum, $p_M = 0.0$. Figure 7.1 is adapted from a review of Cellier and Brunet (1992). It shows typical near neutral dimensionless gradients for heat (ϕ_H) and momentum (ϕ_M) for various vegetation types. Values are taken approximately half-way the depth of the roughness layer as a function of canopy density, here expressed as half of the single sided plant area index. The closed dots are from the current location. This shows that the current location fits well in the idea that very dense canopies show only enhanced mixing for heat and not for momentum.

Figure 7.2 shows dimensionless gradients (ϕ_H) as function of dimensionless height, scaled on canopy height, for various tall forest sites. Full circles are from the current location. Although all sites qualitatively show the same behaviour, quantitatively large differences occur. These differences are presumably related to

158
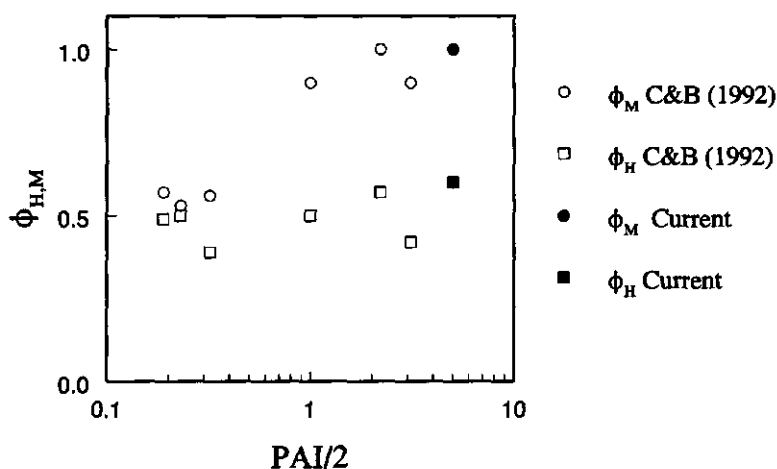
Figure 7.1. Typical ϕ_H and ϕ_M values for various forest roughness layers as function of forest density.

the different geometric structure of the forest. Raupach et al. (1996) put forward the mixing-layer hypothesis. They show that various turbulent quantities in the roughness layer of dense forests show typical characteristics of laboratory mixing-layer flows. In such flows, for example, different transport efficiencies of heat as compared to momentum is found. Perhaps this hypothesis helps to find a more relevant forest geometry related length scale. In the mean time the results suggest that well defined flux-gradient relations exist in the roughness layer of forests, but that for any reasonable desired accuracy these relations have to be derived in situ for each forest. It also points at the importance of determining the forest geometrical structure.

The question has been raised whether roughness layer flux-profile relations based on temperature exchange measurements can be applied for other scalar components. An essential characteristic of the roughness layer is that its turbulent characteristics are affected by the nature of the underlying surface. This may relate to the geometry of the vegetation, but also to the distribution of sources and sinks of the scalar quantity under consideration. Turbulent eddies in the roughness layer carry a signal of the source and sink distribution with them, a signal which is lost when reaching the surface layer. A hint in this direction might be the study of Simpson et al. (1998) who show that CO_2 exchange coefficients in the roughness layer of a mixed deciduous forest differ before and after leaf senescence.

159
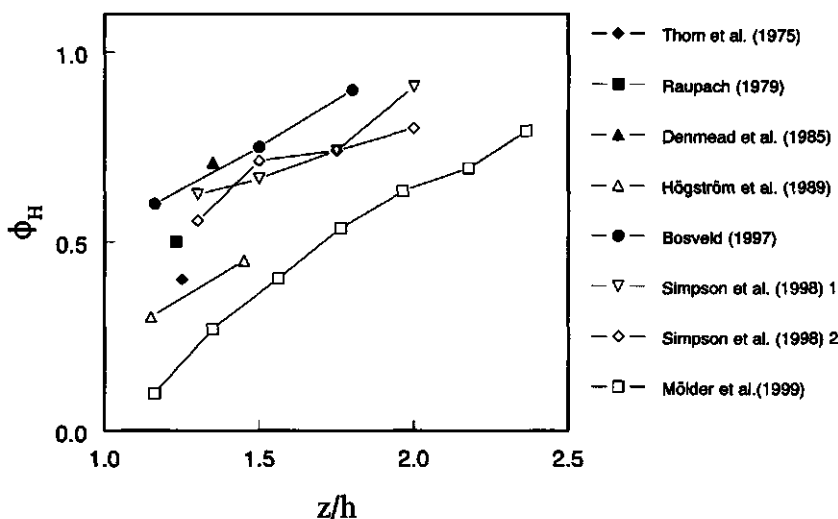
Figure 7.2. ϕ_H values for various forest roughness layers as function of dimensionless height.

The roughness length for heat (z_{0H}) equals 2 m. Together with the value for momentum this leads to an excess resistance of zero. A similar result has been found by Mölder et al. (1999) for a mixed Pine-Spruce Boreal forest (LAI = 3 to 6). The current thesis explains this low value as compared to low vegetation in terms of the enhanced mixing of heat in the roughness layer.

The roughness length related to convection from the crown layer into the forest interior, z_C = 0.23 m. This value has hardly any precedence in the literature. From the study of convection in Maize by Jacobs et al. (1996) we deduce that the soil/air interface has a much smaller roughness length related to convection. This can be understood because the crown layer of the current forest is of a very diffuse nature and extending over a large vertical depth in contrast to the rigid soil air interface.

The observed difference between aerodynamic and radiation surface temperatures is described with a two layer radiation/energy balance model. In this model coefficients arise which describe the distribution of storage heat flux and sensible heat flux over the two layers. The flux mixing coefficient for storage heat flux γ_G is 0.3 times $(1-q^2)$ and for sensible heat flux, γ_H is 0.1 times $(1-q^2)$, where q is the surface fraction occupied by the top layer of the model. These values explain the observed difference between aerodynamic and radiation surface temperatures. No precedence of these coefficients were found in the literature.

160

Canopy convection in forests during clear nights is not exceptional. Geiger (1961) already notes on the basis of nighttime observations of Baumgartner (1956) that cold air from the crown layer penetrates the forest interior. The current forest is exceptional because it has a very dense crown layer. This makes the interpretation of radiation surface temperatures much more simple than for more open forests where the forest floor temperature would interfere.

Daily averaged transpiration of the current forest seems to be in line with findings for other forests in temperate humid climate. A comparison with Thetford forest showed that transpiration rates are about the same despite the large difference in *LAI*. This suggest that transpiration models with canopy resistance inversely proportion to *LAI* overestimate the importance of *LAI*. Roberts (1983) shows, on the basis of a number of forest studies in the temperate climate, that variation of yearly totals of transpiration is small despite the large variation in precipitation amounts among the forest sites, typical transpiration amounts being 330 mm y^{-1}. In their study on long term water balances, Tiktak and Bouten (1994) show that the same holds for the year to year variation of the current forest. They show that variations in rain amounts are reflected primarily in variations of soil water drainage and in variations of interception evaporation. Transpiration variations results mainly from reduction by interception and reduction by soil water stress, of which variations over the years are small. The diurnal variation of transpiration is mainly determined by the light response and the specific humidity deficit of the air. Light response is rather gradual for the current forest, owing to the large *LAI*. The more sophisticated SVATS take this effect into account. The response to atmospheric water vapor deficit is strong, but in line with other temperate forests.

Interaction between evaporation and transpiration as described in this thesis has not been investigated in such detail before. Therefore no comparison can be made with the literature. The described model is equally applicable to other vegetation types. It would be of great interest to have similar studies performed for other canopies to look at the generality of the model formulation. Parameter values for the current model are obtained from drying events after rain. The distribution of water during wetting may be significantly different. This may lead to errors in the estimated fluxes when applying the model for the whole of the wet periods.

The impact of forests on the hydrological balance has been an important issue over the years. Due to high leaf area index many forests are capable of intercepting significant amounts of precipitation. Interception loss has been studied for a large number of forests. Studies of Rutter (1971) and Cooper and Lockwood (1987) show that interception loss is high in temperate humid climates where precipitation is distributed evenly over the seasons. It is estimated that in such climates interception loss amounts to 30-40% of the precipitation (McNaughton and Jarvis, 1983; Morton, 1984). The results of Tiktak and Bouten (1994) for the current forest suggest a 45% interception loss.

McNaughton and Jarvis (1983) show that the evaporation rate is strongly coupled to the atmospheric boundary layer through the atmospheric water vapour deficit. Therefore the actual evaporation depends on the horizontal extend of the wet

161

forest. For very large wetted forested areas evaporation will be at the equilibrium rate, if no other drying mechanisms are active in the atmosphere. For smaller forests surrounded by large stretches of low vegetation, as the current forest, the advection of dryer air may lead to enhanced evaporation. For the current forest it is observed that evaporation lies well above the equilibrium rate.

Outlook

Having summarised the results obtained in this thesis and the results of related studies on forest hydrology, it seems that we have now all the ingredients to answer the research question we have posed ourselves at the onset. Parameters are identified with which we can model: a) the outgoing radiation fluxes, the partitioning of net radiation over the three heat fluxes for dry cases, including forest floor evaporation; b) the distribution of precipitation over interception and throughfall, evaporation of intercepted water under partially wet conditions, the change in transpiration under partially wet conditions; and c) The infiltration of water into the soil, the soil water movement and the feedback of soil water on transpiration. Although we are reaching the end of this thesis, this is not the end of the story. The next step is to couple all these processes into one Soil/Vegetation/Atmosphere scheme. Even a step further is to couple this SVAT scheme to a realistic atmospheric boundary layer scheme. For application in global weather and climate models there remains the problem of parameter choices. In many studies vegetation parameters are derived in different ways. Often the number of parameters are larger than can be estimated from the available measurements. This makes it difficult or at least time consuming to compare results from different studies.

There still remain the processes related to tree physiology, soil nutrients and the deposition of air pollution, that are outside the scope of this thesis, but which may give rise to pronounced variations of forest response over the years (Heij and Erisman, 1994; Jongmans et al., 1997). The few eddy-covariance transpiration measurements available for the year 1988 showed that transpiration amounts were smaller than compared to model values based on the optimalisation for the year 1989. In 1988 a fungi plague was detected in the forest. The TEBEX measurement programme carried out by KNMI during 1995 and 1996 at the forest site, which is analysed at present, may shed some more light on the year to year variation of the forest response.

Finally a data set has been prepared with continuous time series of the forcing variables for the period April to December 1989. The data set also contains validation data for surface fluxes, soil water and interception. At present this data set is used, among others, for the evaluation of a new ECMWF landsurface scheme.

References

Anderson M. C., J. M. Norman, G. R. Diak, W. P. Kustas and J. R. Mecikalski (1997). A two-source time-integrated model for estimating surface fluxes using thermal infrared remote sensing. *Remote Sens. Environ.*, **60**, 195-216.

Ayra S.P. (1991). Finite-difference errors in estimating of gradients in the atmospheric surface layer. *J. Appl. Meteorol.*, **30**, 251-253.

Baldocchi D. D. and Meyers T. P. (1988). Turbulence structure in a deciduous forest. *Boundary- Layer Meteorol.*, **43**, 345-364.

Barr A. G. and T. J. Gillespie (1987). Maximum wetness duration for water drops on leaves in the field. *Agric. For. Meteorol.*, **41**, 267-274.

Bastiaanssen, W.G.M., M. Menenti, R.A. Feddes and A.A.M. Holtslag (1998): A remote sensing surface energy balance algorithm for land (SEBAL): 1. Formulation; *J. Hydrol.*, 198-212.

Baumgartner A. (1956). Untersuchungen ueber den Waerme- und Wasserhaushalt eines jungen Waldes. Ber. DWD 5, Nr 28.

Beljaars A. C. M (1982). The derivation of fluxes from profiles in perturbed areas. *Boundary-Layer Meteorol* , **24**, 35-55.

Beljaars A.C.M., Walmsley J.L. and Taylor P.A. (1987). Modelling of Turbulence over low hills and varying surface roughness. *Boundary-Layer Meteorol.*, **41**, 203-215.

Beljaars A. C. M. and A. A. M. Holtslag (1991). Flux parameterization over land surfaces for atmospheric models. *J. Appl. Meteorol.*, **30**, 327-341.

Beljaars A. C. M. and P. Viterbo (1994). The sensitivity of winter evaporation to the formulation of aerodynamic resistance in the ECMWF model. *Boundary-Layer Meteorol.*, **71**, 135-149.

Beljaars A. C. M., P. Viterbo, M. J. Miller and A. K. Betts (1996). The anomalous rainfall over the united states during july 1993: Sensitivity to land surface parametrization and soil moisture anomalies. *Monthly Weather Rev.*, **124**, 3, 362-383.

Beljaars A. C. M. and F. C. Bosveld (1997). Cabauw data for the validation of land surface parametrization schemes. *J. Climate*, **10**, 1172-1193.

Bergström H. and Högström U. (1989). Turbulent exchange above a pine forest, II organized structures. *Boundary-Layer Meteorol.*, **49**, 231-263.

Berkowicz R. and L. P. Prahm (1982). Sensible heat flux estimated from routine meteorological data by the resistance method. *J. Appl. Meteorol.*, **21**, 1846-1864.

Black T.A. (1979). Evaporation from Douglas Fir stands exposed to soil water deficits. *Water Resour. Res.*, **15**, 164-170.

Blyth E. M. and A. J. Dolman (1995). The roughness length for heat of sparse vegetation. *Boundary-Layer Meteorol.*, **34**, 583-585.

Bosveld F.C. and Beljaars (1987). Complex terrain effects on dry deposition, in: the proceedings of the 16th international technical meeting on air pollution modelling and its application, April 1987, Lindau.

Bosveld F. C. (1991). Turbulent exchange coefficients over a Douglas fir forest. Scientific Report of the Royal Netherlands Meteorological Institute, WR-91-02. KNMI, P.O.Box 201, 3730 AE, De Bilt, The Netherlands.

Bosveld F. C. (1997). Derivation of fluxes from profiles over a moderately homogeneous forest. *Boundary-Layer meteorol.*, **85**, 289-326. (Chapter 2 of this thesis)

Bosveld F. C., A. van Ulden and A. C. M. Beljaars (1998a). A comparison of ECMWF re-analysis data with fluxes and profiles observed in Cabauw. KNMI Memo AO-98-07, to be published in the ECMWF ERA-project series.

Bosveld F.C., J.G. van der Vliet and W.A.A. Monna (1998). The KNMI Garderen Experiment, Micro-meteorological observations 1988-1989, Instruments and data setbos data-set. KNMI TR-208. KNMI, P.O.Box 201, 3730 AE, De Bilt, The Netherlands.

Bosveld F. C., A. A. M. Holtslag and B. J. J. M. van den Hurk (1999a). Interpretation of crown radiation temperatures of a dense Douglas fir forest with similarity theory. *Boundary-Layer Meteorol.* (In Press). (Chapter 3 of this thesis)

Bosveld F. C., A. A. M. Holtslag and B. J. J. M. van den Hurk (1999b). Night time convection in the interior of a dense Douglas-fir forest. *Boundary-Layer Meteorol.* (In Press). (Chapter 4 of this thesis)

Bosveld F. C. and W. Bouten (1999a). Comparing transpiration models with eddy-correlation observations for a Douglas-fir forest. Subm. *Agric. For. Meteorol.*. (Chapter 5 of this thesis)

Bosveld F. C. and W. Bouten (1999b). Evaporation and transpiration reduction of a partially wet Douglas-fir forest. To be subm. *Agric. For. Meteorol.*. (Chapter 6 of this thesis)

Bosveld F. C. (1999). The KNMI Garderen Experiment, Micro-meteorological observations 1988-1989, Corrections. KNMI WR (in press). KNMI, P.O.Box 201, 3730 AE, De Bilt, The Netherlands.

Bouten W., P. J. F. Swart and E. de Water (1990). Microwave transmission, a new tool in forest hydrological research. *J. Hydrol.*, **124**, 119-130.

Bouten W. and F. C. Bosveld (1991). Microwave transmission, A new tool in forest hydrological research-reply. *J. Hydrol.*, **125**, 313-317.

Bouten W., M. G. Schaap, J. C. J. H. Aerts and A. W. M. Vermetten (1996). Monitoring and modelling rainfall interception and canopy wetness in support of acidification research. *J. Hydrol.*, **181**, 305-321.

Brain P. and D. R. Butler (1985). A model of drop size distribution for a system with evaporation. *Plant, Cell and Environment*, **8**, 247-252.

Brutsaert W. and M. Sugita (1992). Regional surface fluxes from satellite-derived surface temperatures: AVHRR) and radiosonde profiles. *Boundary-Layer Meteorol.*, **58**, 355-366.

Brutsaert W. H. (1982). Evaporation into the atmosphere. D. Reidel Publishing Company, Dordrecht, The Netherlands. 299 pp.

Businger J. A. (1986). Evaluation of the accuracy with which dry deposition can be

measured with current micrometeorological techniques. *J. Clim. Appl. Meteorol.*, **25**, 1100-1124.

Butler D. R. (1986). Evaporation from rain drops on leaves in a cereal canopy: a simulation model. *Boundary-Layer Meteorol.*, **36**, 39-51.

Butler D. R. (1985). The energy balance of water drops on a leaf surface. *Boundary-Layer Meteorol.*, **32**, 337-349.

Carson D. J. and P. J. R. Richards (1978). Modelling surface turbulent fluxes in stable conditions. *Boundary-Layer Meteorol.*, **14**, 67-81.

Cellier P. and Y. Brunet (1992). Flux-gradient relationships above tall plant canopies. *Agric. For. Meteorol.*, **58**, 93-117.

Chamberlain A. C. (1966). Transport of gases to and from grass and grass-like surfaces. *Proc. Roy. Soc. London*, **A-290**, 236-265.

Chen W., M. D. Novak, T. A. Black and X. Lee (1997). Coherent eddies and temperature structure functions for three contrasting surfaces. Part II: Renewal model for sensible heat flux. *Boundary-Layer Meteorol.*, **84**, 125-147.

Chen T. H. and Co-authors (1997). Cabauw experimental results form the Project for Intercomparison of Landsurface Parametrization Schemes (PILPS). *J. of Climate*, **10**, 1194-1215.

Cohen Y., T. A. Black and F. M. Kelliher (1985). Determination of sap flow in Douglas fir trees using the heat pulse technique. *Can. J. For. Res.*, **15**, 422-428.

Cooper T. A. and J. G. Lockwood (1987). The influence of rainfall distribution in numerical simulation of evapotranspiration from a multilayer model Pine canopy. *Water Resource Research*, **23**, 1645-1656.

Cuenca H. C., M. Ek and A. A. M. Holtslag (1997). Interaction of soil parameterizations and atmospheric boundary layer simulation. Presented at the special symposium on boundary layer and turbulence, Long Beach California, feb. 2-7 1997.

De Bruin H. A. R. and A. A. M. Holtslag (1982). A simple parametrization of the surface fluxes of sensible and latent heat during daytime compared with the Penman-Monteith concept. *J. Appl. Meteorol.*, **21**, 1610-1621.

De Kort I. (1990). Wood production and water transport capacity of Douglas fir in the ACIFORN-stands in Kootwijk and Garderen. Final report Dutch Priority Programme on Acidification, project nr 111.1, Rijksherbarium/Hortus Botanicus, P.O.Box 9514, 2300RA Leiden, The netherlands, 35pp.

De Vries D. A., (1966). Thermal properties of soils. In: Van Wijk, W. R. ed. Physics of plant environment, 2nd ed.. North-Holland Publishing Company, Amsterdam, Netherlands, 382pp.

Denmead O. T. and Bradly E. F. (1985). Flux gradient relationships in a forest canopy. In: B. A. Hutchison and B. B. Hicks (eds.), The forest-atmosphere interaction. D. Reidel Publishing Company, Dordrecht, The Netherlands, 684pp.

Dickenson R. E., A. Henderson-Sellers, P. J. Kennedy and M. F. Wilson (1986).

Biosphere-Atmosphere Transfer Scheme (BATS) for the NCAR community model. NCAR Tech. Note NCAR/TN-275+STR, 69pp, National Centre of Atmospheric Research, P.O.Box 3000, Boulder, CO 80307.

Dolman J. and D. Gregory (1992). The parametrization of rainfall interception in GCMs. *Q. J. R. Meteorol. Soc.*, **118**, 455-467.

Duyzer J.H. and Bosveld F.C. (1988). Measurements of dry deposition fluxes of O3, NOx, SO2 and particles over grass/heathland vegetation and the influence of surface inhomogeneity, Dutch priority program on acidification Report no 99-3. TNO-MT Report no R 88/111.

Duyzer J. H. , H. L. M. Verhagen, J. H. Westrate and F. C. Bosveld (1992). Measurement of the dry deposition flux of NH3 on to coniferous forest. *Env. Poll.*, **75**, 3-13.

Duyzer J. H., H. L. M. Verhagen, J. H. Westrate, F. C. Bosveld and A. W. M. vermetten (1994). The dry deposition of ammonia onto a Douglas fir forest in the Netherlands. *Atmos. Env.*, **28**, 1241-1253.

Dyer A.J. (1974). A review of flux-profile relationships, *Boundary-Layer Meteorol.*, **7**, 363-372.

Erisman J.- W. (1992). Atmospheric Deposition of Acidifying Compounds in The Netherlands. Thesis State University of Utrecht. ISBN 90-393-0351-7.

Evers P. W. , W. W. P Jans and E. G. Steingroever (eds) (1991). Impact of air pollution on ecophysiological relations in two Douglas fir stands in the Netherlands. Report nr. 637, ISSN 0924-9141, De Dorschkamp, P.O.Box 23, 6700AA, Wageningen, the Netherlands. 306pp.

Evers P., C. J. M. Consten and A. W. M. Vermetten (1987). Acidification research on Douglas fir forest in the Netherlands (ACIFORN-project). In: P. Mathy (Ed.), Proc. Symp. Effects of Air Pollution on Terrestrial and Aquatic Ecosystems, Grenoble, 887-909. Reidel Publishing Co., Dordrecht, the Netherlands.

Fazu C. and P. Schwerdtfeger (1989). Flux-gradient relationships for momentum and heat over a rough natural surface, *Quart. J. Roy. Meterol. Soc.*, **115**, 335-352.

Feijt A. J. and W. Kohsiek (1995). The effect of emissivity variation on surface temperature determined by infrared radiometry. *Boundary-Layer Meteorol.*, **72**, 323-327.

Fitzjarrald D. R. and K. E. Moore (1990). Mechanisms of nocturnal exchange between the rain forest and the atmosphere. *J. Geophys. Res.*, **95**, D10, 16839-16850.

Fowler D., J. H. Duyzer, D. D. Baldocchi, (1991). Inputs of trace gases, particles and cloud droplets to terrestrial surfaces. *Proc. of the Roy. Soc. of Edinburgh*, **97**B, 35-59.

Gao W., R. H. Shaw and K. T. Paw U (1989). Observation of organized structure in turbulent flow within and above a forest canopy. *Boundary-Layer Meteorol.*, **47**, 349-377.

Garratt J.R. (1972). Studies of turbulence in the surface layer over water (Lough

Neagh). Part II. Production and dissipation of velocity and temperature fluctuations. *Quart. J. Roy. Met. Soc.*, **98**, 642-657.

Garratt J. R. (1978a). Flux profile relations above tall vegetation. *Quart. J. Roy. Meteorol. Soc.*, **104**, 199-211.

Garratt J. R. (1978b). Transfer characteristics for a heterogeneous surface of large aerodynamic roughness. *Quart. J. Roy. Meteorol. Soc.*, **104**, 491-502.

Garratt J. R. (1980). Surface influence upon vertical profiles in the atmospheric near-surface layer. *Quart. J. Roy. Meteorol. Soc.*, **106**, 803-819.

Garratt J. R. and B. B. Hicks (1973). Momentum, heat and water vapour transfer to and from natural and artificial surfaces. *Quart. J. Roy. Meteorol. Soc.*, **99**, 680-687.

Geiger R. (1961). Das Klima der bodennahen Luftschicht. Friedr. Vieweg & Sohn, Braunschweig.

Goudriaan J. (1977). Crop micrometeorology: a simulation study. In the serie simulation monographs, PUDOC, Wageningen, The Netherlands. ISBN 90-220-0614-X.

Granier A., Bobay V., Gash J. H. C., Gelpe J. Saugier B. and Shuttleworth W. J. (1990). Vapour flux density and transpiration rate comparisons in a stand of maritime pine (Pinus pinaster Ait.) in Les Landes forest. *Agric. For. Meteorol.*, **51**, 309-319.

Grant A. L. M. and R. D. Watkins (1989). Errors in turbulence measurements with a sonic anemometer. *Boundary-Layer Meteorology*, **46**, 181-194.

Gryning S. E. , A. A. M. Holtslag, J. S. Irwin and B. Sivertsen (1987). Applied dispersion modelling based on meteorological scaling parameters. *Atmos. Env.*, **21**, 79-89.

Heimovaara T.J. and W. Bouten (1990). A computer controlled 36 channel TDR system for monitoring soil water contents. *Water Resour. Res.*, **26**, 2311-2316.

Heij G. J. and T. Schneider (eds.) (1991). Acidification research in the Netherlands. Studies in Environmental Science Volume 46.

Hicks B. B. , Hyson P. and Moore C. J. (1975). A study of eddy fluxes over a forest. *J. Appl. Meteorol.*, **14**, 58-66.

Hicks B. B., G. D. Hess and M. L. Wesely (1979). Analysis of flux-profile relationships above tall vegetation-an alternative view. *Quart. J. Roy. Meteorol. Soc.*, **105**, 1074-1077.

Högström U., Bergstöm H., Smedman A. and Halldin S. (1989. Turbulent exchange above a pine forest, 1: fluxes and gradients, *Boundary Layer Meteorology*, **49**, 197-217.

Holtslag A. A. M. and M. Ek, (1996). Simulation of surface fluxes and boundary layer development over the Pine forest in Hapex-Mobilhy. *J. Applied Meteorolgy*, **35**, 2, 203-213.

Huband N. D. S. and J. L. Monteith (1986, Radiative surface temperature and energy balance of a wheat canopy, I Comparison of radiative and aerodynamic canopy temperature. *Boundary-Layer Meteorol.*, **36**, 1-17.

167

Huber L. and B. Itier (1990). Leaf wetness duration in a field bean canopy. *Agric. Forest Meteorol.*, **51**, 281-292.

Hutchison B. A. and B. B. Hicks (eds.) (1985). The forest-atmosphere interaction. D. Reidel Publishing Company, Dordrecht, The Netherlands, 684pp.

Jackson P.S. (1981). On the displacement height in the logarithmic velocity profile, *J. Fluid Mech.*, **111**, 15-25.

Jacobs A. F. G., J. H. van Boxtel and R.M.M. El-Kilani (1994). Nighttime free convection characteristics within a plant canopy. *Boundary-Layer Meteorol.*, **71**, 375-391.

Jacobs A. F. G., Jacobs, J. H. van Boxtel and J. Nieveen (1996). Nighttime exchange processes near the soil surface of a maize canopy. *Agric. For. Meteorol.*, **83**, 155-169.

Jacobs C. M. J., H. A. R. De Bruin and A. Verhoef (1991). The effects of surface inhomogeneities on the surface fluxes and on the development of the planetary boundary layer. *Annales Geophysicae*, **9**, 510-520.

Jakob M. (1949). Heat transfer, Volume 1. John Wiley and Sons, Inc., New York. (10th printing, 1967), 758pp.

Jans W.W.P., G.M. van Roekel, W.H. van Orden and E.G. Steingröver (1994), Above ground biomass of adult Douglas fir. IBN Research Report 94/1, P.O.Box 23, 6700AA, Wageningen, The Netherlands, 58pp.

Jarvis, P.G., G.B. James and J.J. Landsberg (1976). Coniferous forest. In: J.L. Monteith (ed.), Vegetation and the atmosphere, Vol. 2, Case studies pp. 171-240. Academic press, New York.

Jarvis, P.G., 1976. The interpretation of the variations in leaf water potential and stomatal conductance found in canopies in the field. *Phil. Trans. Roy. Soc. Lond.*, **B-273**, 593-610.

Jarvis P. G., J. L. Monteith, W. J. Shuttleworth and M. H. Unsworth (eds.) (1989). Forest , Weather and Climate. Proceedings of a Royal Society discussion meeting, held on 2 and 3 June 1989, London, UK. University Press, Cambridge.

Kaimal J. C. , J. C. Wyngaard, Y. Izumi and O. R. Cote (1972). Spectral characteristics of surface layer turbulence. *Quart. J. Roy. Meteorol. Soc.*, **98**, 563-589.

Kaimal J. C. and J. E. Goyner (1991). Another look at sonic thermometry. *Boundary-Layer meteorol.*, **56**, 401-410.

Katul G., C.-I. Hsieh, R. Oren, D. Ellsworth and N. Phillips (1996). Latent and sensible haet flux predictions from a uniform forest using surface renewal and flux variance methods. *Boundary-Layer Meteorol.*, **80**, 249-282.

Kohsiek W., H. A. R. de Bruin and H. The and B. van den Hurk (1993, Estimation of the sensible heat flux of a semi arid area using surface radiative temperature measurements. *Boundary-Layer Meteorol.*, **63**, 213-230.

Koorevaar P., G. Menelik and C. Dirksen (1983). Elements of soil physics. Elsevier, Amsterdam.

Kraan C. and W. A. Oost (1989). A new way of anemometer calibration and its

application to a sonic anemometer. *J. Atmos. and Ocean. Technol.*, 6, 516-524.

Kristensen L. (1993). The cup anemometer and other exciting instruments. Thesis Technical University of Denmark. Riso-R-615(EN).

Kristensen L. and D. R. Fitzjarrald (1984). The effect of line averaging on scalar flux measurements with a sonic anemometer near the surface. *J. Atmos. Ocean. Technol.*, 1, 138-146.

Leclerc M. Y., K. C. Beissner, R. H. Shaw, G. den Hartog and H. H. Neumann (1990). The influence of atmospheric stability on the budgets of Reynolds stress and turbulent kinetic energy within and above a deciduous forest. *J. Appl. Meteorol.*, 29, 916-933.

Leclerc M. Y. and Thurtell G. W. (1990). Footprint prediction of scalar fluxes using a Markovian analysis. *Boundary-Layer Meteorol.*, 52, 247-258.

Lee X. (1996, Carbon dioxide exchange and nocturnal processes over mixed deciduous forest. *Agric. For. Meteorol.*, 81, 13-29.

Lhomme J.-P., E. Elguero, A. Chehbouni and G. Boulet (1998). Stomatal control of transpiration: Examination of Monteith's formulation of canopy resistance. *Water Resour. Res.*, 34, 2301-2308.

Lhomme J.-P., B. Monteny, M. Amadou (1994). Estimating sensible heat flux from radiometric temperature over sparse millet. *Agric. For. Meteorol.*, 68, 77-91.

Lindroth A. (1985). Canopy conductance of coniferous forests related to climate. *Water Resour. Res.*, 21, 297-304.

Lohammar T. , S. Larsson, S. Linder and S. O. Falk (1980). FAST-Simulation models of gaseous exchange in Scots Pine. Structure and Function of Northern Coniferous Forests- An Ecosystem Study. *Ecoll. Bull.*, 32, 505-523.

Lumley J. L. and H. A. Panofsky (1964). The structure of atmospheric turbulence. Wiley Interscience, New York, 239pp.

Mahrt L. (1985). Vertical structure and turbulence in the very stable boundary layer. *J. Atmos. Sci.*, 42, 2333-2349.

Mahrt L., J. Sun, J. I. MacPherson, N. O. Jensen and R. L. Desjardins (1997) Formulation of surface heatflux: Apllication to BOREAS. *J. Geophys. Res.*, 102, D24, 29641-29649.

Marshal D. C. (1985). Measurement of sapflow in conifers by heat transport. *Plant. Physiol.*, 33, 385-396.

McNaughton, K.G. and P.G. Jarvis (1983). Predicting effects of vegetation changes on transpiration and evaporation. in: T.T Kozlowski (ed.), Water deficits and plant growth, Academic press, New York. pp 1-47.

McNaughton K. G. and B. J. J. M. van den Hurk (1995). A 'Lagrangian' revision of the resistors in the two-layer model for calculating the energy budget of a plant canopy. *Boundary-Layer Meteorol.*, 74, 261-288.

Meesters A. G. C. A. and H. F. Vugts (1996). Calculation of heat storage in stems. *Agric. For. Meteorol.*, 78, 181-202.

Mölder M. and A. Lindroth (1999). Surface radiation temperature and roughness lengths of a boreal forest. *Agric. For. Meteorol.*, In Press.

Mölder M., A. Grelle, A. Lindroth and S. Halldin (1999). Flux-profile relationships over a boreal forest - roughness sublayer corrections. *Agric. For. Meteorol.*, In Press.

Molion L. C. B. and C. J. Moore (1983). Estimating the zero-plane displacement for tall vegetation using a mass conservation method. *Boundary-Layer Meteorol.*, **26**, 115-125.

Monin A. S. and A. M. Obukhov (1954). Basic laws of turbulent mixing in the atmosphere near the ground. *Tr. Akad. Nauk SSSR Geofiz. Inst.*, **24** (151), 163-187.

Monna W. A. A. (1983). De KNMI windtunnel. Technical Report of the Royal Netherlands Meteorological Institute, TR-32. KNMI, P.O.Box 201, 3730 AE, De Bilt, The Netherlands.De Bilt, The Netherlands. (in Dutch)

Monteith J.L. (1965). Evaporation and environment. In: The state and movement of water in living organisms. 19 th Symp. Soc. Exp. Biol. (G.E. Fogg, ed.), pp205-235. Cambridge University Press, London.

Monteith J. L. (1973). Principles of environmental physics. Edward Arnold publishers limited, London, UK.

Monteith J. L. (ed.) (1976). Vegetation and the Atmosphere, Volume 2, Case studies. Academic Press, London.

Monteith J. L. (1977). Resistance of a partially wet canopy: whose equation fails?. *Boundary-Layer Meteorol.*, **12**, 379-383.

Monteith J.L. (1995). A reinterpretation of stomatal responses to humidity. *Plant, Cell Env.*, **18**, 357-364.

Morton F. I. (1984). What are the limits on forest evaporation?. *J. Hydrol.*, **74**, 373-398.

Mott K. A. and D. F. Parkurst (1991). Stomatal response to humidity in air and helox. *Plant, Cell Env.*, **14**, 509-515.

Noppert F., H. P. de Groot and J. J. Gerritsen (1990). Sapstroomsnelheden in een douglasspar opstand op de Veluwe-Resultaten van het meetseizoen 1989 te Speuld. KEMA report 81277-MOB 91-3514, KEMA, Postbus 9035, 6800 ET, Arnhem, The Netherlands.

Olsthoorn A.F.M. (1991). Fine root density and root biomass of two Douglas-fir stands on sandy soils in the Netherlands. 1. Root biomass in early summer. *Neth. J. Agric. Sci.*, **39**, 49-60.

Olsthoorn A.F.M. and A. Tiktak (1991). Fine root density and root biomass of two Douglas-fir stands on sandy soils in the Netherlands. 2. Periodicity of fine root growth and estimation of below ground carbon allocation. *Neth. J. Agric. Sci.*, **39**, 61-77.

Panofsky H. A. and J. A. Dutton (1984). Atmospheric turbulence. Wiley and Sons, Inc, USA.

Paulson C. A. (1970). The mathematical representation of wind speed and temperature profiles in the unstable atmospheric surface layer. *J. Appl. Meteorol.*, **9**, 857-861.

Paw U K. T. and T. P. Meyers (1989). Investigations with higher-order canopy

turbulence model into mean source-sink levels and bulk resistances. *Agric. For. Meteorol.*, **47**, 259-271.

Paw U K.T., J. Qiu, H.-B Su, T. Watanabe and Y. Brunet (1995). Surface Renewal analysis: a new method to obtain scalar fluxes. *Agric. For. Meteorol.*, **74**, 119-137.

Penman H.L. (1948). Natural evaporation from open water, bare soil and grass. *Proc. Roy. Soc. London*, **A-193**, 120-146.

Press W.H., B.P. Flannery, S.A. Teukolsky and W.T. Vetterling (1986). Numerical recipes, the art of scientific computing. Cambridge university press, Cambridge.

Priestley C.H.B. and R.J. Taylor (1972). On the assessment of surface heat flux and evaporation using large scale parameters. *Monthly Weather Rev.*, **100**, 81-92.

Raupach M. R. (1992). Drag and drag partitioning on rough surfaces. *Boundary-Layer Meteorol.*, **60**, 375-395.

Raupach M. R., J. J. Finnigan and Y. Brunet (1996). Coherent eddies and turbulence in vegetation canopies: the mixing-layer analogy. *Boundary-Layer Meteorol.*, **78**, 351-382.

Raupach M.R. (1979). Anomalies in flux-gradient relationships over forest. *Boundary-Layer Meteorol.*, **16**, 467-486.

Raupach M. R. (1981). Conditionally statistics of Reynolds stress in rough-wall and smooth-wall turbulent boundary layers. *J. Fluid mech.*, **108**, 363-382.

Raupach M. R. and J. J. Finnigan (1988). 'Single layer models of evaporation from plant canopies are incorrect but useful, whereas multilayer models are correct but useless':discuss. *Austral. J. Plant Physiol.*, **15**, 705-716.

Rijtema P. E. (1965). An analysis of actual evapotranspiration. *Agric. Res. Rep.*, **659**, 1-107.

Roberts J. (1983). Forest transpiration: A conservative hydrological process?. *J. of Hydrol.*, **66**, 133-141.

Rotach M. (1994). Determination of the zero plane displacement over an Urban environment. *Boundary-Layer Meteorol.*, **67**, 187-193.

Running W. (1976). Environmental control of leaf water conductance in conifers. *Can. J. For. Res.*, **6**, 104-112.

Schaap M. G. and W. Bouten (1997). Forest floor evaporation in a dense Douglas fir stand. *J. Hydrol.*, **193**, 97-113.

Schmid H. P. (1994). Source areas for scalars and scalar fluxes. *Boundary-Layer meteorol.*, **67**, 293-318.

Schotanus P., Nieuwstadt F.T.M., de Bruin H.A.R. (1983). Temperature measurements with a sonic anemometer and its application to heat and moisture fluxes, *Boundary-Layer Meteorol.*, **26**, 81-93.

Schulze E.-D., J, Cermak, R. Matysek, M. Penka and R. Zimmerman (1985). Canopy transpiration and water fluxes in the xylem of the trunk of Larix and Picea tress- a comparison of xylem flow, porometer and cuvette measurements. *Oecologia*, **66**, 475-483.

Sellers P. J., Y. Mintz, Y. C. Sud and A. Dalcher (1986). A Simple Biosphere

model (SiB) for use with general circulation models. *J. Atmos. Sci.*, **43**, 505-531.

Shaw R. H. and Pereira A. R. (1982). Aerodynamic roughness of a plant canopy: a numerical experiment. *Agric. Meteorol.*, **26**, 51-65.

Shuttleworth W. J. (1976). Experimental evidence for the failure of the Penman-Monteith equation in partially wet conditions. *Boundary-Layer Meteorol.*, **10**, 91-94.

Shuttleworth W. J. (1993). The Soil-Vegetation-Atmosphere interface. In: Energy and Water Cyles in the Climate System (E. Raschke and D. Jacob, eds.). NATO ASI Series, Series 1: Global Environment Change, Vol. 5. Springer Verlag, Berlin.

Simpson I. J., G. W. Thurtell, H. H. Neumann, G den Hartog and G. C. Edwards (1998). The validity of similarity theory in the roughness sublayer above forests. *Boundary-Layer Meteorol.*, **87**, 69-99.

Slob W.H. (1978). The accuracy of aspiration thermometers, Scientific Report of the Royal Netherlands Meteorological Institute, WR-78-1. KNMI, P.O.Box 201, 3730 AE, De Bilt, The Netherlands.

Stewart J. B. (1988). Modelling surface conductance of pine forest. *Agric. For. Meteorol.*, **43**, 19-35.

Stewart J. B. (1977). Evaporation from the wet canopy of a Pine forest. *Water Resour. Res.*, **13**, 6, 915-921.

Stewart J. B. and Thom A. S. (1973). Energy budgets in pine forest. *Quart. J. Roy. Meteorol. Soc.*, **99**, 154-170.

Stewart J.B., and H.A.R. de Bruin (1985). Preliminary study of dependence of surface conductance of Thetford forest on environmental conditions. In: B.A. Hutchison and B.B. Hicks (eds.), The forest atmosphere interaction, pp. 91-104. D. Reidel Publishing Company.

Stewart J. B., W. P. Kustas, K. S. Humes, W. D. Nichols, M. S. Moran and H. A. R. de Bruin (1994). Sensible heat flux-radiometric surface temperature relationship for eight semiarid areas. *J. Appl. Meteorol.*, **33**, 1110-1117.

Stewart R. B. and W. R. Rouse (1977). Substantiation of the Priestley and Taylor parameter $\alpha=1.26$ for potential evaporation in high latitudes. *J. Appl. Meteorol.*, **16**, 649-650.

Sun J. and L. Mahrt (1995). Relationship of surface heat flux to microscale temperature variations: Application to BOREAS. *Boundary-Layer Meteorol.*, **76**, 291-301.

Swanson R. H. and D. W. A. Whitfield (1981). A numerical analysis of heat pulse velocity theory and practice. *J. Exp. Botany*, **126**, 32, 221-239.

Tan C.S. and T.A. Black (1976). Factors affecting the canopy resistance of a Douglas-fir forest. *Boundary-Layer Meteorol.* **10**, 475-488.

Tatarski V. I. (1961). Wave propagation in a turbulent medium. McGraw-Hill Book Company, New York.

Tatarski V. I. (1967). Wave propagation in a turbulent medium. Dover, New York.

Taylor G. I. (1932). The transport of vorticity and heat through fluids in turbulent

motion. *Proc. Roy. Soc.*, **A-135**, 685-705.

Tennekes H. (1982). Similarity relations, scaling laws and spectral dynamics. In: Atmospheric Turbulence and Air Pollution Modelling (Nieuwstadt F. T. M. and H. van Dop (eds.)). D. Reidel Publishing Company, Dordrecht, The Netherlands.

Thom A. S. (1971). Momentum absorbtion by vegetation. *Quart. J. Roy. Meteorol. Soc.*, **97**, 414-428.

Thom A. S. , J. B. Stewart, H. R. Oliver and J. H. C. Gash (1975). Comparison of aerodynamic and energy budget estimates of fluxes over a pine forest. *Quart. J. Roy. Meteorol. Soc.*, **101**, 93-105.

Tiktak A., W. Bouten, W. Jans, A.F.M. Olsthoorn (1990). Temporal dynamics of shoot extension and fine root activity affected by traditional stress factors. Report of the CORRELACI-project. Dorschkamp publication, The Dorschkamp, Wageningen, the Netherlands.

Tiktak A. and W. Bouten (1990). Soil Hydrological system characterization of the two ACIFORN stands using monitoring data and the soil hydrological model "SWIF". University of Amsterdam. Report in the series of Dutch Priority Programme on Acidification nr.102.2.01, 62pp.

Tiktak A. and W. Bouten (1992). Modelling soil water dynamics in a forest ecosystem III: Model description and evaluation of discretisation. *Hydrol. Proc.*, **6**, 455-465.

Tiktak A. and W. Bouten (1994). Soil water dynamics and long -term water balances of a Douglas fir stand in the Netherlands. *J. Hydrol.*, **156**, 265-283.

Townsend A. A. (1962). Natural convection in the earth's boundary layer. *Quart. J. Roy. Meteorol. Soc.*, **88**, 51-56.

Turner J. S. (1973). Buoyancy effects in fluids. Cambridge University Press, UK, 368pp.

Van Ulden A. P. and A. A. M. Holtslag (1985). Estimation of atmospheric boundary layer parameters for diffusion application. *J. Clim. Appl. Meteorol.*, **24**, 1196-1206.

Van den Hurk B., W. Bastiaanssen, H. Pelgrum and E. van Meijgaard (1997). A feasibility study for the use of METEOSAT and NOAA data for assimilation of initial soil moisture fields. *J. Appl. Meteorol.*, **36**, 1271-1283.

Verhoef A., H. A. R. De Bruin and B. J. J. M. van den Hurk (1997). Some practical notes on the parameter kB^{-1} for sparse vegetation. *J. Appl. Meteorol.*, **36**, 560-572.

Vermetten A. W. M. , Hofschreuder P. and Harssema H. (1986). In: H. -W Gergii ed., Deposition of gaseous pollutants in a Douglas fir forest. Atmospheric pollutants in forest areas, 3-11.

Vermetten A. W. M., P. Hofschreuder, J. H. Duyzer, F. C. Bosveld and W. Bouten (1991). Dry deposition of SO_2 onto a stand of douglas fir: the influence of canopy wetness. Proceedings of the 5th IPSAEP-conference, Richland WA, USA, July 14-19, 1991.

Vermetten A.W.M., L. Ganzeveld, A. Jeuken, P. Hofschreuder and G.M.J. Mohren

(1994). CO_2 uptake by a stand of Douglas fir: flux measurements compared with model calculations. *Agric. For. Meteorol.*, **72**, 57-80.

Viterbo P. and A.C.M Beljaars (1995). An improved land surface parametrization scheme in the ECMWF model and its validation. *J. of Climate*, **8**, 2716-2748.

Voght R. and Jaeger L. (1990). Evaporation from a pine forest - using the aerodynamic method and Bowen ratio method. *Agric. For. Meteorol.*, **50**, 23-38.

Webb E. K. , G. I. Pearman and R. Leuning (1980). Correction of flux measurements for density effects due to heat and water vapour transfer. *Quart. J. Roy. Meteorol. Soc.*, **106**, 85-100.

Wessels H. R. A. (1983). Distortion of the wind field by the cabauw meteorological tower. KNMI scientific report 83-15. De Bilt The Netherlands

Wyngaard J. C. and O. R. Cote (1971). The budgets of turbulent kinetic energy and temperature variance in the atmospheric surface layer. *J. Atmos. Sci.*, **28**, 190-201.

Wyngaard J. C. , Y. Izumi and S. A. Collins Jr. (1971). Behaviour of the refractive-index-structure parameter near the ground. *J. Optical Sci. of Am.*, **61**, 1646-1650.

Summary

This thesis deals with the research question: which processes are relevant in controlling the exchange fluxes between the forest and the atmosphere and how can this control be quantified? Answering this question is relevant for research in the fields of air pollution, weather and climate and remote sensing. To answer this question a measurement program has been performed over and in a dense Douglas fir forest (Speulderbos), near the village of Garderen, the Netherlands. Variables were monitored related to, the state of the atmosphere, the state of soil water and the state of the trees. Forest response was determined by measuring outgoing radiation fluxes and the surface fluxes of momentum, sensible and latent heat. Well-known concepts from micro-meteorology and hydrology were used for the interpretation of the measurement. At times, these concepts had to be adapted for the specific forest situation. One concept is surface layer similarity theory, which enables to categorise observations in a convenient way. A second concept, related to surface layer similarity, is on resistances relating spatial differences in variables to their corresponding fluxes. A third concept is the Penman-Monteith equation, which enables the discrimination between atmospheric control and plant control on transpiration.

Turbulent exchange within the roughness sublayer is investigated. The importance of terrain inhomogeneity is studied with footprint analysis and with an inhomogeneous surface layer model. A windspeed dependence of roughness length for momentum and displacement height is found. Surface layer similarity theory is extended to describe the roughness-sublayer influence. This involves the introduction of an additional length scale related to the geometry of the forest. It is found that well- defined flux profile relations exist for momentum and sensible heat in the roughness layer of the current forest. In the roughness layer the exchange of temperature is more efficient than the exchange of momentum. This is in contrast to results for the surface layer, but in concord with previous findings for dense forests.

The scalar excess resistance, which describes the difference between momentum transport and scalar transport at the surface/atmosphere interface, is investigated by using measurements of infrared surface temperature. Surface radiation temperature and aerodynamic surface temperature, obtained by extrapolating the air-temperature profile to the surface, are not necessarily equal. By assuming equality between the two, it is shown that a consistent description of the relation between sensible heat flux and temperature difference between the surface and the atmosphere is obtained, at least for daytime cases. The excess resistance for the current forest is much smaller than values found for low vegetation. It is shown that the enhanced exchange efficiency of heat, relative to momentum, in the roughness sublayer attributes to this low value. An alternative analysis is presented to separate this roughness layer effect from the transfer resistance at the forest/atmosphere interface. The value found for this alternative excess resistance, is more in line with low vegetation values. For neutral cases the two methods give the same results for temperature differences between the surface and the surface layer.

It is shown that stability effects give rise to a discrepancy between the two methods. The observations show some evidence in favour of the alternative method. The difference between forest interior air temperature and air temperature at canopy height is related to storage heat flux and sensible heat flux by applying the concepts of gust penetration and surface renewal. The analysis suggests that the renewal of interior air caused by gust penetration is slow due to the presence of a very dense crown layer.

For night-time cases, the equality between aerodynamic and radiation surface temperature breaks down when wind speeds are low and longwave cooling is high. The analysis shows that forest air becomes decoupled from the air aloft. Longwave cooling at the crown layer triggers canopy convection which transports cooled air from the crown layer to the forest interior. The existence of a convective surface temperature in the crown layer is deduced from the measurements. A two-layer radiation/energy balance model is constructed. The model explains the difference between radiation- and aerodynamic surface temperature in terms of the distribution of storage heat and sensible heat over the two model layers.

Transpiration for dry conditions is investigated by using the Penman-Monteith equation with a Jarvis type of formulation for the surface resistance. First the closure of the surface energy balance is checked. Overall closure is within the range of estimated measurement error. However, at times deviations occur which can be attributed to wind direction. With respect to transpiration it is found that surface resistance reacts strongly to water vapour deficit changes. This is related to the good aerodynamic coupling of the rough forest to the atmosphere. In spring, a clear increase in transpiration is observed after shoot growth. Soil water response is clearly present before mid summer, after that the forest seems less susceptible to draught. Probably the root system adapts to the dry situation. An analysis of residuals between observed and modelled transpiration shows that deviations occurred at the same wind direction where the energy balance closure broke down. The variance in the residuals appears to be two times larger than estimated from atmospheric statistics. Important contributions to this variance are correlated over periods of one day. This suggests that standard statistical techniques lead to an underestimation of the confidence intervals of estimated model parameters. Two other models are evaluated. A new formulation suggested by Monteith, where stomatal response to moisture deficit is replaced by a response to transpiration itself, is investigated. This formulation appears to be equivalent to the Jarvis formulation with an atmospheric moisture deficit response. The Priestley-Taylor formula is adapted to include soil water response. It performs reasonably well given the simple nature of the formulation.

Interception measurements and xylem sapflow measurements are exploited to investigate the interaction between evaporation and transpiration in a partially wet forest. The Penman-Monteith equation is generalised to describe this interaction. Explicit expressions are obtained for evaporation and transpiration. After optimisation the model is capable of describing both evaporation and transpiration reduction fairly well. Due to parameter interdependency, error bounds on individual

parameter estimates, related to evaporation, are large. Independent estimates of the parameters, although crude, are shown to be within the confidence region of the optimisation results. It is shown that evaporation rates are smaller than the frequently used formula: wet fraction times potential evaporation. Most of the transpiration reduction comes from energy consumption by the process of evaporation and the impact of the humidity conditions close to the needles. Only a small amount of stomatal blocking due to intercepted water is needed to explain the remaining reduction. This is in concord with the observation that stomata of the Douglas fir are at the lower side of the needle, which is only partially wetted during rain.

The response of the forest to external forcings can be described by a number of parameters related to model descriptions of various processes. The results for the current dense Douglas-fir forest are compared with other forest studies. A good agreement is found for the relation between the geometric parameters, canopy height, displacement height and roughness length for momentum. The exchange coefficients in the roughness layer for momentum and heat agree qualitatively with typical values found for other dense forests. Quantitatively significant and as yet unexplained differences remain. The very small scalar excess resistance found for the current forest is in agreement with the only other comparable dense forest study, which appeared recently in the literature. Transpiration rates as a function of external conditions are broadly in line with results found at other forest sites in the temperate climate.

New in this thesis are the results on; the estimation of displacement height; the difference between aerodynamic surface temperature and radiation surface temperature at night time; night time convection; changing transpiration response to soil water stress during the season; and the interaction between evaporation and transpiration reduction during wet conditions.

Samenvatting

Dit proefschrift behandelt de vraag welke processen de uitwisselingsfluxen tussen een bos en de atmosfeer bepalen en hoe dit gekwantificeerd kan worden. Deze vraag is van belang voor onderzoek naar luchtverontreiniging, weer en klimaat, en remote sensing. Om deze vraag te beantwoorden is een meetprogramma opgezet in een dicht Douglas sparren opstand (Speulderbos), nabij Garderen, Nederland. Metingen van atmosferische grootheden werden verricht, naast metingen van bodemwater en boomkarakteristieken. De response van het bos werd vastgesteld doormiddel van metingen van uitgaande stralingsfluxen en de oppervlaktefluxen van impuls en voelbare- en latente warmte. Gangbare concepten uit de micro-meteorologie en hydrologie werden toegepast voor de interpretatie van deze metingen. Soms werden deze concepten aangepast aan de specifieke situatie van het huidige bos. Eén zo'n concept is oppervlaktelaag-similariteit, welke het mogelijk maakt metingen verricht onder wisselende condities te ordenen. Een tweede concept, gerelateerd aan oppervlaktelaag-similariteit, is het weerstanden-transportmodel, waarin ruimtelijke verschillen in een grootheid gerelateerd worden aan de corresponderende flux. Een derde concept is de Penman-Monteith vergelijking voor transpiratie, die het mogelijk maakt atmosferische invloeden op verdamping te onderscheiden van plant invloeden.

Turbulente uitwisseling in de ruwheidslaag boven het bos is onderzocht. De invloed van terrein-inhomogeniteiten is afgeschat met behulp van 'foot-print' analyse en met een model voor de inhomogene oppervlaktelaag. De ruwheidslengte voor impuls en de verplaatsingshoogte blijken beiden afhankelijk te zijn van de windsnelheid. De theorie van oppervlaktelaag-similariteit is uitgebreid om de invloed van de ruwheidslaag op flux-profielrelaties te beschrijven. Hiertoe is een extra lengteschaal, gerelateerd aan de geometrie van het bos, ingevoerd. Goed gedefinieerde flux-profielrelaties zijn gevonden voor impuls en warmte. Het blijkt dat de uitwisseling van warmte efficiënter plaats vindt dan de uitwisseling van impuls. Dit is in tegenstelling tot de uitwisseling in de oppervlaktelaag, maar in overeenstemming met eerdere resultaten voor dichte bossen.

De exces weerstand voor warmte, welke het verschil beschrijft tussen impulstransport en scalartransport over het scheidingsvlak tussen vegetatie en atmosfeer, is onderzocht met behulp van stralingstemperatuur metingen. Stralings-oppervlaktetemperatuur en aerodynamische- oppervlaktetemperatuur, verkregen door extrapolatie van het temperatuurprofiel in de lucht naar het oppervlak, zijn niet noodzakelijk gelijk. De aanname dat ze wel gelijk zijn leidt voor dit bos, althans overdag, tot een consistente beschrijving van de relatie tussen warmteflux en het temperatuur verschil tussen het oppervlak en de atmosfeer. De exces weerstand voor het huidige bos is veel kleiner dan die voor lage vegetatie. De efficiëntere menging van warmte ten opzichte van impuls, in de ruwheidslaag, draagt hier in belangrijke mate toe bij. In een alternatieve analyse is getracht dit ruwheidslaag effect te scheiden van de transportweerstand over het scheidingsvlak van vegetatie en atmosfeer. De waarde voor de exces weerstand volgens deze nieuwe analyse komt

178

meer overeen met waarden die voor lage vegetatie worden gevonden. In de neutrale limiet geven beide methoden dezelfde relatie tussen warmteflux en temperatuur verschil tussen de vegetatie en oppervlaktelaag. Theoretisch kan aannemelijk gemaakt worden dat stabiliteitseffecten tot verschillen tussen de twee methoden leidt. De waarnemingen geven enige steun voor de alternatieve methode. Door gebruik te maken van de concepten van windvlaag-penetratie en oppervlakte-ververversing kan het temperatuurverschil tussen de lucht in het inwendige van het bos en de lucht bij de boomtoppen gerelateerd worden aan de bodem/biomassa warmte flux en de voelbare warmte flux. De analyse suggereert dat de ververversing van bos interieur lucht slechts langzaam plaats vindt omdat de kronenlaag erg dicht is.

Voor nachtelijke situaties met weinig wind en heldere lucht ontstaat een verschil tussen stralings-oppervlaktetemperatuur en aërodynamische-oppervlakte-temperatuur. De lucht tussen de boomtoppen raakt ontkoppeld van de luchtlagen daarboven. Langgolvige koeling in de kronenlaag initiëert convectie, die koude lucht naar het bos interieur transporteert. Op grond van de metingen kan het bestaan van een convektieve-oppervlaktetemperatuur afgeleid worden. Een twee-lagen stralings/energiebalans model is geconstrueerd. Dit model verklaard het verschil tussen stralings- en aërodynamische-oppervlaktetemperatuur door een voorgeschreven verdeling van bodem/biomassa warmte flux en voelbare warmte flux over de twee modellagen.

Transpiratie is onderzocht door gebruik te maken van de Penman-Monteith vergelijking, met een beschrijving van de oppervlakteweerstand volgens de methode van Jarvis. Eerst is de sluiting van de energiebalans onderzocht. Gemiddeld over de meetperiode ligt de imbalans binnen de geschatte meetfout. Nu en dan treden grotere afwijkingen op, deze blijken gerelateerd aan specifieke windrichtingen. De oppervlakteweerstand blijkt sterk te reageren op veranderingen in het atmosferische vochtdeficit. Dit is gerelateerd aan de goede aërodynamische koppeling tussen het ruwe bos en de atmosfeer. Na de scheutgroei in de lente worden beduidend hogere transpiratiesnelheden gevonden. Bodemwaterrespons is duidelijk aanwezig tot het midden van de zomer, daarna lijkt het bos minder gevoelig te worden voor droogte. Wellicht dat aanpassing van het wortelstelsel hier een rol speelt. Een analyse van de residuen tussen waargenomen en gemodelleerde verdamping toont aan dat deze gecorreleerd zijn met de afwijkingen in de energiebalans. De variantie in de residuen is twee keer groter dan op grond van de atmosferische statistiek verwacht mag worden. Een belangrijk deel van deze extra variantie is gecorreleerd over tijdsintervallen van een dag. Dit suggereert dat standaard statistische technieken tot een onderschatting van de betrouwbaarheidsintervallen voor de geschatte model parameters leiden. Een nieuwe formulering volgens Monteith, waarin de stomataire response op het atmosferisch vochtdeficit is vervangen door een response op verdamping zelf, is onderzocht. Deze formulering blijkt equivalent te zijn aan de formulering van Jarvis met een atmosferisch vochtdeficit respons. De Priestley-Taylor formule is aangepast door het toevoegen van een bodemwaterrespons. In deze vorm blijkt het model de waarnemingen redelijk goed te kunnen beschrijven ondanks de eenvoudige formulering.

179

Interceptiemetingen en xylem-sapstroommetingen zijn gebruikt om de interactie tussen evaporatie en transpiratie te onderzoeken in een gedeeltelijk nat bos. Hiertoe is de Penmann-Monteith vergelijking gegeneraliseerd. Expliciete uitdrukkingen voor evaporatie en transpiratie zijn afgeleid. Na optimalisatie blijkt het model de waarnemingen van evaporatie en transpiratie reductie goed te kunnen beschrijven. Door de statistische afhankelijk van parameters in het evaporatie deel van het model zijn de betrouwbaarheidsintervallen rond deze parameters groot. Onafhankelijke schattingen van deze parameters liggen binnen deze betrouwbaarheidsgebieden in de parameterruimte. Evaporatie is kleiner dan de vaak gebruikte formule: natte fractie maal potentiële verdamping. De belangrijkste factoren in transpiratie reductie zijn de energie consumptie door evaporatie en de beïnvloeding van het micro-klimaat rond de vegetatie. Slechts een kleine fractie stomataire blokkade door het opliggend water is nodig om de resterende transpiratie reductie te verklaren. Dit stemt overeen met het feit dat de stomata van Douglas-spar zich aan de onderzijde van de naald bevind. Deze zijde wordt in het algemeen slechts gedeeltelijk bevochtigd tijden regen.

De resultaten gevonden voor het huidige, dichte Douglas sparrenbos zijn vergeleken met andere bosstudies. De relatie tussen de geometrische parameters, boomhoogte, nulvlaksverplaatsing en ruwheidslengte voor impuls blijken overeen te komen met resultaten van eerdere studies. De uitwisselingscoefficiënten in de ruwheidslaag voor impuls en warmte komen kwalitatief overeen met typische waarden voor andere dichte bossen. Kwantitatief blijven er significante en onverklaarde verschillen bestaan. De kleine waarde voor de scalaire exces weerstand is in overeenstemming met de enige andere vergelijkbare studie voor dicht bos die onlangs in de literatuur is verschenen. Transpiratiesnelheden als functie van externe omstandigheden stemmen globaal overeen met resultaten van andere bossen in het gematigde klimaat.

Nieuw in dit proefschrift zijn de resultaten over; het schatten van de verplaatsingshoogte; het verschil tussen stralings- en aërodynamische oppervlaktetemperatuur voor nachtelijke situaties; nachtelijke convectie in het bos; veranderende response van transpiratie op bodemwater tekort over de seizoenen en de interaktie tussen evaporatie en transpiratie onder natte omstandigheden.

180

Curriculum Vitae

Fred Bosveld werd geboren op 14 september 1956 te Oosterbeek. In 1975 behaalde hij het diploma Atheneum B aan het Christelijk Atheneum te Arnhem. In dat jaar begon hij aan de studie Natuurkunde aan de Univerteit van Utrecht, waar hij in 1978 zijn kandidaatsexamen (cum laude) deed. In 1983 studeerde hij aldaar af in de hoofdrichting gemengd theoretisch/experimentele natuurkunde met bijvakken wiskunde en milieukunde en de didactische aantekening natuurkunde. Het experimentele afstudeerwerk werd verricht bij de vakgroep stromingsleer aan de Technische Universiteit Delft, op het onderwerp turbulente spots in een laminaire grenslaag. In 1984 trad hij in dienst van het KNMI bij de afdeling Fysische Meteorologie. Van 1985 tot en met 1987 deed hij ervaring met experimenteel veldwerk op in een samenwerkingsproject met MT-TNO Delft op het gebied van droge depositie van luchtverontreiniging op natuurlijke vegetatie. In 1988 werd een herfst-school op het gebied van oppervlaktefluxen gevolgd in Banyuls, Frankrijk. Vanaf 1988 werd binnen het kader van het additioneel verzuringsprogramma van VROM in een groter samenwerkingsverband gestart met micro-meteorologische metingen in het Speulderbos nabij Garderen. In 1991 werd een herfst-school gevolgd in Glücksburg, Duitsland, op het gebied van klimaatonderzoek. Daarna verplaatste de aandacht zich naar het verkrijgen van lange en continue reeksen van oppervlaktefluxen voor het evalueren van onderdelen van weer- en klimaatmodellen. Deze meetprogramma's werden uitgevoerd in Garderen en te Cabauw bij de 200 m hoge meteorologische meetmast van het KNMI.